CODEN:TRITA/SKP-90/1065

KUNGL
TEKNISKA
HÖGSKOLAN

Royal Institute of Technology
Department of Naval Architecture
S-100 44 Stockholm, Sweden

Combined Wave Induced Stresses in an OBO Carrier

Application of a Rationally Based Direct Calculation Method

Part 2

by

Mikael Huss

1990

Report TRITA-SKP 1065

ISSN 0349-0025

COMBINED WAVE INDUCED STRESSES IN AN OBO CARRIER;

APPLICATION OF A RATIONALLY BASED DIRECT CALCULATION METHOD

PART 2

by
Mikael Huss
1990

Report TRITA-SKP 1065

Royal Institute of Technology
Department of Naval Architecture
S-100 44 Stockholm, Sweden

ABSTRACT

This report presents calculations of wave induced stresses in side frames and bottom girders of an OBO carrier. Calculations have been performed with a direct, rationally based method incorporating all major low-frequency wave load components. Structural response was calculated using ordinary hull beam idealization for global loads and FE-analysis for local hydrodynamic pressure loads and for inertia loads from ship cargo. Results from structural analysis were coupled to strip calculations with influence coefficients. Non-linear stress response close to the still water line was evaluated using a time step procedure. Stress responses are presented for regular waves, short-term irregular seas, and long-term wave statistics for the North Atlantic Sea. Results from fatigue analysis of different weld joints are presented. A semi-continuous Weibull distribution for long-term stresses is proposed that is suitable for determination of extreme stresses as well as for fatigue analysis. The influence of speed reduction and non-linear pressure loads on the long-term stress distribution is discussed. The additional information that can be achieved by the present direct method in comparison with ordinary methods based on static design loads is emphasized.

Key words:
wave loads, stress response, ship structural design, fatigue, dynamic, direct analysis, long-term distribution, Weibull, hydrodynamic pressure, non-linear

CODEN: TRITA/SKP-90/1065

ISSN 0349-0025

CONTENTS

1 INTRODUCTION

This report represents the second part of a project aimed to investigating the combined wave induced stresses in ship hulls with respect to all major low frequency load components.

In a previous report by the author, [1], a direct rationally based calculation method was presented. Results from nominal stress calculations of different structural members at the midships hold of a lo/lo containership were presented in the form of response functions for regular waves and irregular seas. The main girder structures in sides and bottom of the containership were "isotropic" with approximately equal spacing and thickness in the transverse and longitudinal direction.

In this report results are presented for a completely different girder structure. The OBO-carrier studied here has solely transverse frames at side and solely longitudinal girders at the bottom between bulkheads. Stress response functions for this hull structure together with the previously presented results for the containership form a comprehensive material from which conclusions can be drawn about the relative importance and combined effect of the various wave induced load components.

1.1 Calculation method

Three major types of low frequency wave induced loads are of importance when calculating the local stress response in the structure.

* Global moments and forces on the ship hull girder.
* Local external hydrodynamic pressure on sides and bottom.
* Local internal inertia and gravity forces from the cargo due to ship motions.

Ship motions and global loads calculated with strip-theory become linear with respect to the wave height and periodic with the same frequency as the encountering waves.

The combined stress response depends on both the amplitude and the relative phase of the various load components. Since the phase lag varies with the frequency and with the position of the structural member, the combined stress must be calculated for each stress spot separately. With the assumption of elastic material properties the stress response in a regular harmonic wave also becomes linear and harmonic.

The hydrodynamic pressure distribution below the still water line calculated with strip theory, is based on the assumption of small wave amplitudes. However, for larger wave amplitudes a harmonic pressure variation on the area within the relative motion between ship and wave does not fulfil the condition of zero pressure above the wave surface.

In the computer program WAIST, [2], stress response functions are determined with use of results from strip calculations of ship motions, global moments and forces, and local hydrodynamic pressures together with hull sectional properties for global loads, and stress influence coefficients from FE-calculations for local external and internal loads. The non-linear pressure distribution close to the still water line is calculated using a time step procedure where the harmonic pressure is corrected or extrapolated in accordance with the actual position of the wave surface.

2 STRUCTURAL MODELS

The ship structure studied in this report is from a 55 000 dwt OBO Carrier designed and built by Uddevallavarvet. Main particulars and profile is shown in fig.2.1 and the midship section with scantlings in fig.2.2. The cargo compartment is divided in 8 full breadth holds. Between hopper tanks and top wing tanks the single side shell is stiffened by vertical frames with 0.9 m spacing. Every fourth frame is a stiff webframe that continues into the tanks. The double bottom is solely longitudinally stiffened with full height bottom girders with 0.9 m spacing. Stress responses have been calculated at the bottom side girder and at three positions along the side frame midway between webframes as indicated in fig.2.2.

Main Particulars:

Length over all	207,00	m
Length between perpendiculars	200,00	m
Breadth, moulded	32,23	m
Depth, moulded to upper deck	17,35	m
Design draught	11,58	m
Scantling draught	12,65	m
Deadweight at scantling draught	54600	mton
Trial speed at design draught	16,6	knots
Service speed 50% scantling/50 % ballast draught, 12% sea margin on power	15,5	knots

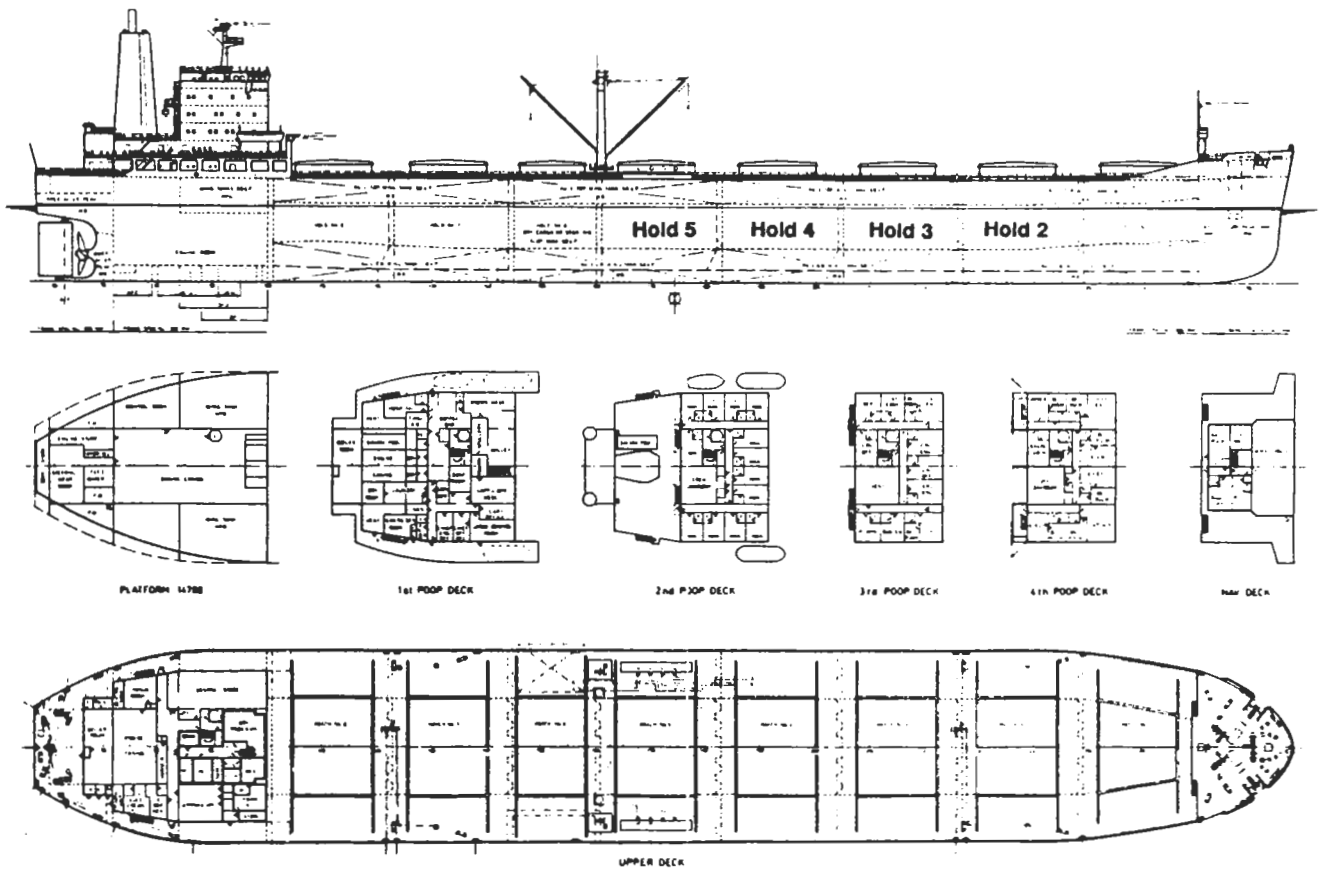

Fig.2.1 Uddevallavarvet 55 000 dwt OBO carrier, main particulars

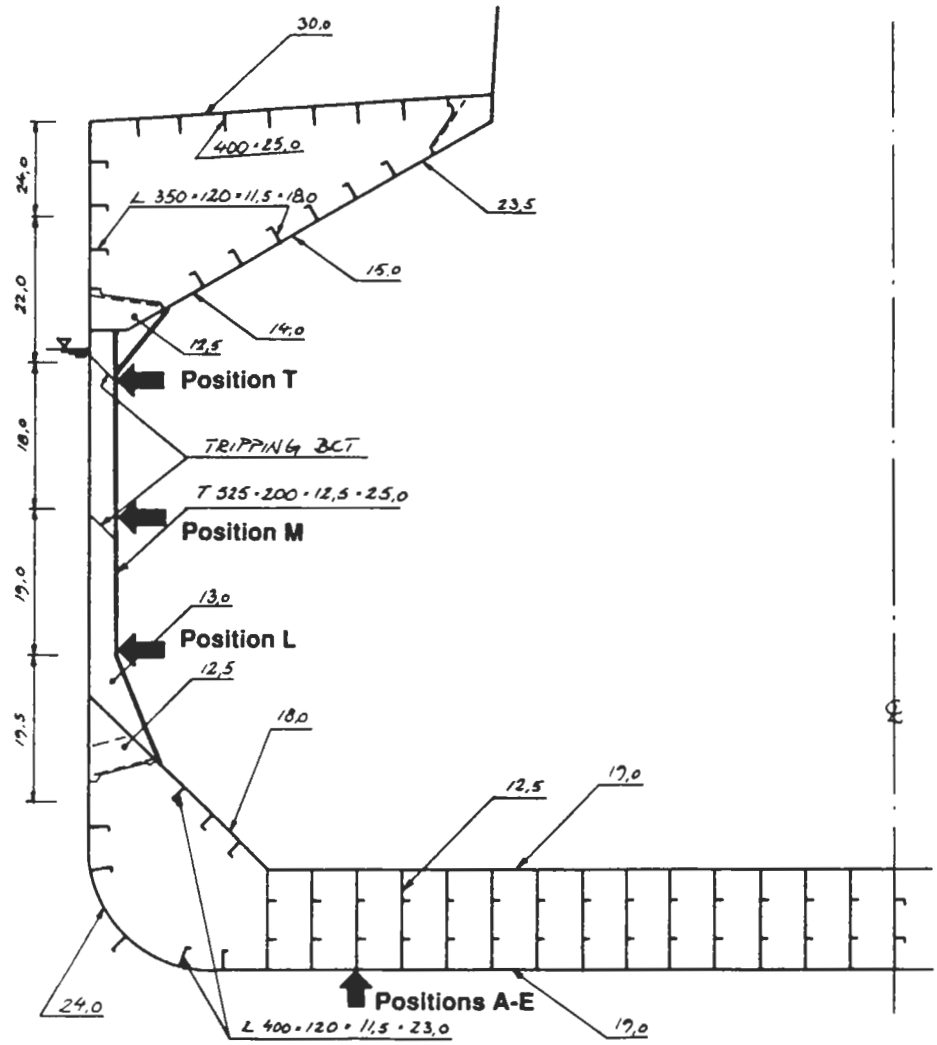

Fig.2.2 Midship section

2.1 Bottom side girder

Normal stresses from global vertical- and horizontal hull girder bending were calculated with use of a vertical moment of inertia I_y=198,1 m^4 with a neutral axis 7.08 m above keel, and a horizontal moment of inertia I_z=505,9 m^4. Shear stresses in girders from global hull shear forces were considered insignificant. Stresses from global torsional moment were also considered negligible due to the wide transverse deck strips between hatch openings, and to the large closed cells at top and bottom.

Local influence coefficients for external hydrodynamic pressures and for internal mass forces were calculated with a simple 2-dimensional FE-model covering one hold and half of the adjacent holds. Boundary conditions at the ends of the modelled girder were free vertical displacements, and zero longitudinal displacements, assuming symmetry of loads and structure. The transverse corrugated bulkheads were modelled as vertical beams. External pressure on the bottom shell and internal mass force load on the tank top were applied at four longitudinal stations, and stress responses were evaluated at five positions, A-E, along the bottom of the girder.

Fig 2.3 shows model and load cases, fig.2.4 shows model deformations under external bottom load and fig.2.5 shows an example of influence coefficient distribution for the four load cases. The stations for calculation of hydrodynamic pressure were not symmetric with respect to the holds, which explains the non-symmetric distribution of influence coefficients for position C in fig.2.5.

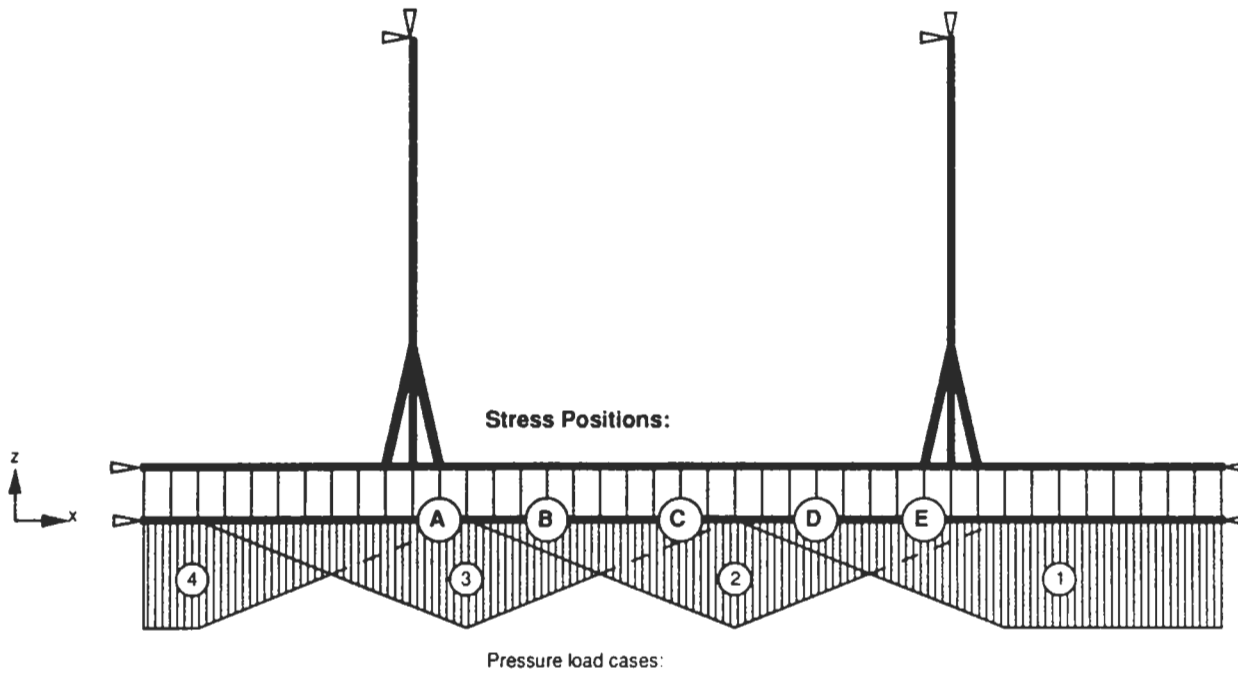

Fig.2.3 FE-model of bottom girder

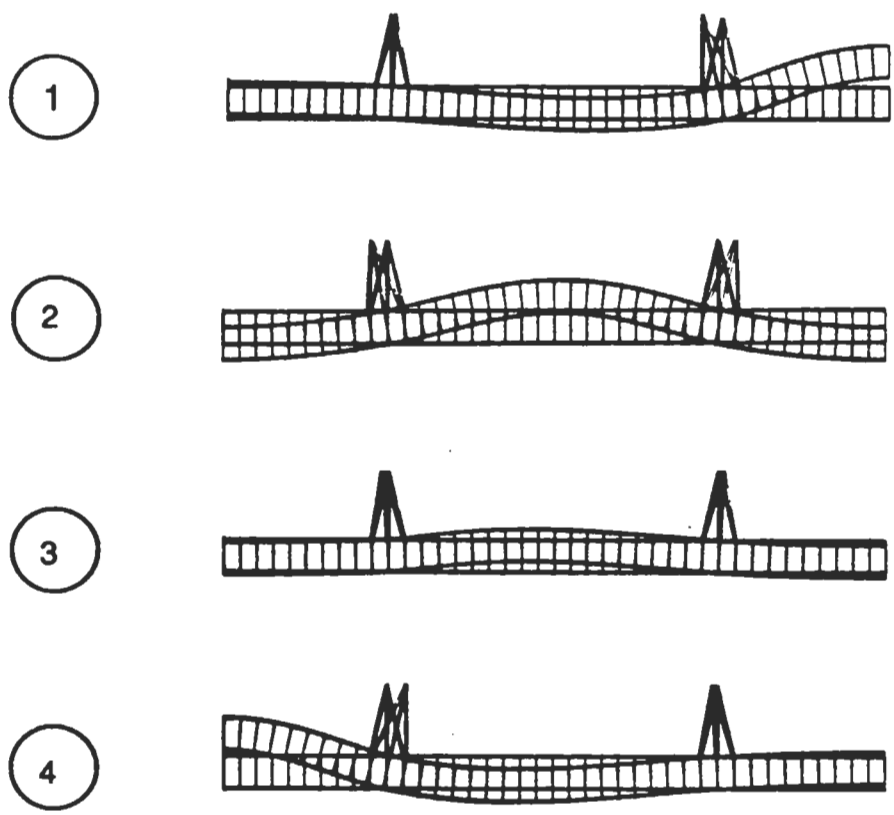

Fig.2.4 Plot of deformations for load cases 1-4

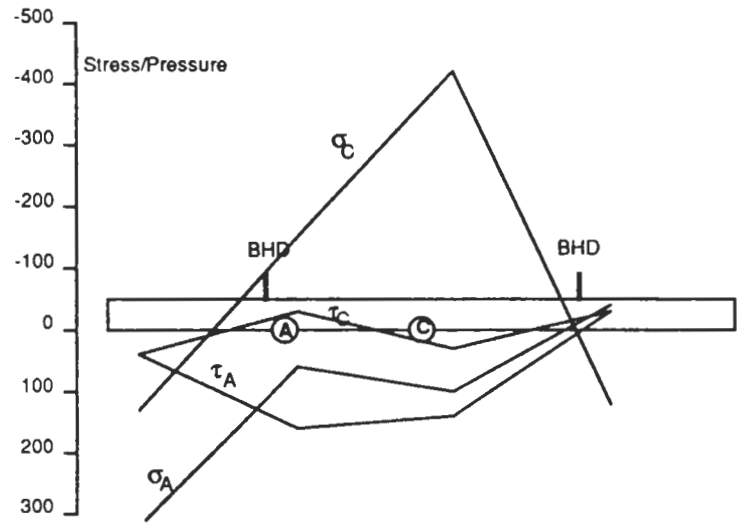

Fig.2.5 Distribution of stress/pressure influence coefficients for positions A and C

2.2 *Side frame*

Stress responses to local loads were calculated using a 3-dimensional FE-model including two frame spaces, from one webframe half way to the next webframe, fig.2.6. The boundary conditions were: zero rotation around the vertical axis at aft and fore end of the model, zero lateral displacement at the web, and free lateral displacement at the mid frame between the webframes. External pressure load was applied at 10 different positions from bilge to deck and internal mass force was applied at 10 positions from hopper tank to top wing tank. Nominal normal stresses were evaluated in the frame flange at three positions: close to the bracket toe (T) below top wing tank, close to the flange knuckle (L) above hopper tank, and at the tripping bracket 9,4m above keel (M).

Fig.2.7 shows examples of deformations under external load and fig.2.8 shows examples of stress influence coefficients along the frame.

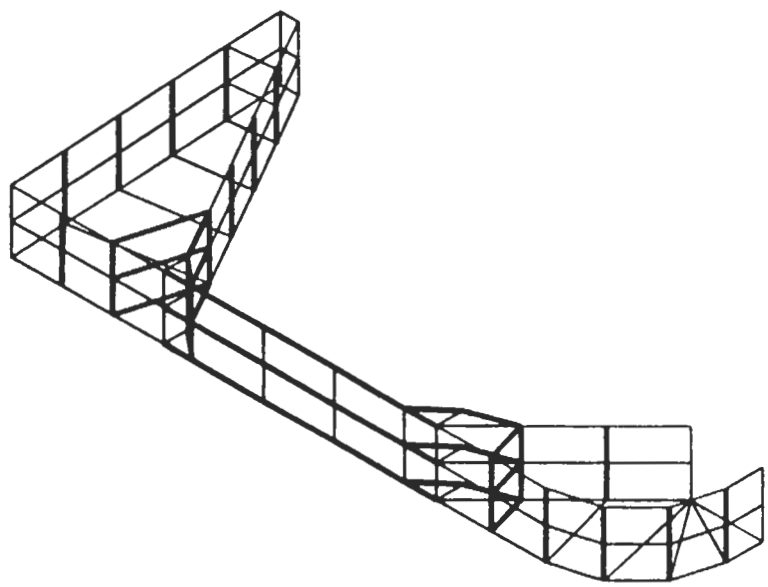

Fig.2.6 FE-model of side frame

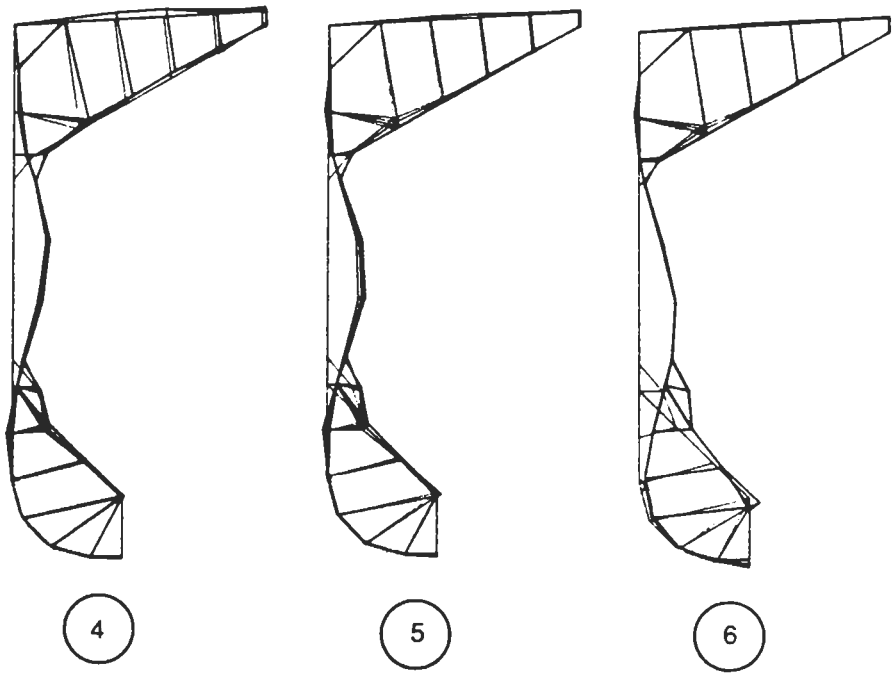

Fig.2.7 Plot of deformations for pressure load positions 4-6

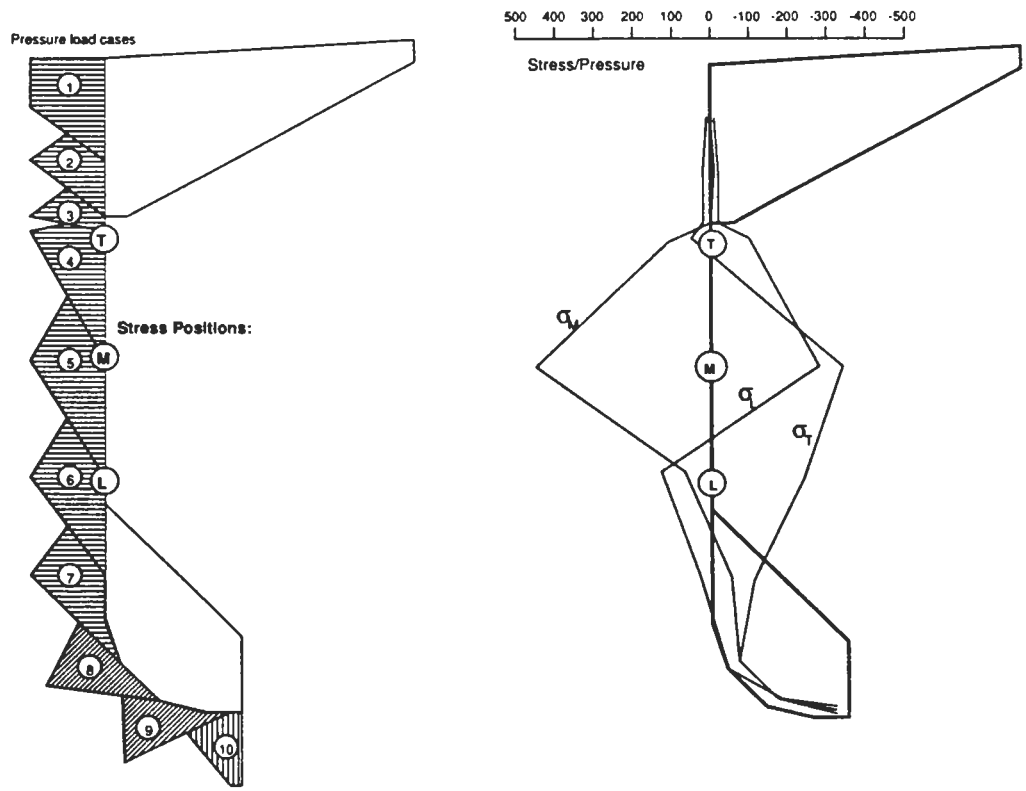

Fig.2.8 Distribution of stress/pressure influence coefficients for positions L, M, T

3 WAVE LOADS

Ship motions in 5 degrees of freedom, global hull girder moments, and hydrodynamic pressure distributions were calculated with the strip program SGENS, [3], based on the theory of Salvesen, Tuck, and Faltinsen, [4]. The previous WAIST program, described in [2], was connected with the SCORES strip program, [5,6]. In comparison with the old one, the new version gives a more significant speed effect on the global loads. Also the coordinate system of motions is redefined in the new version, fig.3.1. Since the hull forms are smooth with U-shaped sections, ordinary 3-parameter Lewis transformation was used to calculate the hydrodynamic sectional properties. This is, however, no general limitation of the system, since SGENS also includes a more general panel representation of the sectional geometry.

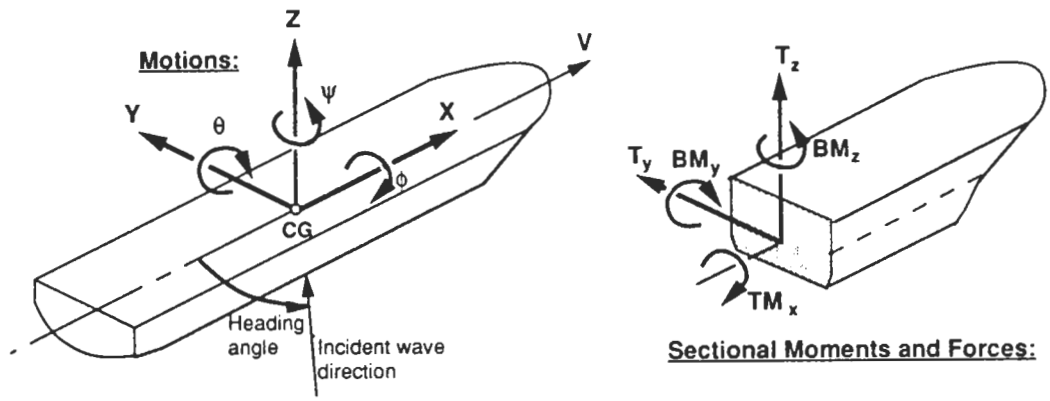

Fig.3.1 Definition of coordinate system

3.1 Global loads

A full load oil cargo departure condition at scantling draught 12.65 m and speed 15 kn was used for response calculation. This condition gives a maximum still water bending moment of 900 MNm in hogging at Hold 6, corresponding to nominal hull girder bending stresses of 49 MPa at deck and -32 MPa at bottom. For comparison of the long term bottom stresses also a bulk cargo departure condition was studied, see fig.5.18.

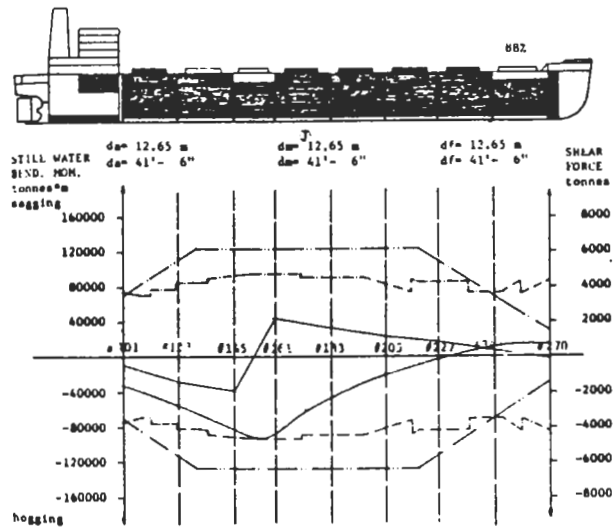

Fig.3.2 Load condition with distribution of still water bending moment and shear force. From the Trim and Stability Book

3.2 Local hydrodynamic pressures

Hydrodynamic pressure distributions at the hull sections are calculated using the general method described by de Jong, [7]. The total harmonic pressure is separated in four components:

* Pressure calculated from wave potential without influence from ship hull
* Variation in hydrostatic pressure due to vertical motion (3 dof)
* Diffracted wave pressure on the hull surface when the ship is maintained fixed
* Wave pressure from radiation due to vertical and horizontal motions (5 dof)

Close to the still water line (SWL) the harmonic pressure variation is modified in accordance with a method described in [1].

* Pressure variation from wave potential and from ship vertical motion is assumed to be linearly distributed from the value at the wave surface to zero at SWL when the surface is below SWL, and from the value at SWL to zero at the wave surface when it is above SWL
* Pressure variation from diffraction and radiation is cut at the wave surface when it is below SWL, and kept constant from SWL up to the surface when it is above SWL

Fig.5.25 shows examples of the time variation of stresses induced by harmonic as well as modified non-harmonic pressure close to SWL.

3.3 Local mass forces

Local inertia forces on the hull structure are calculated from the variation of the quasi hydrostatic pressure distribution in liquid cargo holds due to ship accelerations in waves. Accelerations at position k are evaluated from ship motions according to eqs.(3.1-3.3). The surge acceleration is not calculated by the strip program, and therefore not included in eq.(3.1).

$$\ddot{x}_k = \omega_e^2 (- z_k \theta + y_k \psi) \tag{3.1}$$

$$\ddot{y}_k = \omega_e^2 (- y + z_k \phi - x_k \psi) \tag{3.2}$$

$$\ddot{z}_k = \omega_e^2 (- z - y_k \phi + x_k \theta) \tag{3.3}$$

where

$$y = y_0 \cos(\omega_e t + \varepsilon_y) \quad \text{(sway)}$$
$$z = z_0 \cos(\omega_e t + \varepsilon_z) \quad \text{(heave)}$$
$$\phi = \phi_0 \cos(\omega_e t + \varepsilon_\phi) \quad \text{(roll)}$$
$$\theta = \theta_0 \cos(\omega_e t + \varepsilon_\theta) \quad \text{(pitch)}$$
$$\psi = \psi_0 \cos(\omega_e t + \varepsilon_\psi) \quad \text{(yaw)}$$

In addition to the inertia forces, linearized variations of gravity forces from pitch and roll are included in the local mass forces. If the "active" mass at position k is $(m_x, m_y, m_z)_k$ in the ship's longitudinal, transverse and vertical direction, then the mass force components for solid cargo become

$$F_{mx_k} = m_{x_k} (- \ddot{x}_k + g\,\theta) \tag{3.4}$$

$$F_{my_k} = m_{y_k} (- \ddot{y}_k - g\,\phi) \tag{3.5}$$

$$F_{mz_k} = m_{z_k} (- \ddot{z}_k) \tag{3.6}$$

Solid cargo mass forces are generally not coupled and can be treated separately. For liquid cargo however, mass forces arise from quasi "hydrostatic" pressure variation due to accelerations. For small accelerations the coupling effect can be taken into account according to eqs.(3.7-3.9) and fig.3.3. Here *Cposx* and *Cposy* are internal normalized tank coordinates with values in the interval -1 to +1 and with origo at the centre of the hold. For side structures, *Cposy* is -1 at starboard side and +1 at portside and for bulkhead structures, *Cposx* is -1 at aft and +1 at forward end of the hold.

$$F_{mx_k} = m_{x_k} (- \ddot{x}_k + g\,\theta) + Cposx_k\, Cposy_k\, m_{y_k} (- \ddot{y}_k - g\,\phi) - Cposx_k\, m_{z_k} (- \ddot{z}_k) \tag{3.7}$$

$$F_{my_k} = Cposx_k\, Cposy_k\, m_{x_k} (- \ddot{x}_k + g\,\theta) + m_{y_k} (- \ddot{y}_k - g\,\phi) - Cposy_k\, m_{x_k} (- \ddot{z}_k) \tag{3.8}$$

$$F_{mz_k} = - Cposx_k\, m_{x_k} (- \ddot{x}_k + g\,\theta) - Cposy_k\, m_{y_k} (- \ddot{y}_k - g\,\phi) + m_{z_k} (- \ddot{z}_k) \tag{3.9}$$

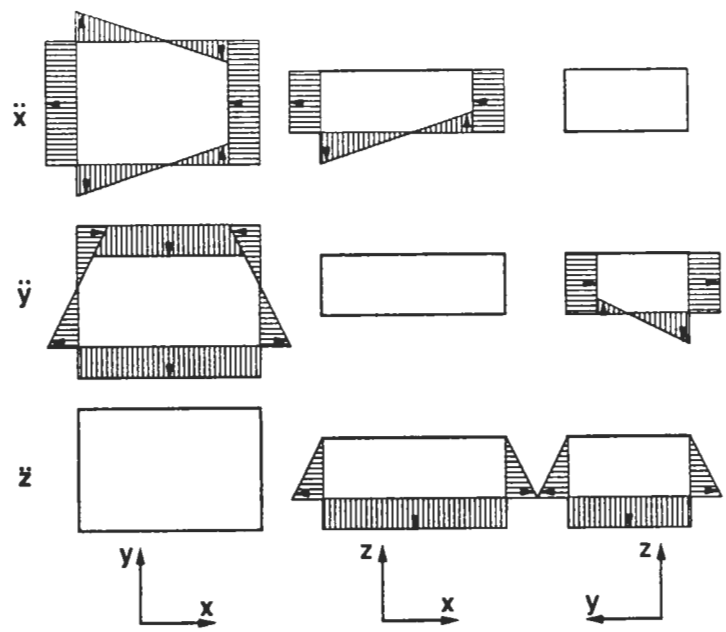

Fig.3.3 Quasi-hydrostatic inertia forces from liquid cargo

The values of the "active" liquid mass components must be determined with respect to the load case, the arrangement of holds and load carrying structures, as well as to how the stress per mass force influence coefficients have been calculated. Eq.(3.10) and fig.3.4 below illustrate how the "active" mass is calculated for a certain position k at the side frame in a liquid cargo hold. Note that m_{xk} and m_{yk} as used in eqs.(3.7-3.9), become independent of the position of k. The load area A_k is the one used for calculation of influence coefficient C_{myik} in eq.(4.5).

$$(m_x, m_y, m_z)_k = \rho A_k \left(\frac{l}{2}, \frac{b}{2}, h_k \right) \qquad (3.10)$$

where

ρ = density of liquid cargo
l = hold length between transverse bulkheads
b = hold breadth
h_k = height of liquid above position k
A_k = load (pressure) carrying area related to position k

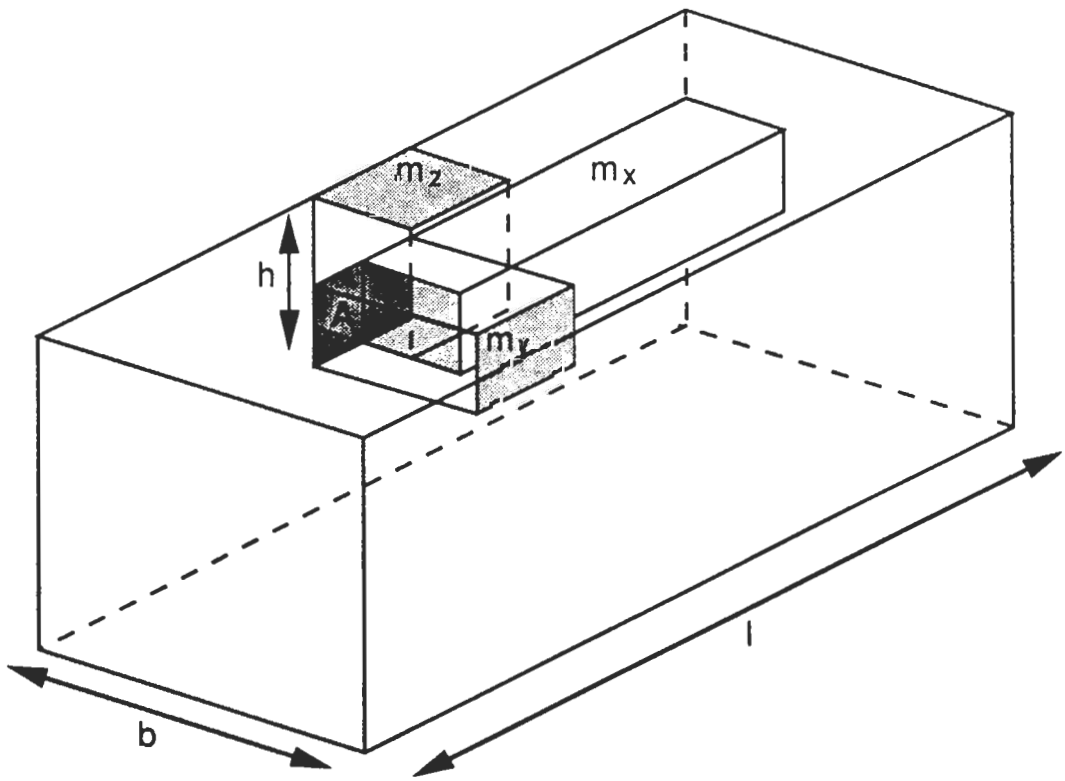

Fig.3.4 Illustration of "active" mass components for mass force position k

Figs.3.5-3.6 show examples of stress transfer functions from combined mass forces and separately from the m_y- and m_z-components. In the bottom side girder, fig.3.5, the main m_z-component is naturally dominating but there is a significant contribution to the combined mass force induced stresses also from the coupled m_y-component especially for -90° wave heading. The m_x-component is of the order of 1% of the combined mass force stress response, and is not shown in the figure. In the side frame, fig.3.6, there is a significant contribution from the coupled m_z-component for both -135° and -90° headings.

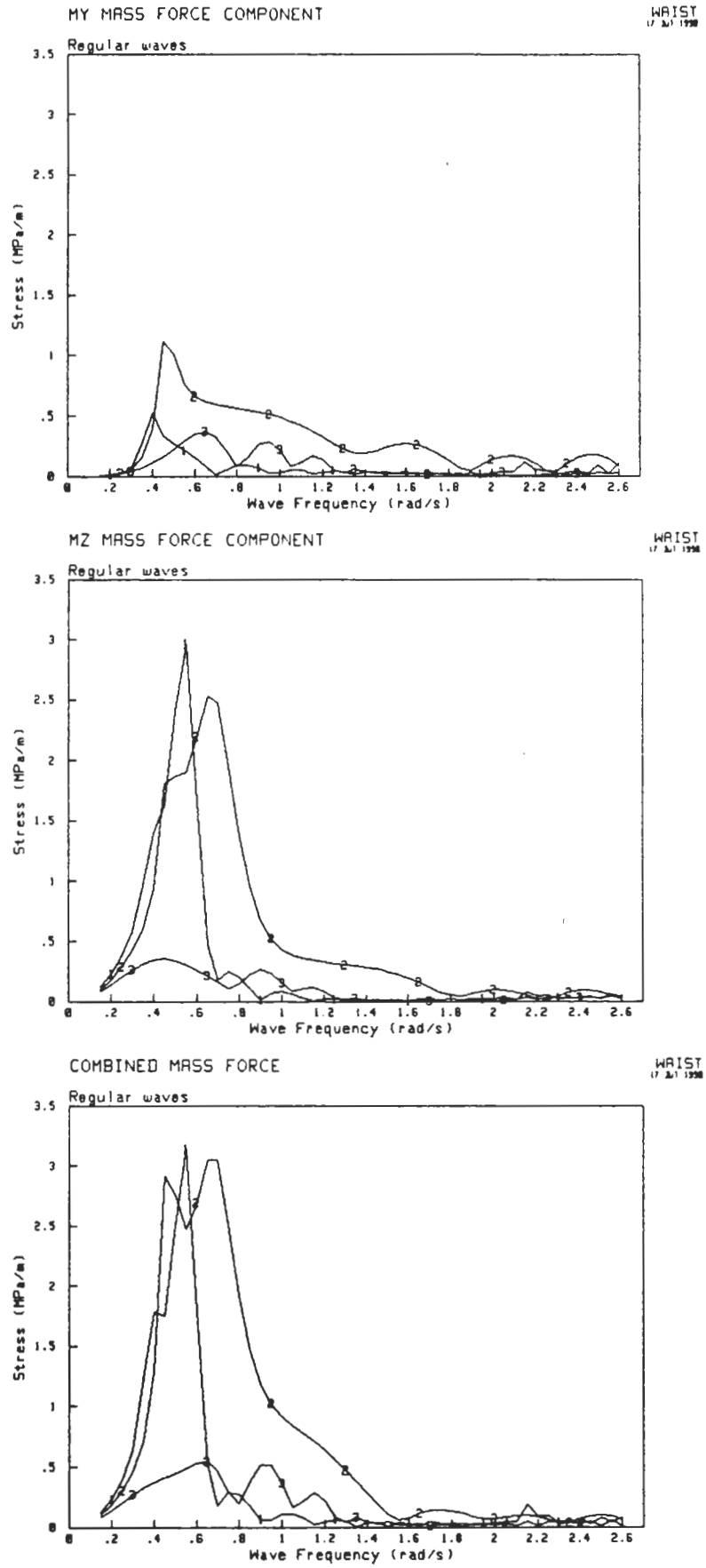

Fig.3.5 **Example of stress transfer functions from internal liquid mass forces. Bottom side girder position A, Hold 4. Curve 1: -135°, 2: -90°, 3: -45° wave heading**

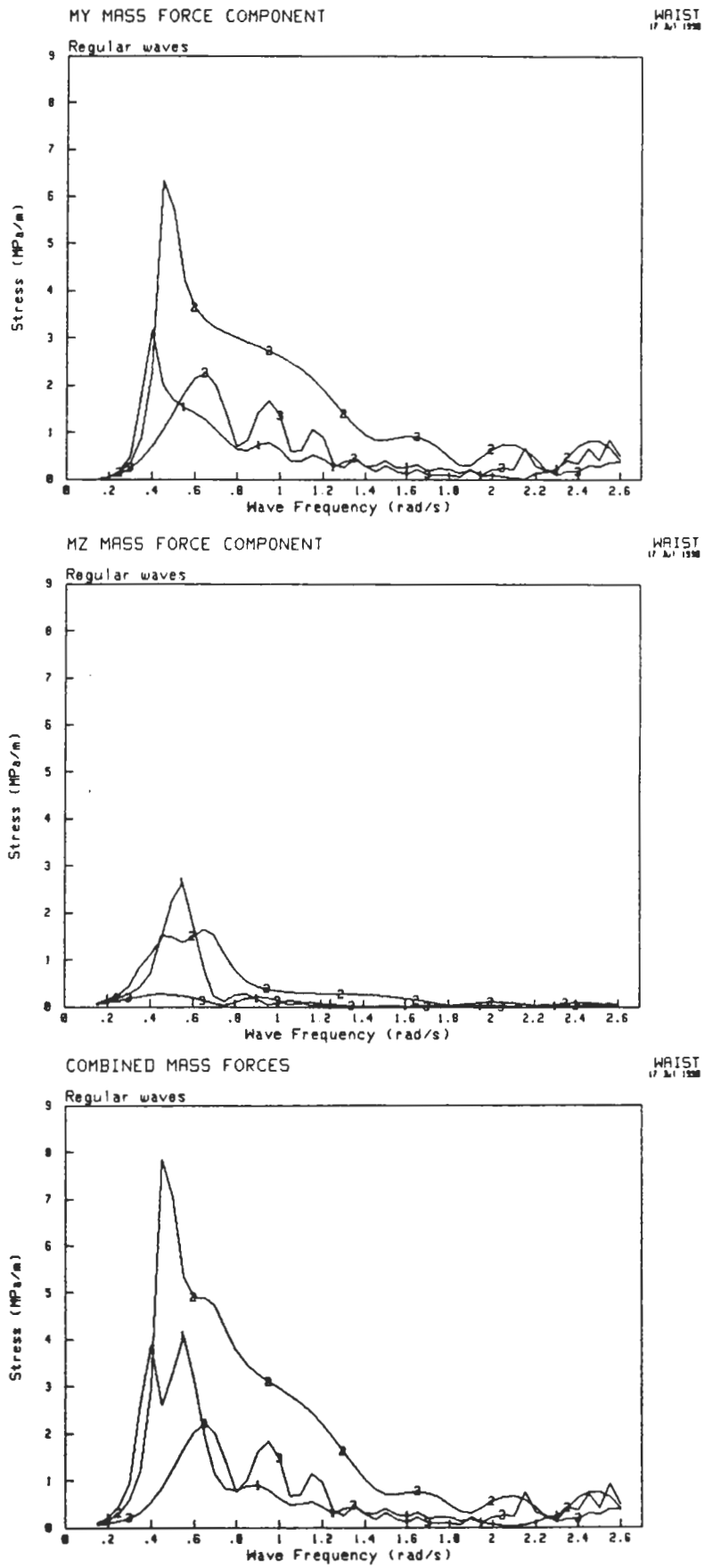

Fig.3.6 **Example of stress transfer functions from internal liquid mass forces. Side frame position M, Hold 2. Curve 1: -135°, 2: -90°, 3: -45° wave heading**

4 STRESS RESPONSE

Combined nominal stress response at position i is in program WAIST generally calculated according to

$$\sigma_{c_i} = \sigma_{g_i} + \sigma_{p_i} + \sigma_{m_i} \tag{4.1}$$

The global stress component is in the general case calculated from hull girder bending moments and shear forces according to eq.(4.2) for normal stress, and eq.(4.3) for shear stress.

$$\sigma_{g_i} = C_{Mx_i} TM_{x_i} + C_{My_i} BM_{y_i} + C_{Mz_i} BM_{z_i} \tag{4.2}$$

where

$$TM_{x_i} = TM_{x0_i} \cos(\omega_e t + \varepsilon_{TMx_i}) \quad \text{(torsional moment)}$$
$$BM_{y_i} = BM_{y0_i} \cos(\omega_e t + \varepsilon_{BMy_i}) \quad \text{(vertical bending moment)}$$
$$BM_{z_i} = BM_{z0_i} \cos(\omega_e t + \varepsilon_{BMz_i}) \quad \text{(horizontal bending moment)}$$

$$\tau_{g_i} = C_{Tx_i} TM_{x_i} + C_{Ty_i} T_{y_i} + C_{Tz_i} T_{z_i} \tag{4.3}$$

where

$$T_{y_i} = T_{y0_i} \cos(\omega_e t + \varepsilon_{Ty_i}) \quad \text{(horizontal shear force)}$$
$$T_{z_i} = T_{z0_i} \cos(\omega_e t + \varepsilon_{Tz_i}) \quad \text{(vertical shear force)}$$

C_M and C_T are stress coefficients, defined as local stress per global moments or forces. C_{Mx} and C_{Tx} consist of one part related to sectional properties and one part related to an assumed ratio warping moment / total torsional moment, see [1]. In the present study only hull girder bending moments are taken into account in the calculation of global stresses in the bottom side girder. C_{My} and C_{Mz} are equal to the sectional modulus for vertical bending and horizontal bending respectively.

Local normal or shear stress response from hydrodynamic pressure is calculated from the sum of pressures at position j multiplied by influence coefficients representing stress at position i per pressure at position j.

$$\sigma_{p_i} = \sum_j [C_{p_{ij}} p_j] \tag{4.4}$$

where

$$p_j = p_{0_j} \cos(\omega_e t + \varepsilon_{p_j}) \quad \text{(hydrodynamic pressure)}$$

5 STRESS RESULTS

5.1 Stress response in regular waves

5.1.1 Bottom side girder

A complete set of stress transfer functions in regular waves for the various normal stress components in the bottom side girder at position C, Hold 4, is presented in Appendix 1, pp.A1.2-A1.5. Maximum stress amplitudes at this position are shown in table 5.1.

Component	Max.stress MPa/m	Wave heading	ω rad/s	λ m
Vertical Bending	13,3	180°	0,50	250
Horizontal Bending	5,5	45°	0,75	110
Pressure	3,8	-90°	0,45	305
Mass Force	3,4	-135°	0,55	205
Combined	14,2	180°	0,50	250

Table 5.1 Maximum values of stress amplitude per meter wave amplitude at position C, Hold 4.

5.1.2 Side frame

Transfer functions for pressure and mass force induced normal stress components in the side frame at position M, Hold 2, is presented in Appendix 1, pp.A1.6-A1.9. The figures also include combined linear stresses and combined non-linear stresses from time simulations in regular waves with heights 8m and 16m. The non-linear stresses are here represented by "equivalent harmonic amplitudes" calculated as $\sqrt{2}$*RMS of the time step values.

The transfer functions show a typical resonance peak at wave frequencies 0,50-0,55 rad/s for forward incoming waves (135°,180°,-135°), with a maximum pressure induced component of 18,7 MPa/m and a maximum combined linear amplitude of 14,6 MPa/m in -135° waves. Even higher stress values are found for forward waves at very high wave frequencies. However, in ordinary irregular wave spectra these waves include very little energy. The maximum mass force induced component is 7,8 MPa/m and appears for -90° waves with frequency 0,45 rad/s.

The non-linear equivalent amplitudes are in all cases smaller then the linear amplitude. At the resonance peak 0,55 rad/s in -135° waves, the combined non-linear equivalent amplitude is about 75% of the linear amplitude for H = 4m and less then 60% for H > 8m. An example of non-linear transfer functions for position L,M, and T respectively in Hold 2 is shown in fig.5.1. The non-linear effect is shown to be less significant for the lower part of the frame (L).
The lower stress levels obtained with non-linear calculations can be explained by the fact that the still water line is very close to the stiff top wing tank. Pressure variation above SWL will then have little influence on stresses in the side frame, while pressure variation below SWL will have a large influence. This is clearly shown by the distribution of influence coefficients in fig.2.8.
In the first part of this report series, non-linear stresses in a web between double side plates were calculated. Close to SWL, non-linear normal stress amplitudes were increased with the wave height in comparison to linear stresses. The side structure of the studied container ship was not significantly stiffer close to deck, and consequently pressure variation did have larger importance above SWL than below, (see e.g. p.A1.66 in reference [1]).

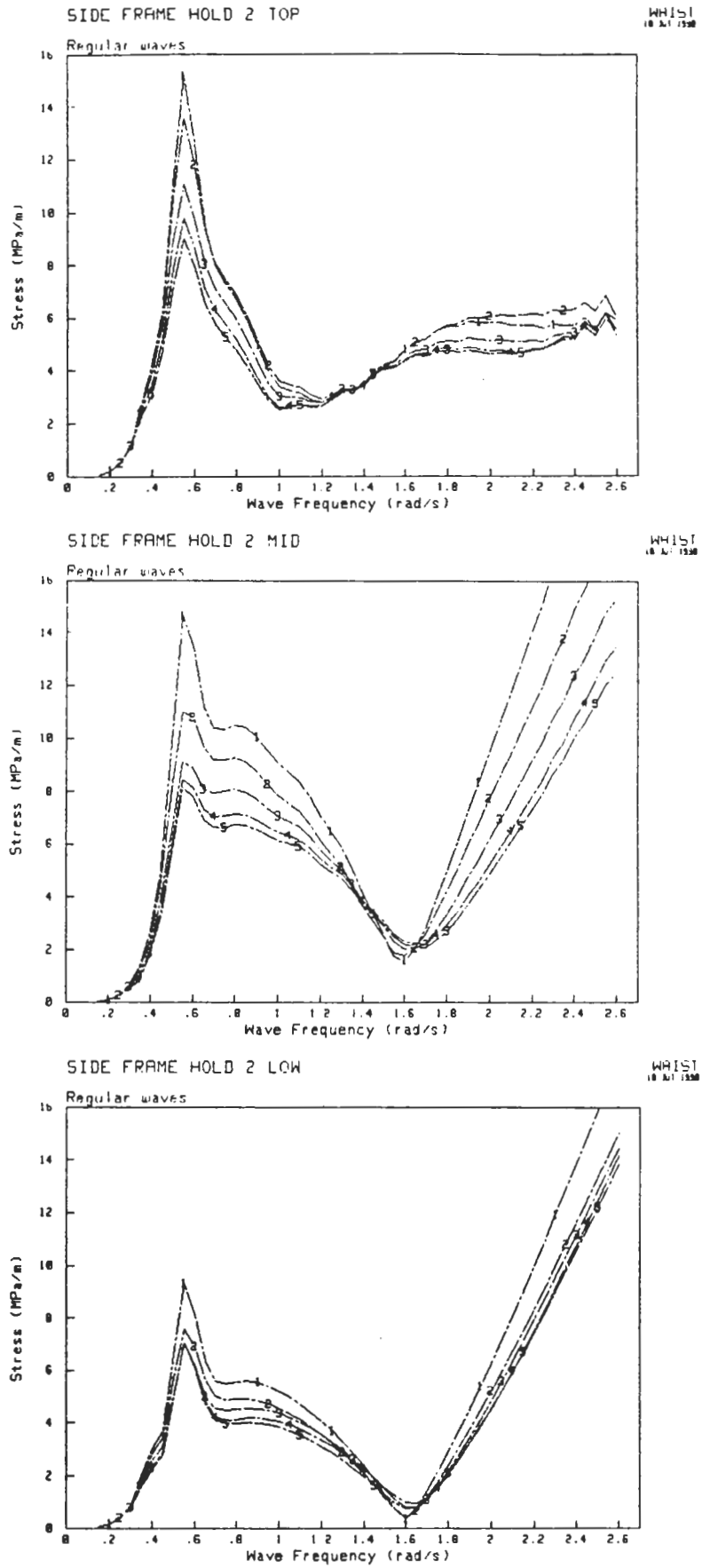

Fig.5.1 **Transfer functions for combined non-linear stresses in the side frame. Positions T (top), M (mid), L (low) in Hold 2. Wave heading -135°. 1: Combined linear 2-5: Combined non-linear; H=4m,8m,12m,16m**

5.2 Short-term stress response in irregular seas

Stress responses in irregular seas have been calculated using 2-parameter Pierson-Moskowitz spectra defined by the significant wave height and the mean zero upcrossing period according to

$$S_w(\omega) = \frac{\bar{H}_{1/3}^2 \bar{T}}{8\pi^2}\left(\frac{2\pi}{\omega\bar{T}}\right)^5 e\left(-\frac{1}{\pi}\left(\frac{2\pi}{\omega\bar{T}}\right)^4\right) \qquad (5.1)$$

where

$\bar{H}_{1/3}$ = significant wave height

$\bar{T}$ = mean zero upcrossing period

ω = wave frequency

Significant stress amplitudes are evaluated from stress spectra according to

$$S_\sigma(\omega) = S_w(\omega)\, T_\sigma(\omega)^2 \qquad (5.2)$$

where

$T_\sigma(\omega)$ = transfer function for stresses

$$\bar{\sigma}_{1/3} = 1.416\sqrt{R_\sigma}$$

$$R_\sigma = 2\int_0^\infty S_\sigma(\omega)\, d\omega \qquad (5.3)$$

where

R_σ = parameter of the Rayleigh distribution: $Q(\sigma) = e^{-(\sigma^2/R_\sigma)}$

Both sea- and stress spectra are assumed to be narrow banded with Rayleigh distributed wave- and stress amplitudes. Significant values (index 1/3) are by definition the mean value of the upper third fractile of the distributions. Only linear response can be calculated using this ordinary frequency based analysis and hence the significant stress amplitude per meter significant wave amplitude is determined only by the mean period of the sea state. All the stress results shown in Appendix 2 and in the following figures of this section, are presented in this form, both significant stress response and significant wave height either double or single amplitude

The statistical correlations between different stress components in irregular seas are represented by correlation coefficients defined according to

$$\rho_{AB} = \left(\left(\overline{\sigma_A + \sigma_B}\right)_{1/3}^2 - \bar{\sigma}_{A_{1/3}}^2 - \bar{\sigma}_{B_{1/3}}^2\right) / \left(2\,\bar{\sigma}_{A_{1/3}}\,\bar{\sigma}_{B_{1/3}}\right) \qquad (5.4)$$

5.2.1 Bottom side girder

In Appendix 2, pp.A2.2-A2.17, stress responses in irregular seas are presented for the girder at position A and C in Hold 4. At position A close to the bulkhead, shear stress response and correlation between shear and normal stresses are included while at position C in the middle of the hold, where shear stresses are insignificant, correlations between the different normal stress components are presented.

The highest combined normal stress response is found for 180°, -135°, and -45° seas. For 180° seas the vertical bending moment is the very dominating component while for the other headings, horizontal bending and local stress components contribute significantly to the combined stress, see e.g. p.A2.17. For 180° seas the highest stress response is found for a mean wave period of 9-10s, for -135° seas 8-9s, and for -45° seas 7s. The horizontal and vertical bending moments show for all mean periods a strong correlation with positive correlation coefficients for portside incoming waves. The correlation between pressure- and mass force components is negative for all mean periods above 5s and for all headings except for 0°. The most significant correlation is found in portside beam seas, see p.A2.16.

Shear stress response from local load components at position A shows a maximum of 2,2 MPa/m for 180° sea with mean period 5s, p.A2.6. Like for normal stresses, the pressure and mass force components mostly counteract each other so that the combined stress is less than the largest component.

Longitudinal distribution of stress response along the bottom side girder from Hold 5 to Hold 2 in longcrested irregular sea with 9s mean period is shown in figs.5.2-5.6. The region ranges from 0,44Lpp to 0,84Lpp. The studied four holds have approximately the same structural geometry, and in the full load oil cargo condition also the same static local load condition. Hence the same influence coefficients from the FE-analysis have been used for all holds and only the positions for calculation of wave loads have been changed.

Fig.5.2 shows the combined normal stress response. The maximum dynamic stress level appears in the middle of Hold 4 for 180° sea. The figure very clearly shows the positive correlation between local and global stresses in the middle of the holds, and the negative correlation at the bulkheads, see also fig.5.5. This tendency is found for all headings except for -90°. The vertical and horizontal hull girder bending moments and the combined global stress response have maximum levels in Hold 4, fig.5.3. The correlation between vertical and horizontal bending moments is strong all along the ship with positive correlation coefficients in the order of 0,4-0,9 for portside incoming waves, fig.5.5. Pressure induced as well as mass force induced local normal stresses have local maxima at the bulkheads and in the centre of the holds. The levels increase in the forward part of the ship, fig.5.4, but due to the predominantly negative correlation, fig.5.5, the combined local stress levels are unchanged for the four holds considered. The same phenomenon is found for local shear stresses, fig.5.6.

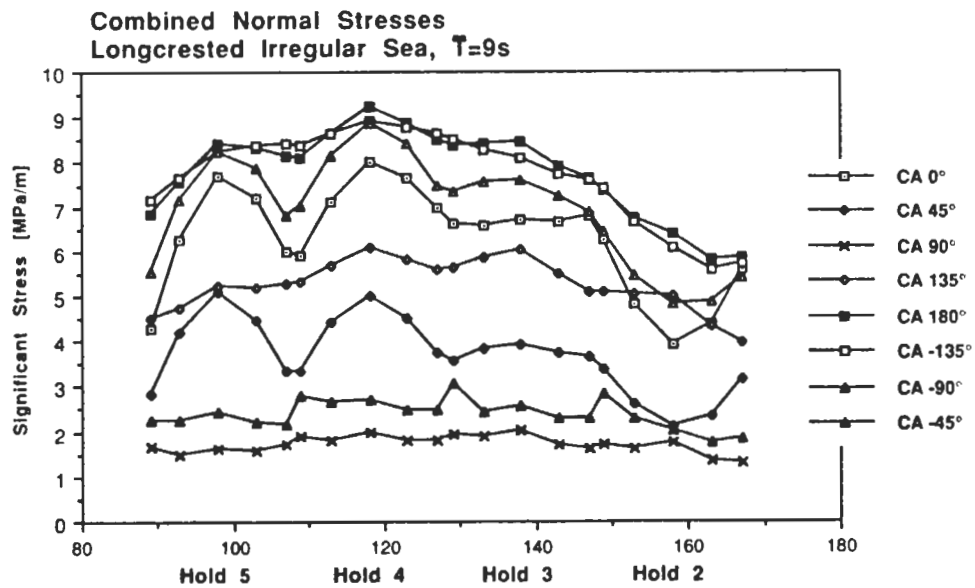

Fig.5.2 Short-term combined normal stress distribution in bottom side girder

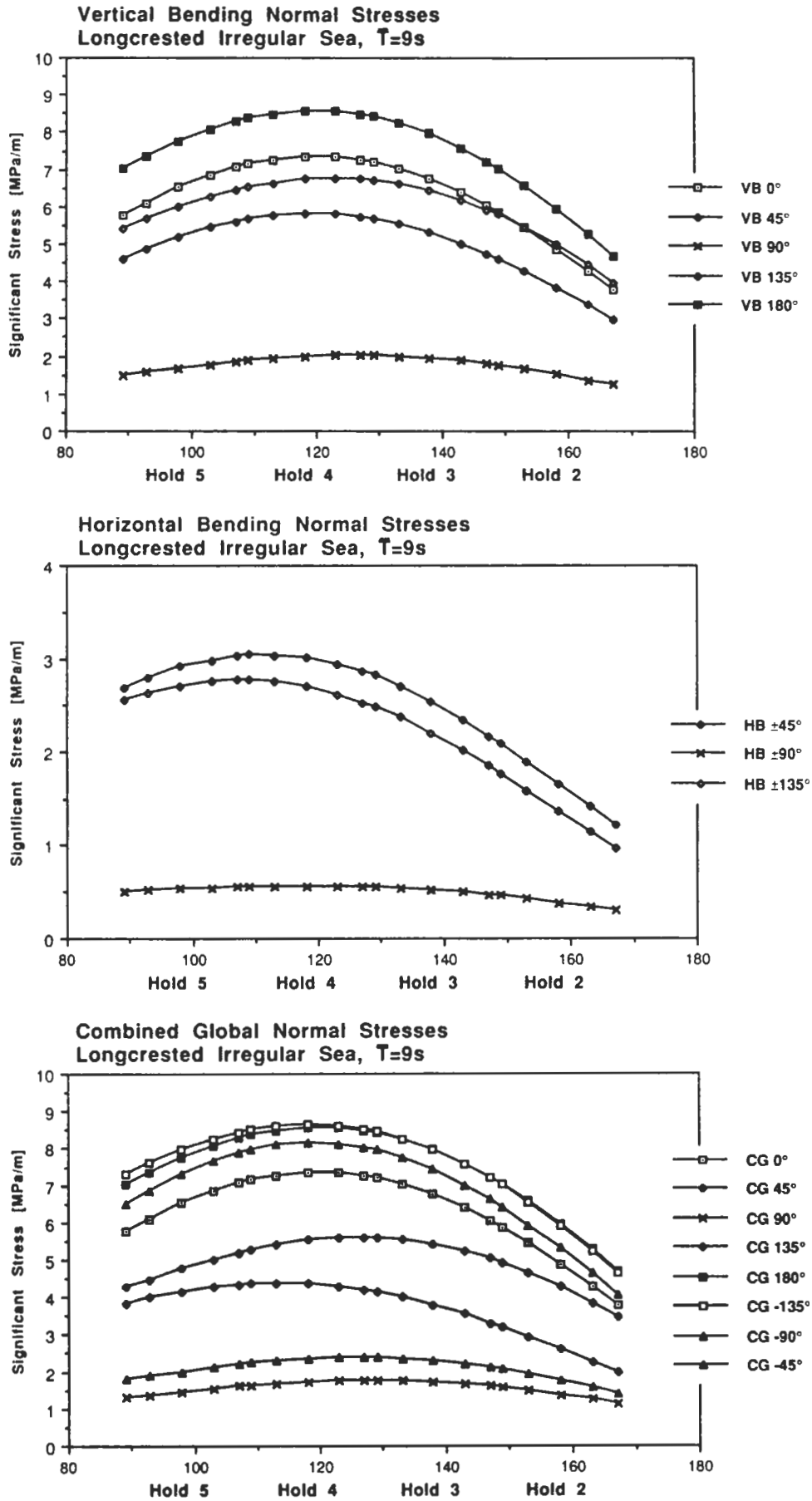

Fig.5.3 Short-term global normal stress components in bottom side girder

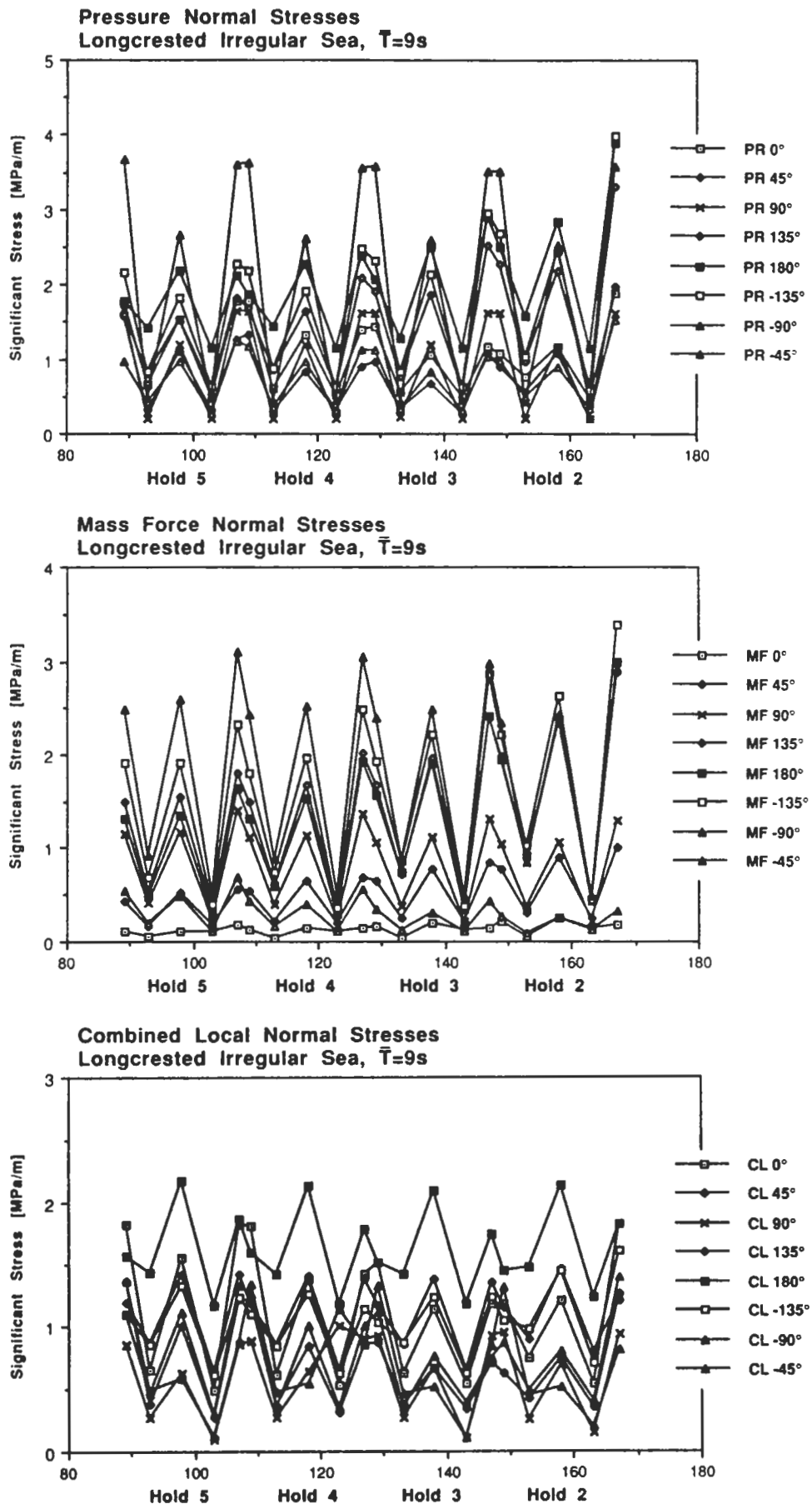

Fig.5.4 Short-term local normal stress components in bottom side girder

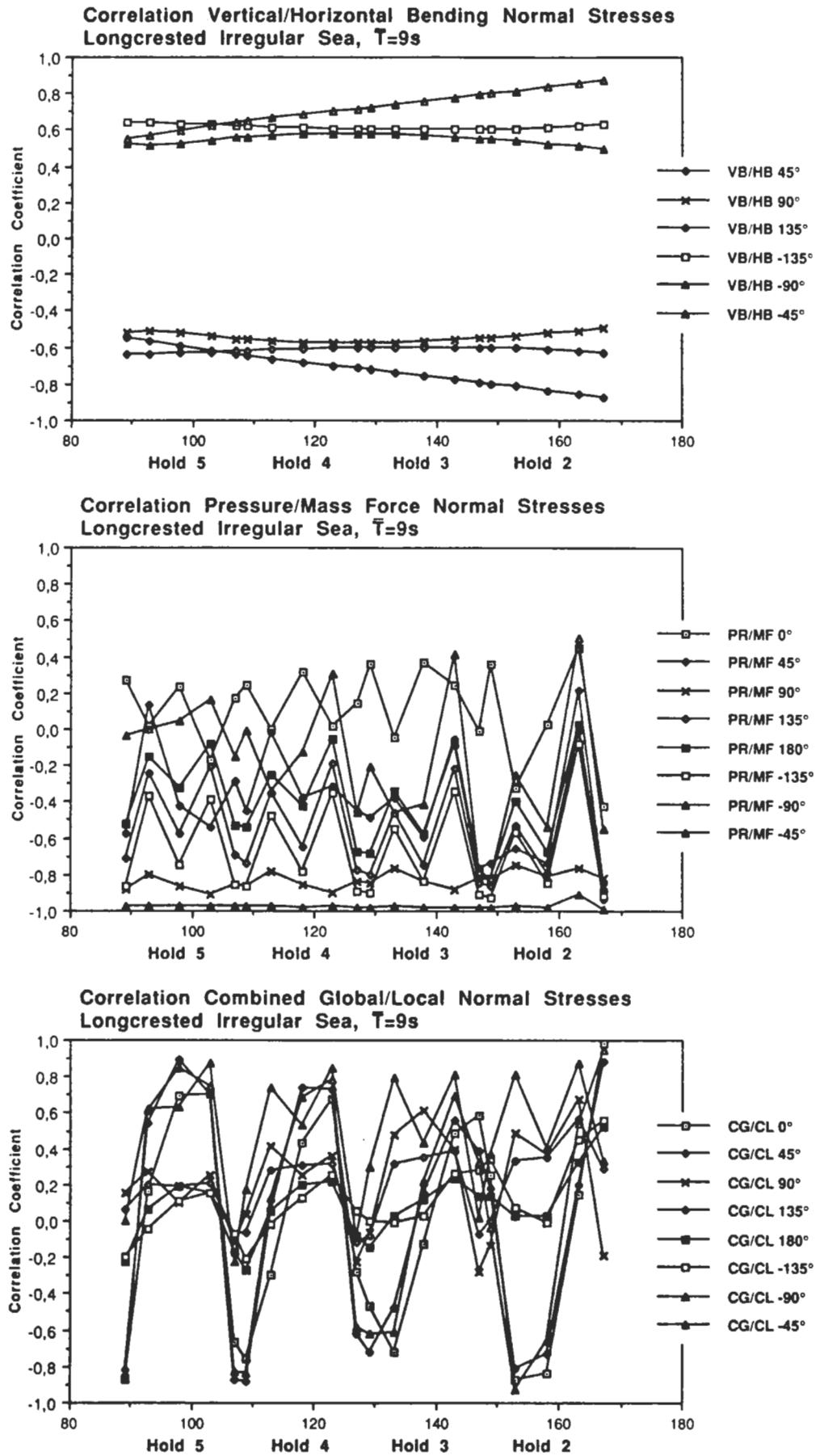

Fig.5.5 Short-term correlation between normal stress components in bottom side girder

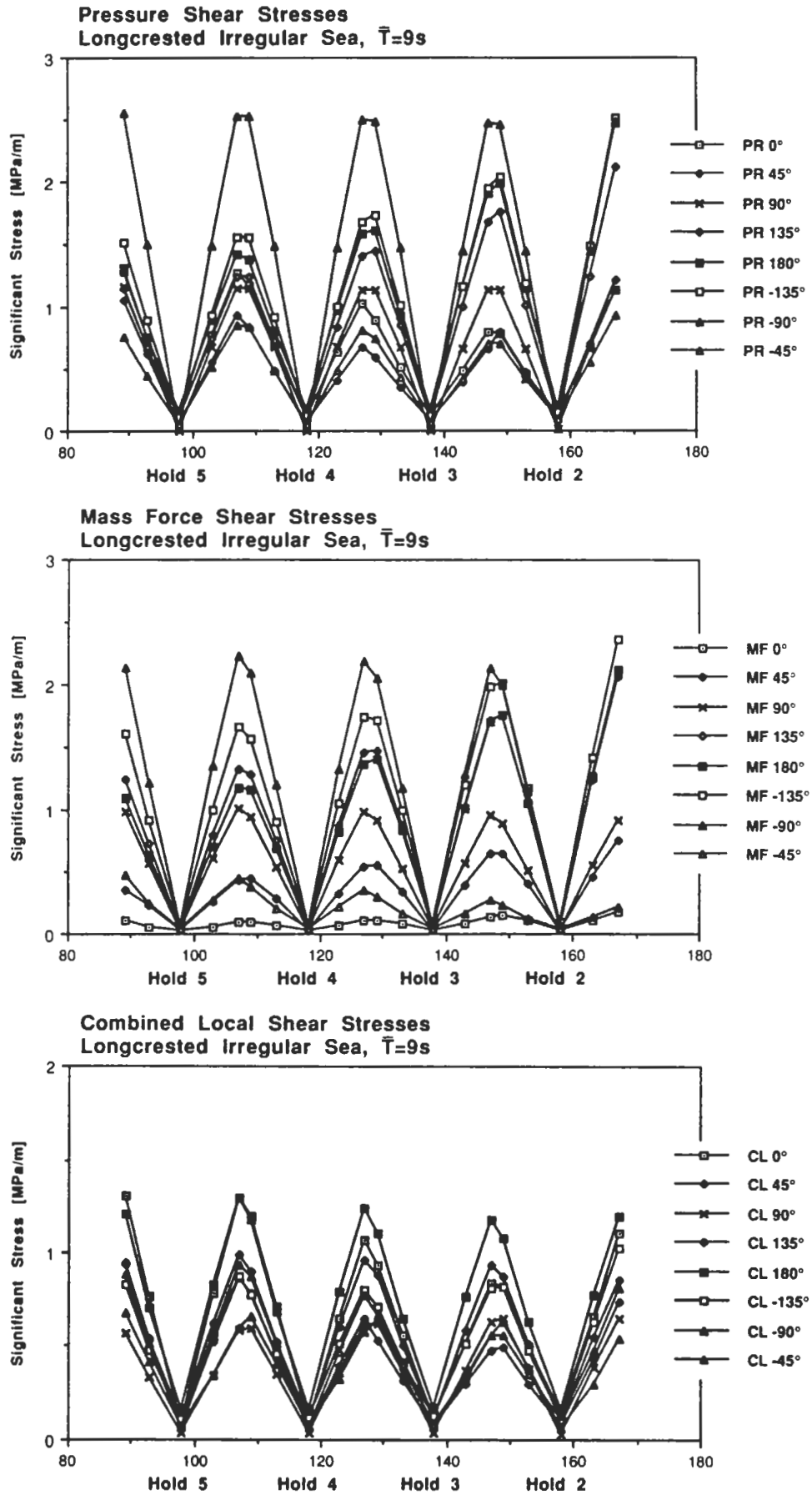

Fig.5.6 Short-term local shear stress components in bottom side girder

5.2.2 Side frame

In Appendix 2, pp.A2.18-A2.29, linear normal stress responses in irregular seas are presented for the side frame at positions L,M, and T in Hold 2. The highest stresses are found at the middle (M) and top (T) positions for headings 135°,180°,and -135°, and for mean wave periods of 8s-10s. The most important load component is the pressure which gives significantly higher stresses then the mass force component for all studied headings and positions except for 90° seas at position M. The correlation between the two components is predominantly negative at positions M and T, and positive at position L. The strongest correlation is found for all positions in -90° seas, see pp. A2.21, A2.25, and A2.29.

The influence of non-linear transfer functions on short-term irregular stress response, must be studied using extensive time simulations in irregular seas. A general picture of the relative importance of the non-linearity can in a simplified way be achieved by comparing significant stress responses obtained with transfer functions based on different wave heights. Such a comparison is presented in figs.5.7-5.8 for position M. The non-linearity is shown to be of great importance for wave headings 135°, 180°, -135°, and -90°. A linear analysis will here obviously give conservative stress levels.

The variation in stress response for the different holds is shown in figs.5.9-5.11. For forward incoming seas, the pressure induced stresses and combined stresses are increased forward in the ship. For beam seas and following seas the levels are in practical terms constant over the ship length.
For forward seas, an important part of the mass force induced stresses arise from vertical accelerations (m_Z-component), with increased levels forward in the ship. At position L the mass force stresses are small and have maxima for forward seas while at positions M and T mass force stresses are of larger importance with maxima for beam seas, constant over the four studied holds.

Fig.5.12 shows correlation between pressure and mass force components. At positions M and T for forward and portside beam seas where the maximum stress response occur, the correlation coefficients are decreasing forward in the ship with values below -0,8 in Hold 2.

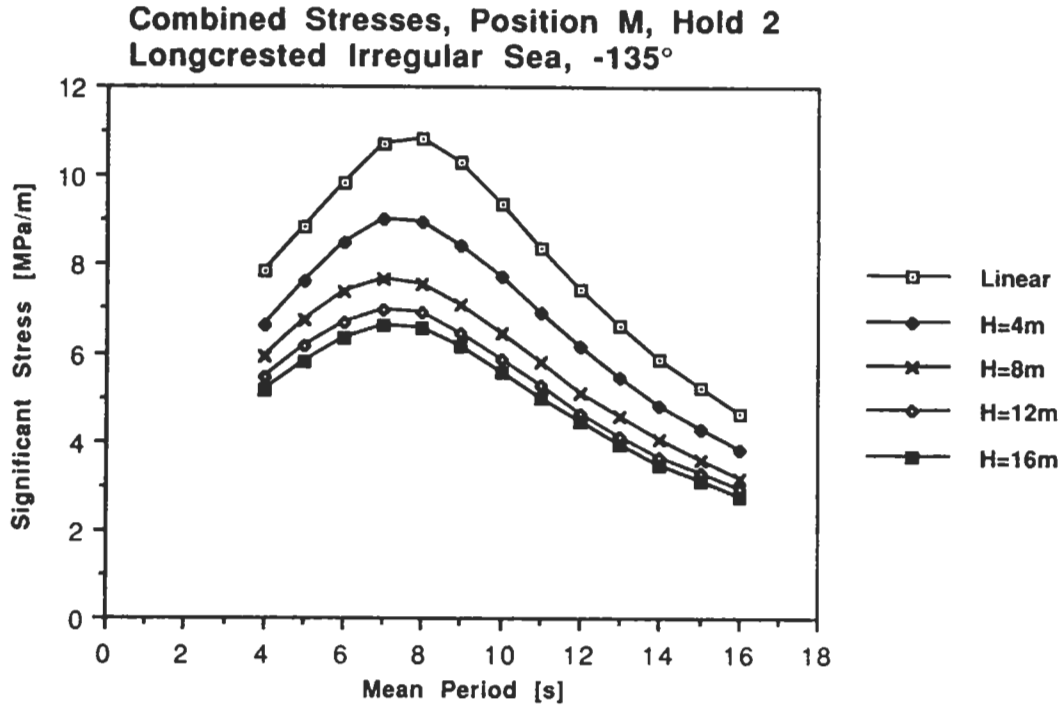

Fig.5.7 Comparison between responses in irregular seas based on non-linear transfer functions calculated for different wave amplitudes

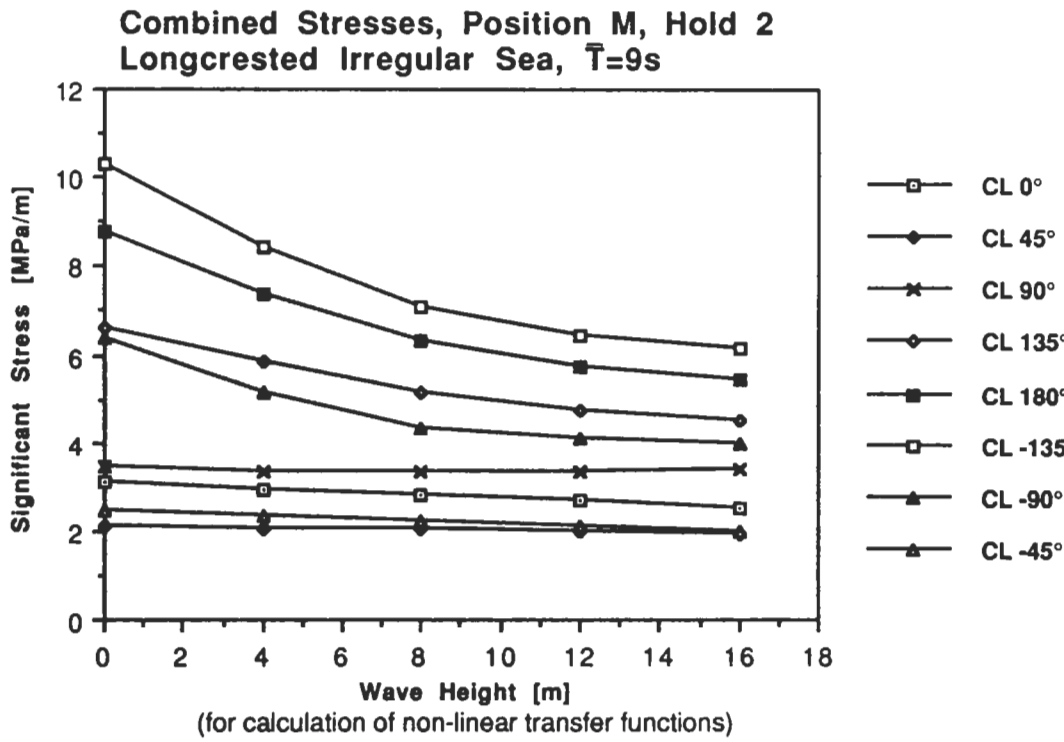

Fig.5.8 Comparison between responses in irregular seas based on non-linear transfer functions calculated for different wave amplitudes

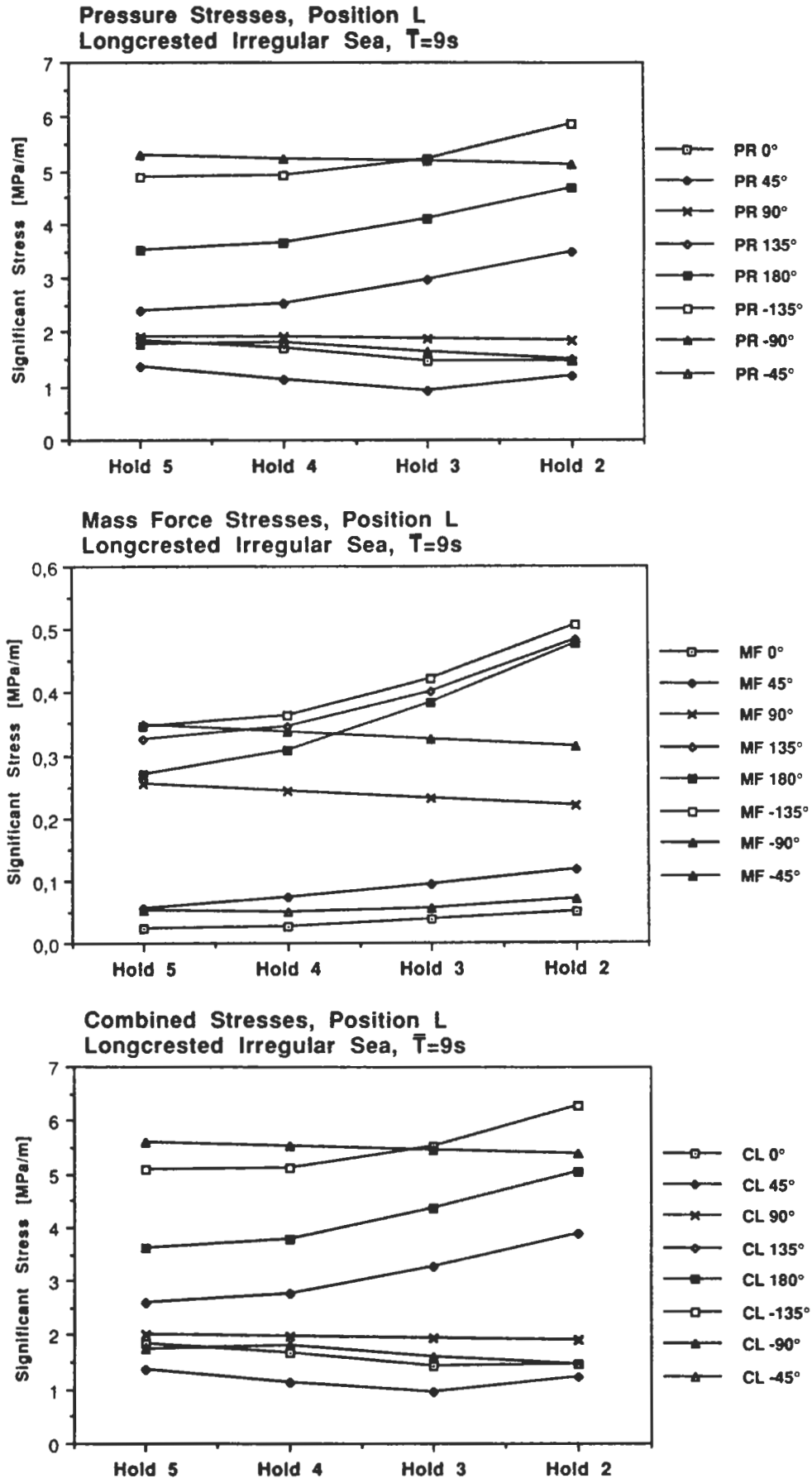

Fig.5.9 Short-term linear normal stress components in side frames, position L

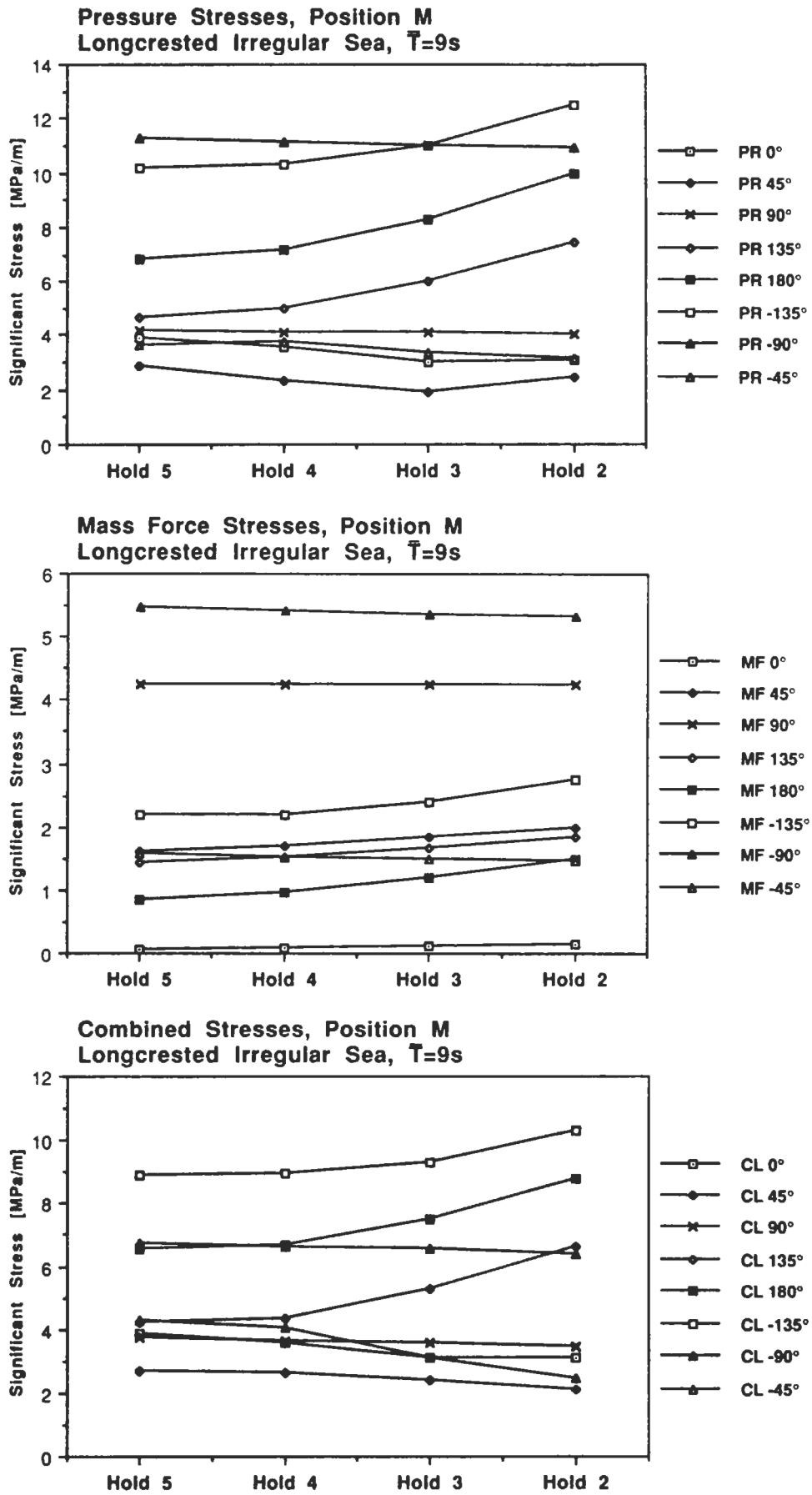

Fig.5.10 Short-term linear normal stress components in side frames, position M

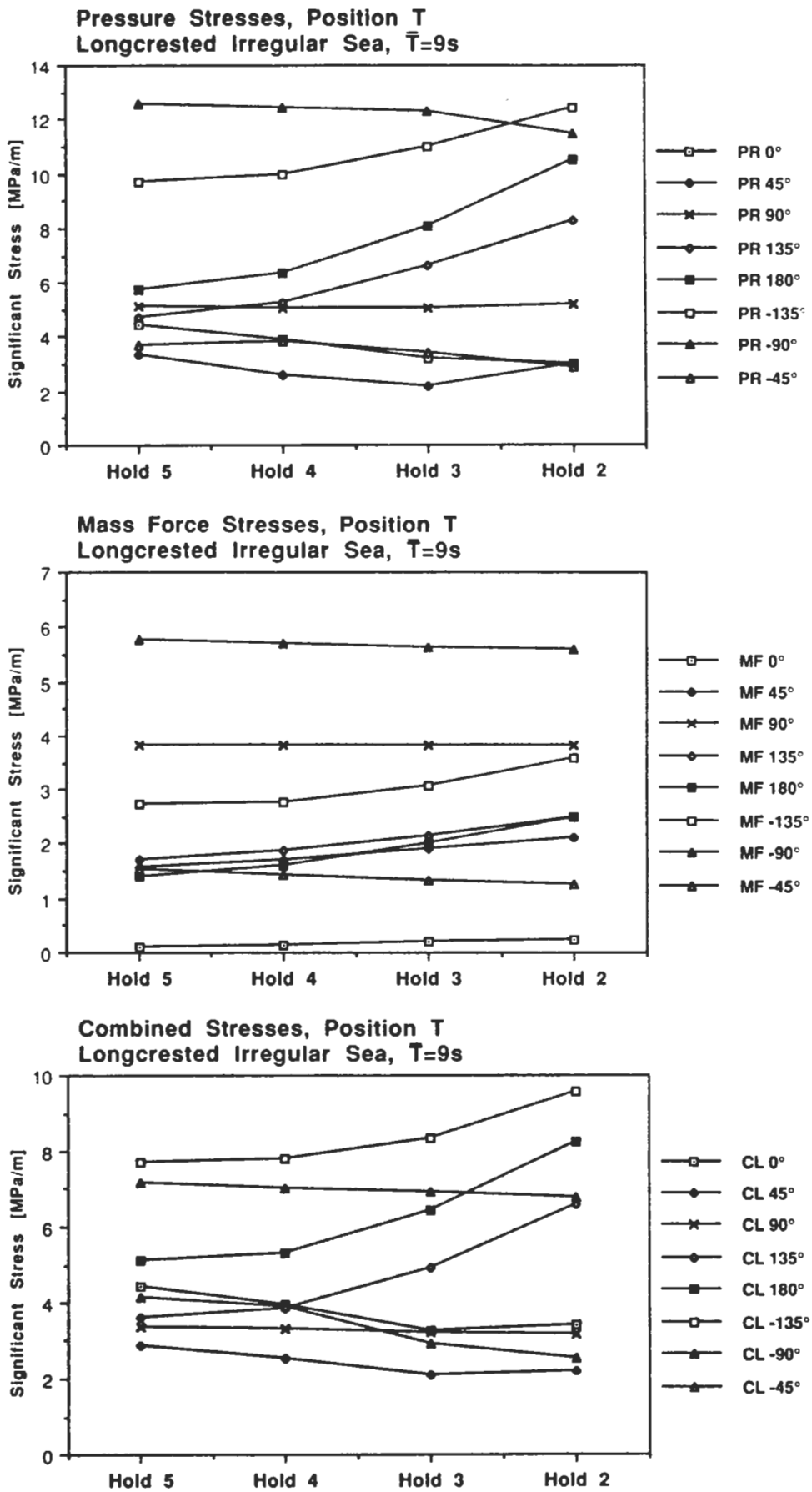

Fig.5.11 Short-term linear normal stress components in side frames, position T

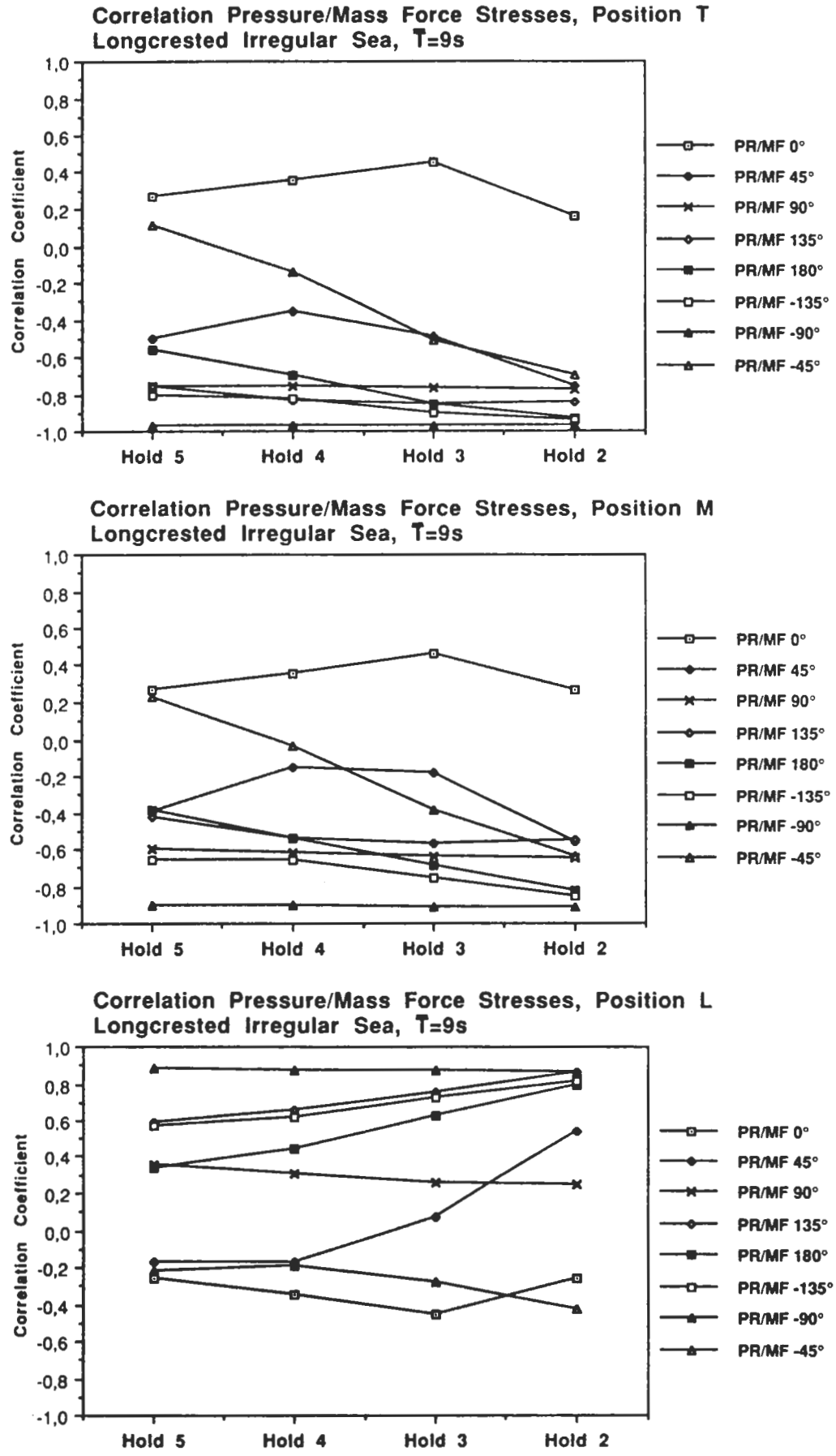

Fig.5.12 Short-term correlation between normal stress components in side frames

5.3 Long-term stresses

5.3.1 Summed long-term stress distribution from joint wave height and period statistics

Long-term stress distributions have been evaluated using statistics from "Global Wave Statistics", [8], North Atlantic Area 16 according to figs.5.13-5.14.

The summed probability of exceeding 20 different stress (double) amplitudes in the range from 2 MPa to 400 MPa have been calculated according to

$$Q_{LT}(\sigma) = \sum_i \sum_j \sum_k p(\beta_i)\, p(\bar{H}_{1/3j}, \bar{T}_k)\, Q_{ijk}(\sigma) \qquad (5.5)$$

where

$Q_{LT}(\sigma)$ = long-term probability of exceedance

$p(\beta)$ = relative probability of heading β

$p(\bar{H}_{1/3}, \bar{T})$ = long-term coupled probability of significant wave heights and mean periods from wave statistics

$Q_{ijk}(\sigma)$ = Rayleigh distributed short-term probability of exceedance

With use of regression analysis the long-term probabilities of exceedance have further been represented by a 2-parameter Weibull distribution according to eq.(5.6), from which stress ranges at certain probability levels can been determined.

$$Q_{LT}(\sigma) = e^{-(\sigma/B)^h} \qquad (5.6)$$

where B and h are parameters of the long-term distribution

Fig 5.15 shows an example of calculated actual probabilities together with correlated Weibull approximations. All the long-term stress distributions show the same typical reversed "S"-form with significantly lower stress levels than the Weibull distribution for probabilities less then 10^{-8}. This might be a true effect but might also be explained by insufficient wave data for the extreme conditions. With regression analysis performed for values in the interval $10^{-10} < Q < 10^{-2}$, the approximate Weibull distribution is in reasonable agreement with direct calculated values for all probabilities above 10^{-8}. The approximation of calculated probabilities of exceedance with a simple long-term distribution is further discussed in Chapter 6.

For a large number of stress cycles n, the most probable largest stress range will have the long-term probability of exceedance $Q = 1/n$. This is the peak value of the extreme distribution and will on the average be exceeded in 63% of a large number of samples, each including n cycles. Maximum values for design of ships are usually evaluated from the long-term distribution at $Q = 10^{-8}$. This corresponds to the most probable maximum stress among $n = 10^8$ stress cycles which is the approximate number of low frequency cycles during 20 years of ocean service.

Fig.5.16 shows the most probable maximum long-term normal stresses in the bottom side girder. The relative longitudinal distribution of long-term maxima follows very close to the envelope of the short-term responses for different heading angles shown in figs.5.2-5.4.

The long-term correlation between the different components is shown in fig.5.17, represented by an equivalent "long-term correlation coefficient" similar to eq.(5.4) but evaluated at the long-term probability $Q = 10^{-8}$.

$$\rho_{AB_Q} = ((\sigma_A + \sigma_B)_Q^2 - \sigma_{A_Q}^2 - \sigma_{B_Q}^2) / (2\,\sigma_{A_Q}\,\sigma_{B_Q}) \qquad (5.7)$$

For comparison, long-term stresses have also been examined in Hold 4 for a full load bulk cargo condition shown in fig.5.18. Hold 4 is in this load condition empty with the surrounding Hold 5 and Hold 3 full, so the boundary conditions used in the structural model is still valid here. Figs.5.19-5.20 show long-term maximum stress components and long-term correlation coefficients for the bulk cargo condition. The major difference in comparison with the homogeneous oil cargo condition is the very strong correlation between local pressure and mass force induced stresses, resulting in high local combined stresses in the centre of the hold. However, the correlation between local and global stresses is for the bulk cargo condition low and the total combined stresses are less than for the oil cargo condition. Long-term correlation coefficient for pressure-mass force components shown in fig.5.30, is slightly above the theoretical maximum 1,0 at the centre of the hold, which is an indication of inaccuracy in the Weibull representation.

Long-term stresses in the side frames are shown in fig.5.21. The pressure induced stresses at positions M and T are significantly higher than the combined stresses including internal mass forces from cargo. The long-term correlation coefficients for pressure-mass force components are shown in fig.5.22.
For the bulk cargo condition only pressure induced stresses are present in the side frames in Hold 4. The levels are approximately the same as for the oil cargo condition.

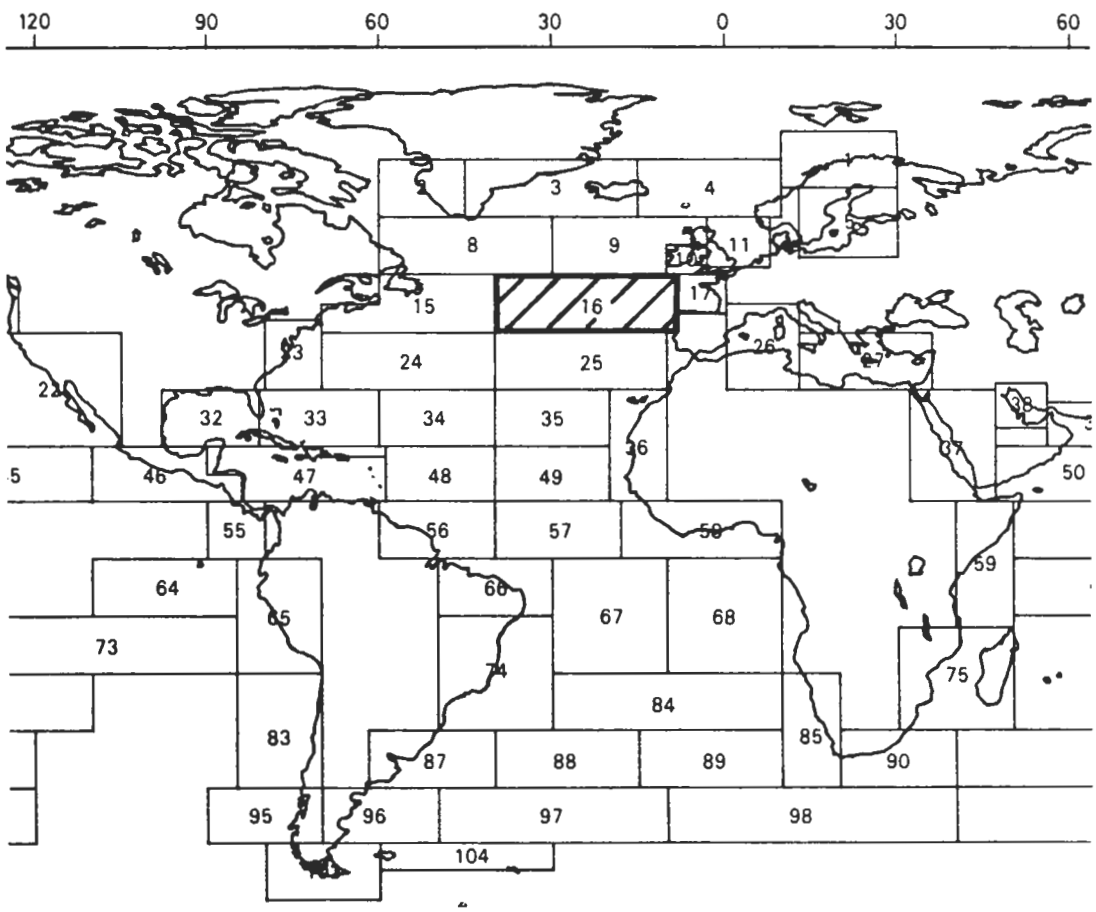

Fig.5.13 Geographic area for long-term wave statistics, from [8]

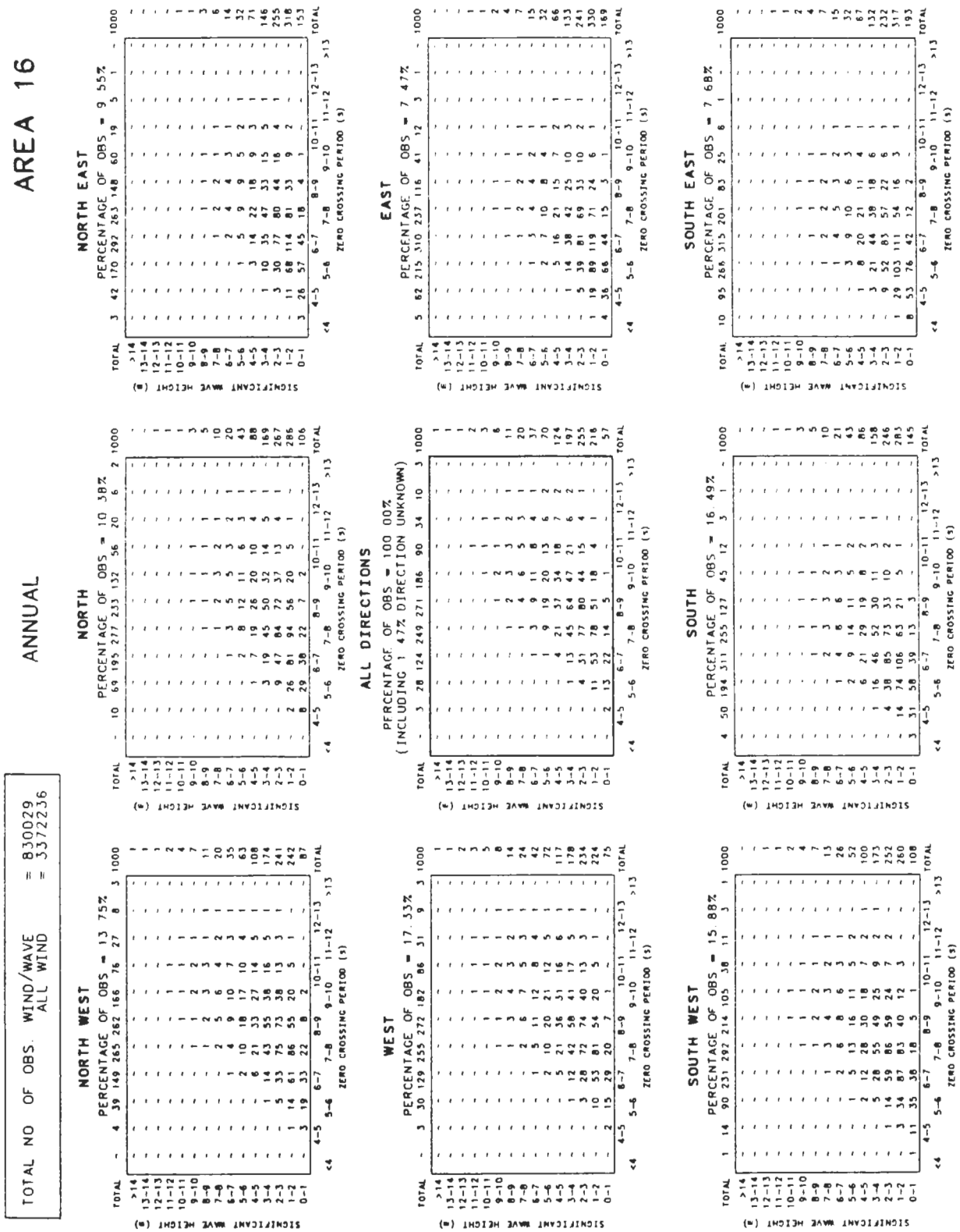

Fig.5.14 Long-term wave statistics for Area 16, from [8]

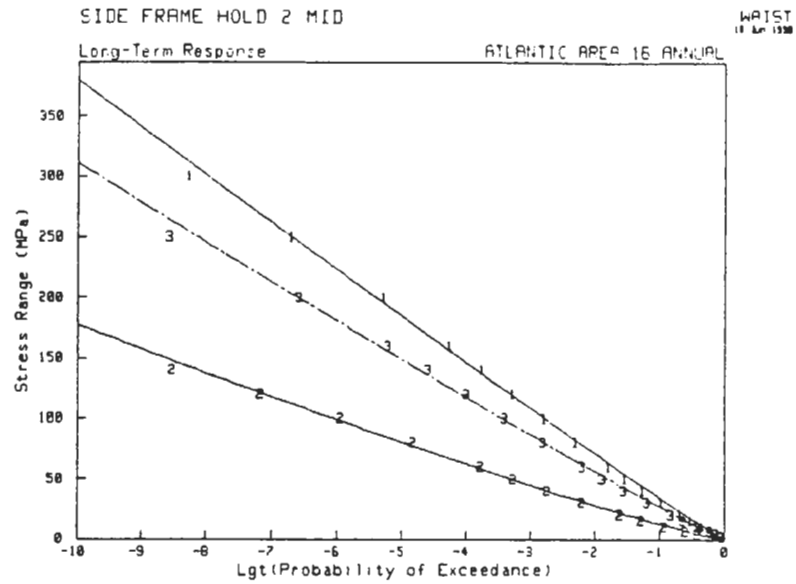

Fig.5.15 Long-term stress distributions. Side frame, position M Hold 2. Centre of numbers indicate calculated values, lines indicate Weibull distributions. Pressure (1), Mass Force (2) and Combined (3), stresses

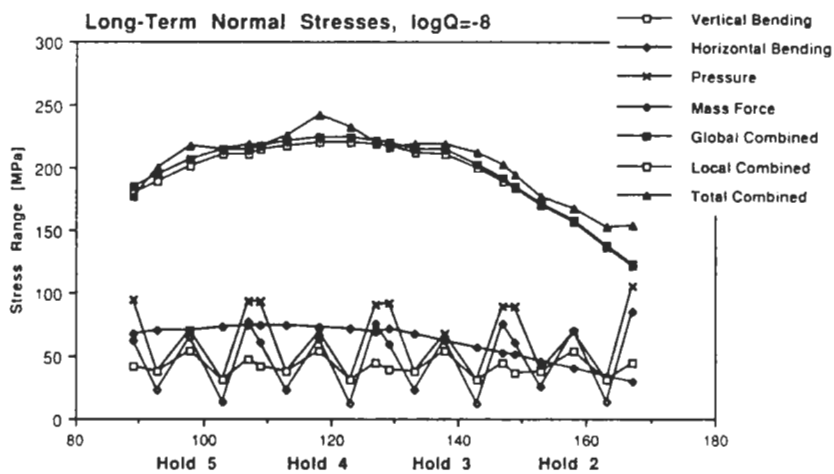

Fig.5.16 Distribution of most probable maximum long-term normal stresses in the bottom side girder. Homogeneous oil cargo condition.

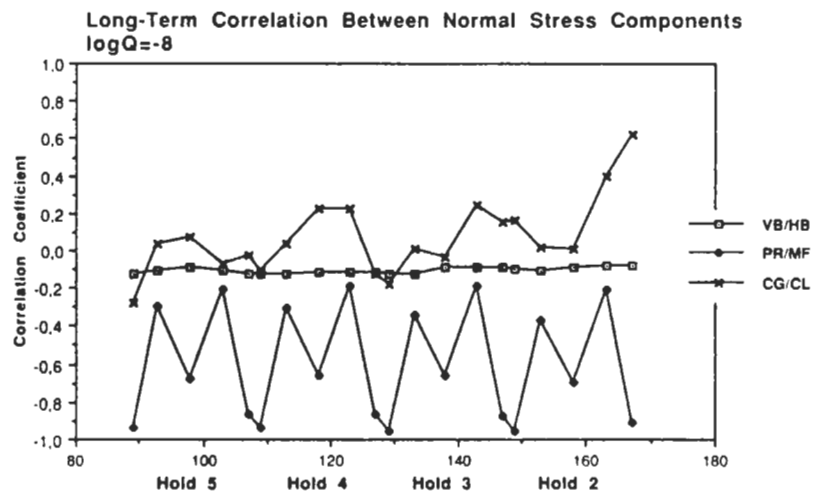

Fig.5.17 Long-term correlation coefficients for normal stress components in the bottom side girder. Homogeneous oil cargo condition.

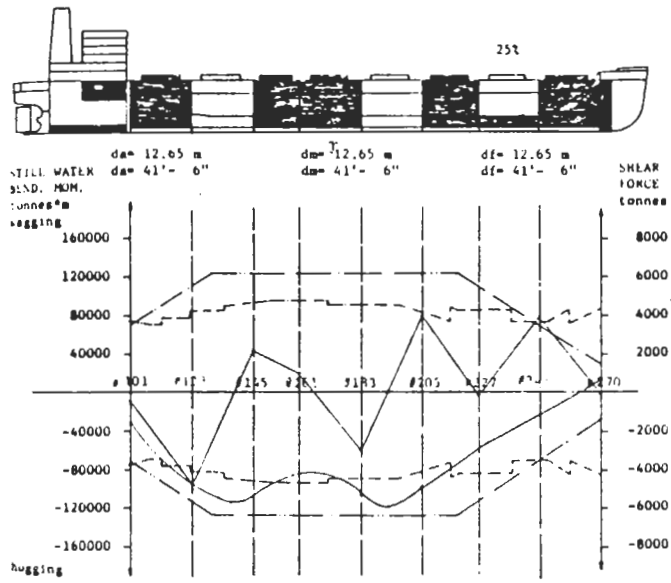

Fig.5.18 Full load bulk cargo departure condition.

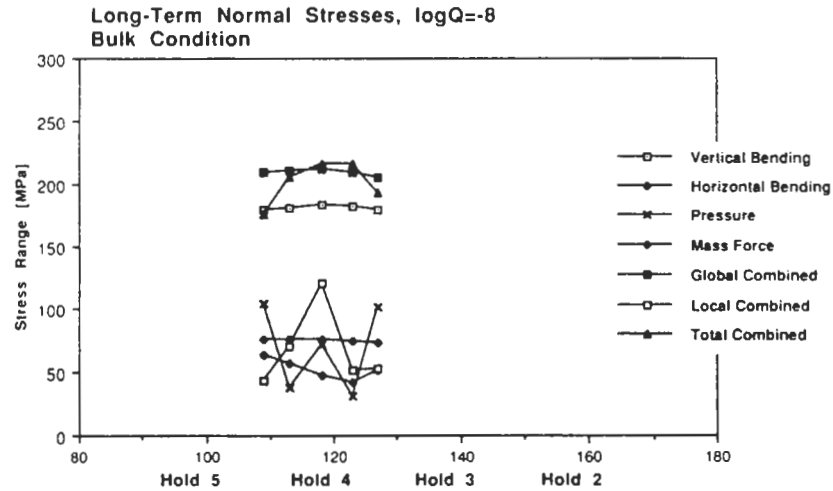

Fig.5.19 Distribution of most probable maximum long-term normal stresses in the bottom side girder, Hold 4. Bulk cargo condition.

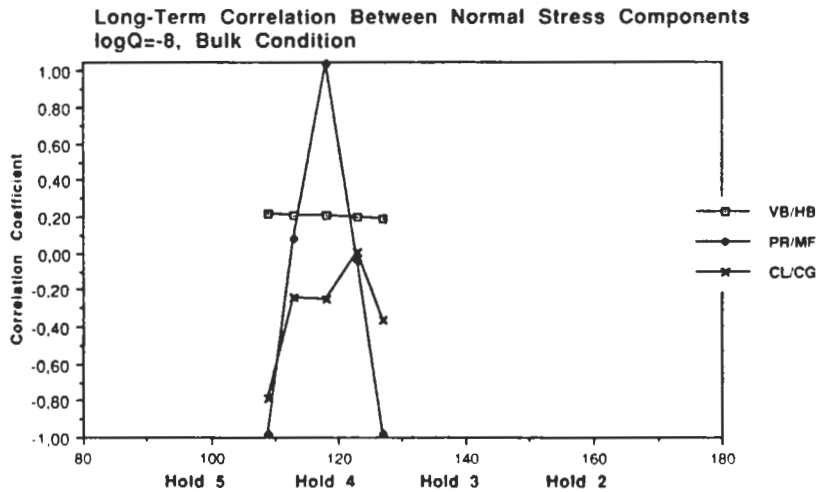

Fig.5.20 Long-term correlation coefficients for normal stress components in the bottom side girder, Hold 4. Bulk cargo condition.

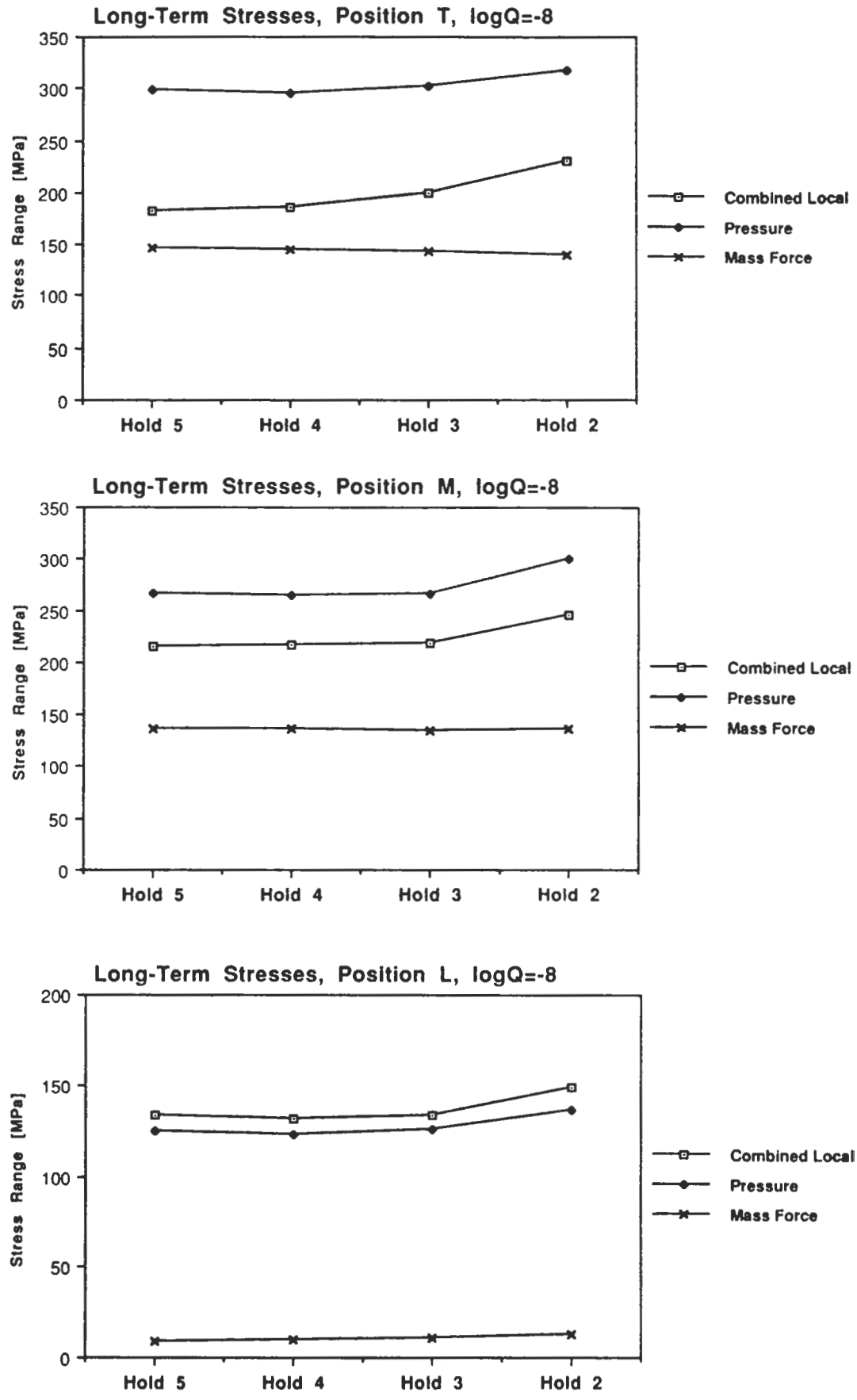

Fig.5.21 Most probable maximum linear long-term normal stresses in side frames.

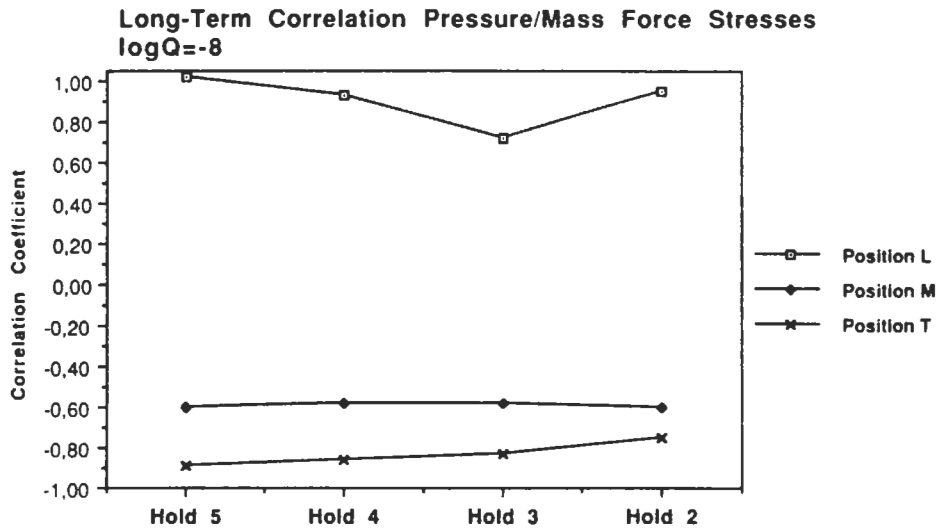

Fig.5.34 Long-term correlation coefficients for normal stress components in side frames

5.3.2 Extreme short-term sea condition, influence of speed reduction

The long-term stress distributions calculated from the scatter diagram, fig.5.24, are based on assumptions of constant load condition and speed over the entire life time of the ship. In severe seas however, the speed cannot possibly be kept at 15 kn. It will be reduced by increased resistance and by voluntary speed reductions made for the safety of ship and cargo. Therefore the maximum long-term stresses for constant condition must be adjusted in accordance to the actual conditions in extreme sea states.

The worst sea state indicated in the N Atlantic wave statistics has a significant wave height of over 14 m with a mean wave period of 10-11 s. This condition will occur in a total average corresponding to one week during 20 years. For comparison is here used an extreme sea state with 15 m significant wave height and a mean wave period of 11 s. As shown in the previous figures in this chapter, the worst stress responses will be found for head (180°) or portside bow (-135°) incoming seas, at the centre of Hold 4 for the bottom side girder, and at position M for the side frame in Hold 2.

The most probable maximum response among n in an irregular short-term sea state is calculated from the significant response according to eq.(5.8), based on the assumption of narrow banded response spectrum with Rayleigh distributed linear response amplitudes.

$$\sigma_{1/n} = \sqrt{R_\sigma \ln(n)} = \frac{\bar{\sigma}_{1/3}}{1{,}416}\sqrt{\ln(n)} \qquad (5.8)$$

Table 5.2 shows the equivalent time duration in the short-term sea state that will give the same maximum stress levels as those calculated from the long-term distributions. The response mean period is here assumed to be equal to the encountering mean wave period.

	Bottom Side Girder, Pos.C, Hold 4		Side Frame, Pos.M, Hold 2	
	180°	-135°	180°	-135°
15 kn long-term combined stress range:	242,4		245,5	
15 kn significant short-term stress range (H_s=15 m, $\bar{T}$=11 s):	135,4	118,2	113,4	125,8
Average number of stress cycles to obtain long-term maximum:	620	4590	12060	2072
Equivalent time duration $\bar{T}$ = 7,6 s - 8,3 s (15 kn):	1,3 h	10,6 h	25,5 h	4,8 h

Table 5.2

Figs.5.23-5.24 show the influence of speed reduction on different stress responses at the extreme short-term sea state. Most probable maximum stress ranges are evaluated for a time duration of 4 hours. The figures includes both the effect of reduced response due to speed reduction and the effect of reduced number of stress cycles due to changed mean response period. The stress reduction due to changed mean period is however less then 2,5% of the total stress level. Combined stresses in bottom side girder is reduced about 20%, and in the side frame, 60% for 180°, and 40% for -135° seas, when the speed is reduced from 15 kn to 0 kn. At zero speed the largest stress response in the side frame occurs for -90° seas.

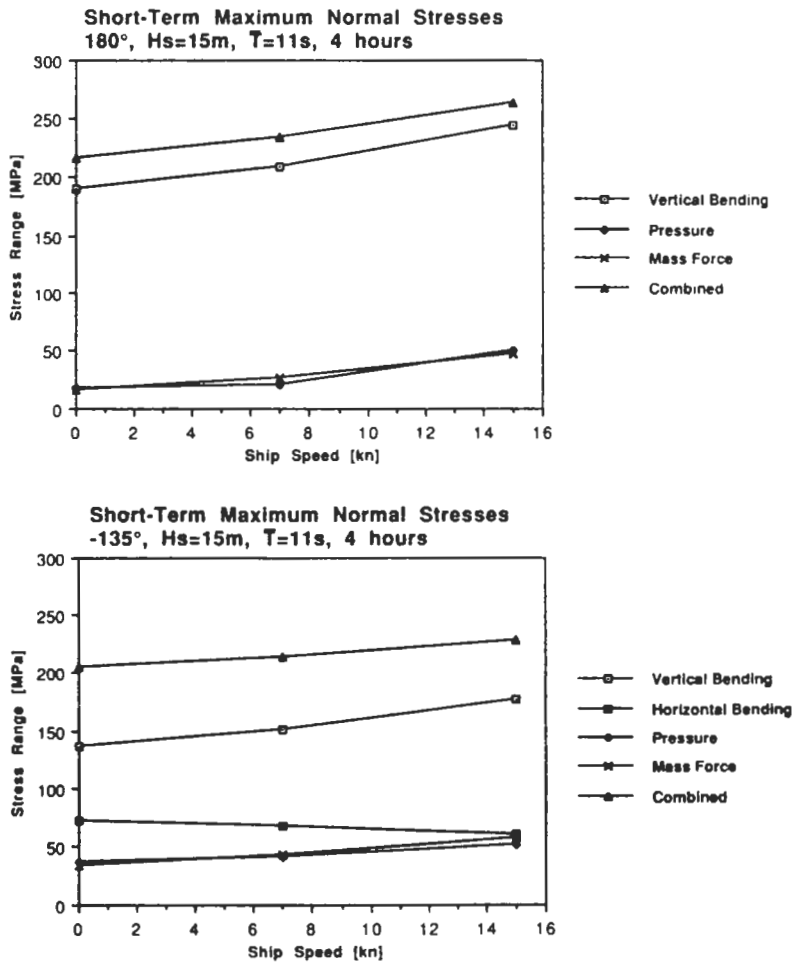

Fig.5.23 Most probable maximum linear stress response as function of ship speed. Bottom side girder, position C Hold 4.

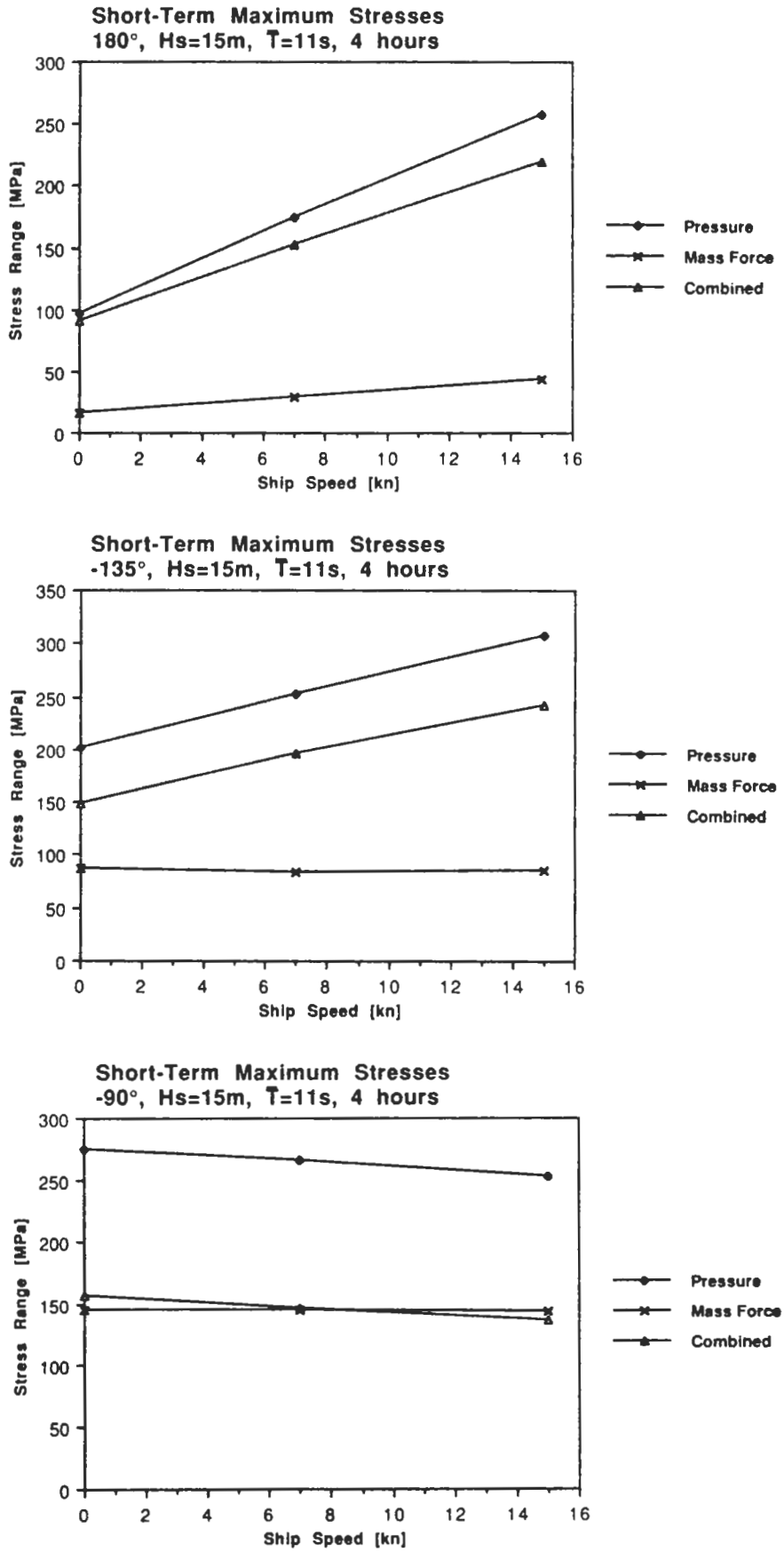

Fig.5.24 Most probable maximum linear stress response as function of ship speed. Side frame, position M Hold 2

5.3.3 Extreme regular waves, influence of speed reduction and non-linearity

The non-linear stress response in the side frames due to the non-linear pressure variation around the still water line is shown to be significantly less then the linear response even for moderate wave amplitudes. Linear long-term stress distributions as well as linear extreme short-term responses are therefore likely to overestimate the actual maximum stresses in the frame. In extreme waves however, none of the linear strip theory assumptions are valid. Breaking waves on deck as well as non-linear hydrostatic and hydrodynamic coefficients may have a significant influence on the stress response. It is far beyond the scope of this report to discuss all the problems that are involved in a complete non-linear analysis in extreme waves. Yet, to get a picture of the magnitude of the stress non-linearity studied here, calculations have been performed for a 28 m wave, corresponding to the most probable extreme single wave height in the short-term sea condition above. It must be emphasized that the ship motions relative to the wave in this approach still are assumed to be linear with respect to the wave height.

As an example, fig.5.25 show results from time simulations of stress responses at zero speed for regular harmonic waves with a period of 14,0 s (ω=0,45 rad/s, λ=305 m) and wave headings 180°, -135°, and -90°. The figure clearly shows that the maximum stress peak hardly is affected by the non-linearity while the stress range (peak-to-trough) is significantly reduced. Especially for the -90° heading the pressure induced stresses are cut off during nearly half the wave period when the ship side is raised above the wave surface.
The figure also shows the important each other counteracting effect of mass force and pressure components. The combined non-linear stress for headings -135° and -90° have two marked positive peaks during one wave period, one following the combined linear stress during half the wave period, and one following the mass force component during the other half period. Since the mass force induced stress component is larger then the combined stress, the maximum non-linear stress is larger than the maximum linear stress for this example.

Fig.5.26 shows comparisons between linear stress ranges at 15 kn and 0 kn and non-linear peak-to trough amplitudes at 0 kn for different wave periods. Reduced speed is shown to have much larger influence on the stress range than non-linearity for headings 180° and -135°.

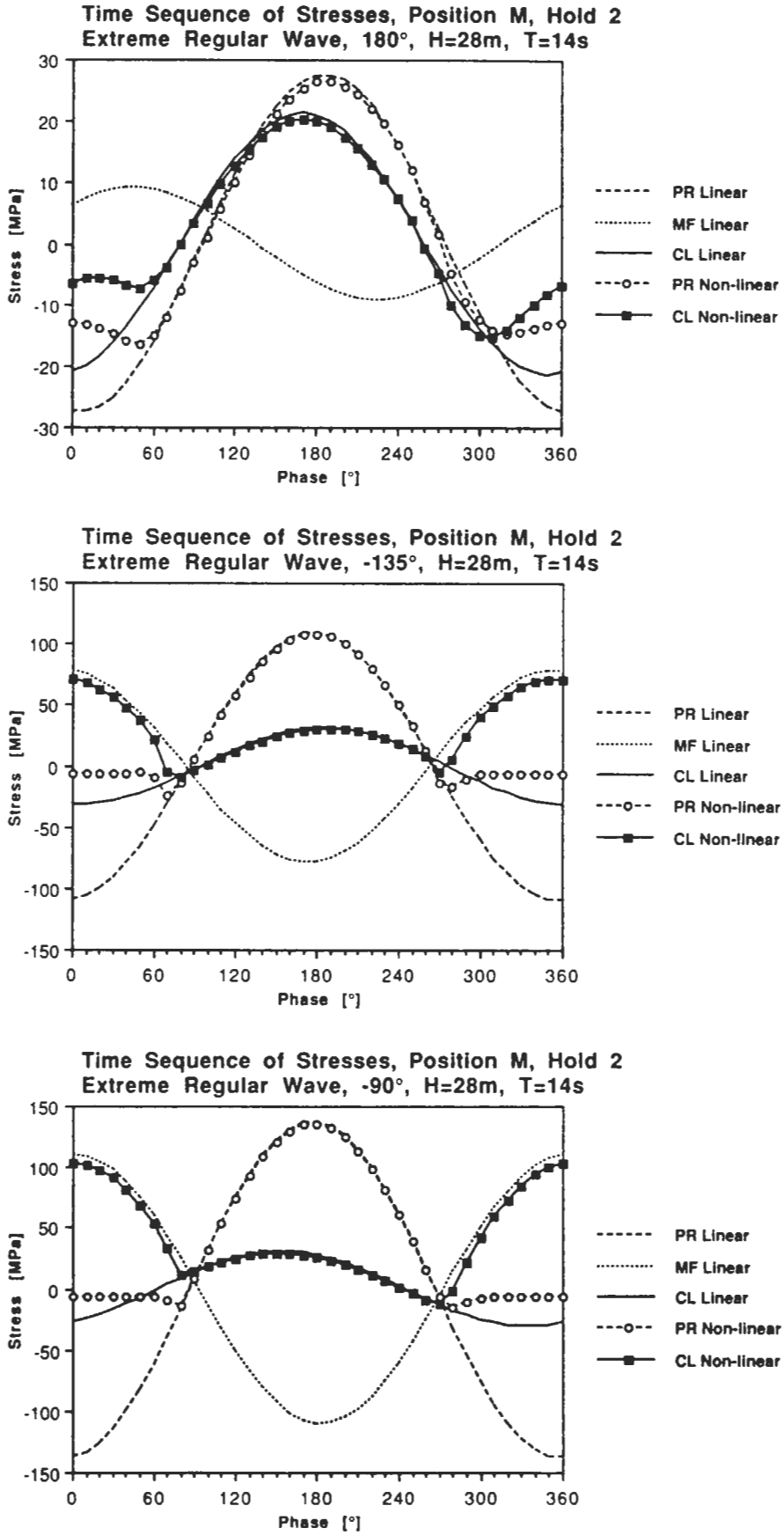

Fig.5.25 Linear and non-linear stress variation in the side frame during one period of an extreme regular wave.

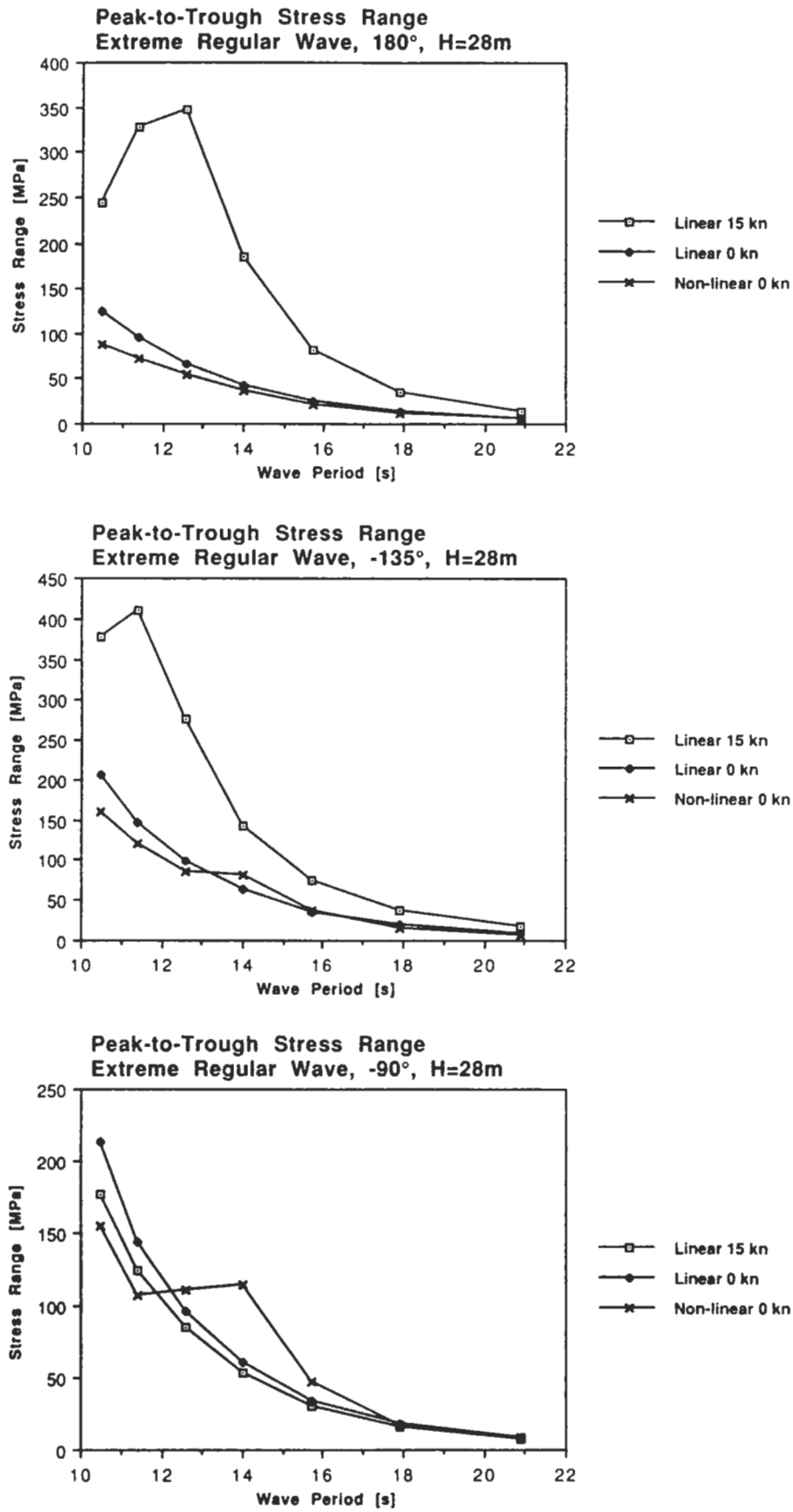

Fig.5.26 Comparison between linear and non-linear stress amplitudes for extreme regular waves with different periods. Side frame, position M Hold 2.

6 FATIGUE ANALYSIS

6.1 General analysis based on long-term stress distributions

The calculation method for long-term combined stress distributions from wave loads can be used both for estimating maximum stresses during the ship's life time for ultimate strength analysis, and for fatigue life estimate. For design purposes fatigue life is normally determined by the general Miner-Palmgren hypothesis for cumulative damage.

$$D = \sum_{i=1}^{k} \frac{n_i}{N_i} \tag{6.1}$$

where

D = cumulative damage ratio

k = number of stress range levels σ_i

n_i = number of stress cycles at level σ_i

N_i = number of cycles to failure at constant stress range σ_i

The cumulative damage approach can be used in different ways dependent on which fatigue test data to be used and which stress to be applied.

If the actual maximum material stress could be obtained, fatigue life could in theory be calculated from the direct relation between actual stress ranges and stress ranges to failure for fatigue tested material specimens having no inherent imperfections. The obvious difficulty is here to calculate the actual material stress for complicated structures with weld joints and imperfections from production.

The opposite approach is based on fatigue tests with real structural details from production, and the reference stress ranges are here nominal tensile-, shear- or bending stresses. An extensive description of this procedure including test results is given by Munse et al in [9]. The major disadvantage is here the large amount of fatigue tests necessary to enclose all details of interest. This approach might also act conservative in the sense that it is difficult to use for new improved detail designs.

Between the two approaches above, is for marine structures mostly used the weld joint class approach. It is based on fatigue tests with simple weld joints statistically analysed and grouped in a number of different classes. The relevant class for a detail is chosen based on the geometrical arrangement, the direction of the stresses and the method of fabrication and inspection of the detail. The reference stress for fatigue life estimate is here the "hot-spot" stress at the weld, including all geometrical stress concentrations from the structure, but excluding the influence from weld geometry. The most extensive analyses of fatigue tests of weld joints have been presented by the British Welding Institute, [10]. It forms the basis for recommendations and rules for fatigue design of offshore structures such as those from UK Department of Energy, [11], and Det norske Veritas, [12].

Fatigue lifes for the joint classes under constant amplitude loading are represented by a group of SN-curves based on linear relationships between $\log \sigma$ and $\log N$.

$$\log N = \log a - m \log \sigma \tag{6.2}$$

For design of offshore structures, the design curves are defined as the mean minus two standard deviations of $\log N$, corresponding to 2,3% probability of failure.

$$\log N = \log a - 2 \log s - m \log \sigma = \log \bar{a} - m \log \sigma \tag{6.3}$$

For a ship that is regularly inspected, and that might avoid the worst sea states, design curves for offshore structures is probably too conservative and would result in significantly increased scantlings in comparison with todays design rules which are not explicitly fatigue based, but are based on service experience from thousands of ship years at sea.

For weld joints exposed to sea water but cathodicly protected, a fatigue cut-off stress level (fatigue limit) S_Q at $N = 2 \cdot 10^8$ is introduced, below which no fatigue damage is assumed to occur. Basic data for SN-curves are presented in table 6.1 and fig.6.1 below. For a long-term Weibull distribution of stresses, the major part of the cumulative damage occurs for stresses within the probability interval $10^{-4}<Q<10^{-0,5}$ as shown in fig.6.2. Fig.6.3 shows a comparison of damage ratios calculated with and without cut-off level. The introduction of a cut-off level S_Q has little influence on the total damage for $D \geq 1$.

Class	Log a	Logs	Log ā	m	S_o (MPa)
B	15.3697	0.1821	15.01	4.0	48
C	14.0342	0.2041	13.63	3.5	33
D	12.6007	0.2095	12.18	3.0	20
E	12.5169	0.2509	12.02	3.0	18
F	12.2370	0.2183	11.80	3.0	15
F2	12.0900	0.2279	11.63	3.0	13
G	11.7525	0.1793	11.39	3.0	11
W	11.5662	0.1846	11.20	3.0	10
T	12.6606	0.2484	12.16	3.0	19

Table 6.1 Details of basic SN-curves - Sea water and cathodic protection, [12]

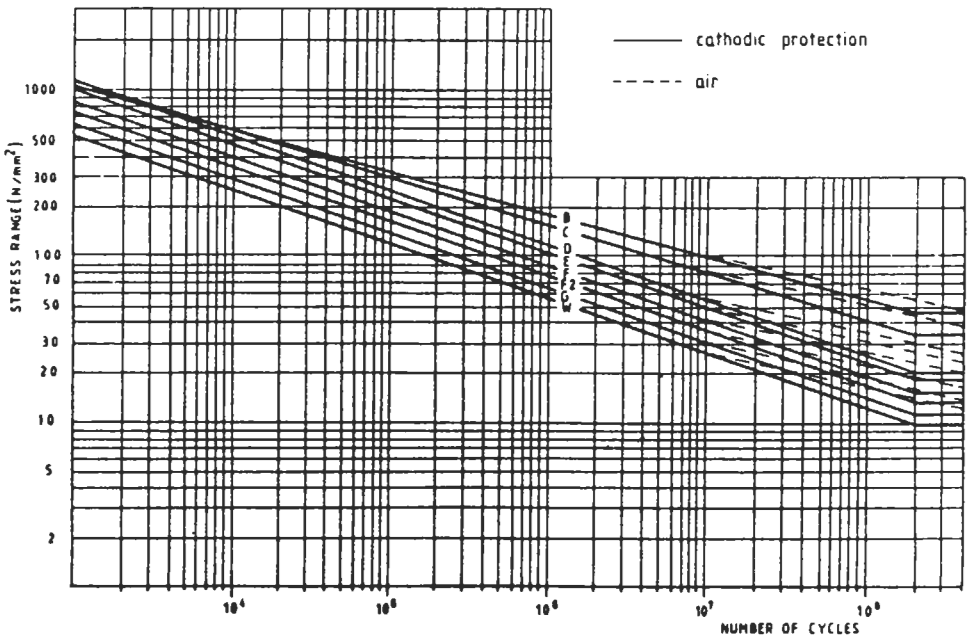

Fig.6.1 SN design curves based on mean minus two standard deviations, [12]

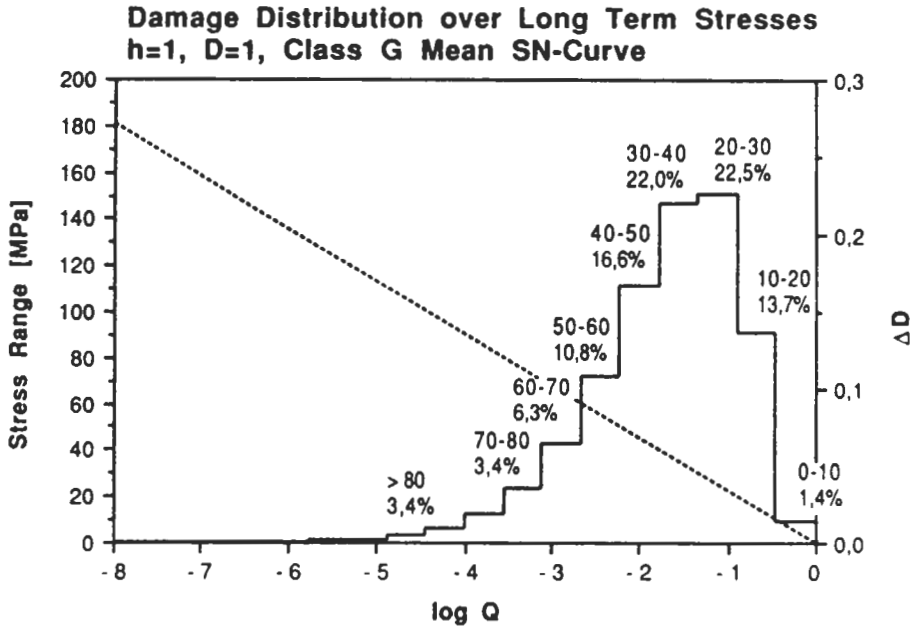

Fig.6.2 Example of distribution of cumulative damage ratio for Weibull distributed long-term stresses, $n=10^8$

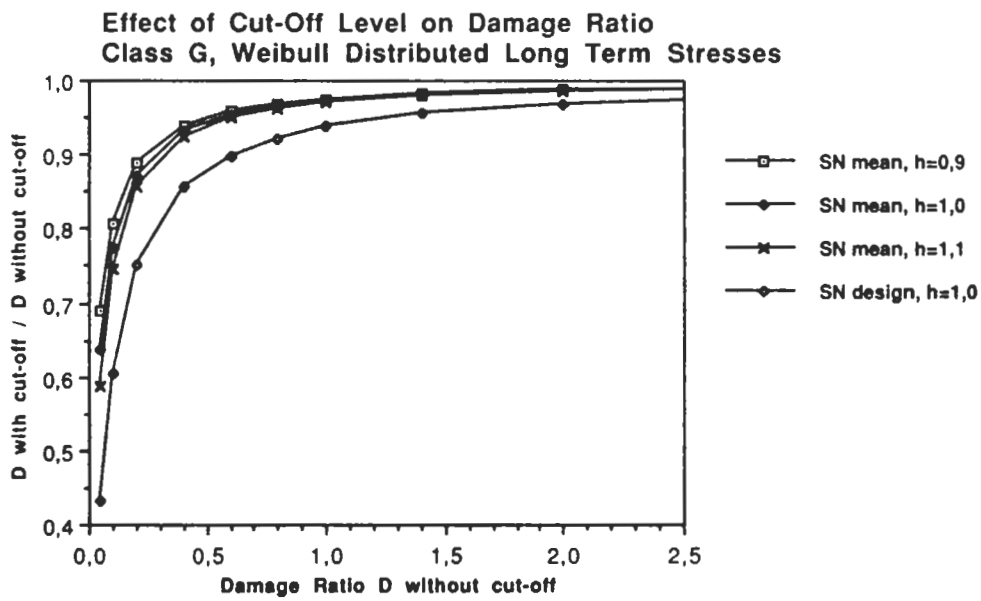

Fig.6.3 Comparison between damage ratios calculated with and without cut-off level. Weld joint class G, Weibull parameter $h=1,0$

If the cut-off level is neglected and the random long-term probability of stress ranges is represented by a continuous Weibull distribution according to eq.(5.6), then the cumulative damage can be calculated analytically

$$D = \frac{n}{a} B^m \Gamma\left(1+\frac{m}{h}\right) \tag{6.4}$$

where

n = total number of stress cycles

B,h = parameters of the long-term stress distribution

$\Gamma\left(1+\frac{m}{h}\right)$ is the complete gamma function

$$= \int_0^\infty e^{-t} t^{\left(\frac{m}{h}\right)} dt$$

for the $\frac{m}{h}$ of interest, it can be approximated as

$$\approx 10^{\left(0{,}2934\left(\frac{m}{h}-1\right)^{1{,}4107}\right)}$$

Eq.(6.4) illustrates the importance of the shape parameter *h* in the long-term stress distribution. The parameter *h* depends on both the long-term wave statistics and on the shape of the stress response functions in irregular seas. It is usually suggested to be estimated from full scale measurements of vertical bending moments on ships, such as [13] and [14]. However, records of ship damages reveal a large number of fatigue cracks also in transverse members subjected to local loads, see e.g [15], [16], [17]. The stress distribution in these members are governed by the local structural arrangement, and cannot be generalized in the same way as calculations and measurements of hull girder bending moments. The major advantage of the calculation procedure presented in this study is that it is able to calculate the long-term stress distribution directly, with respect both to the local structural design and to all wave load components of importance.

As mentioned on p.29, the actual calculated long-term distribution of stresses shows a reversed "S"-form. Because of this, if the whole stress range for the ship life time is used for the Weibull approximation, the fatigue damage ratio will be overestimated of the order of 10%-20%. A better representation of long-term probabilities over the whole stress range can be achieved by a combination of two Weibull distributions, one for higher probabilities and one for lower probabilities according to eq.(6.5). The first one should be used for fatigue design and the second one for ultimate strength design. An example of a curve fit according to eq.(6.5) is shown in fig.6.4. Figs.6.5-6.6 show comparisons between shape parameters *h* calculated for all probabilities and for probabilities only above 10^{-4} respectively. All the results presented in this chapter are based on Weibull parameters calculated for long-term stresses with probabilities of exceedance above 10^{-4}.

$$\begin{aligned} Q_{LT}(\sigma) &= e^{-(\sigma/B)^h} && Q \geq 10^{-4} \\ Q_{LTe}(\sigma) &= 10^{-4}\, e^{-((\sigma-\sigma_*)/B_e)^{h_e}} && Q < 10^{-4} \\ \sigma_* &= B\,(-\ln(10^{-4}))^{1/h} \end{aligned} \tag{6.5}$$

In a recent extensive survey by Svensson, [18], different long-term distribution formulations are penetrated and also the problem of finding one single appropriate distribution to represent all probabilities of exceedance is emphasised.

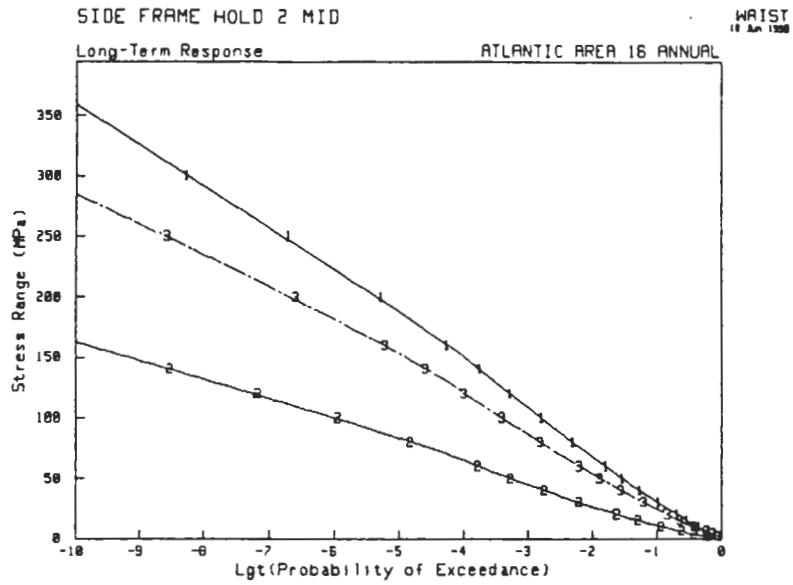

Fig.6.4 Example of a semi-continuous long-term distribution, (eq.(6.5)) Knuckle point at $Q=10^{-4}$. (Compare with fig.5.15)

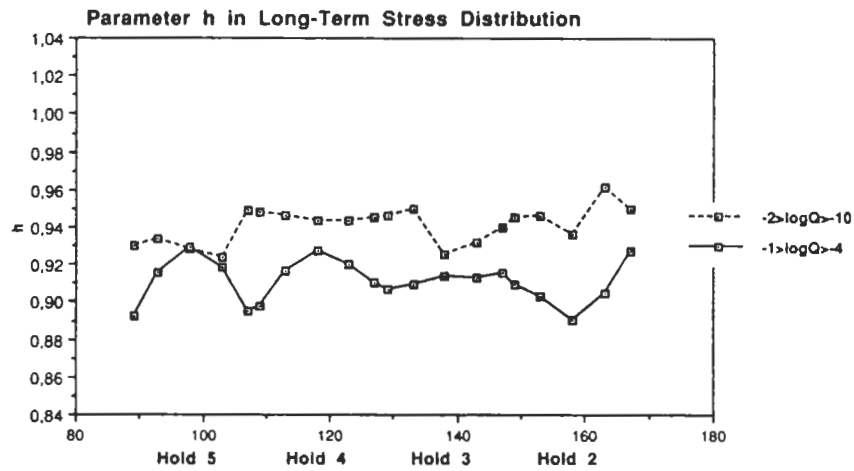

Fig.6.5 Variation of Weibull parameter h at different longitudinal positions. Bottom side girder, combined stresses.

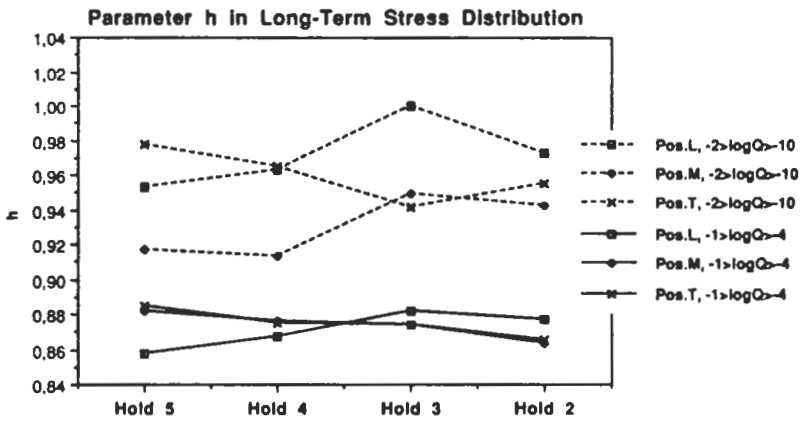

Fig.6.6 Variation of Weibull parameter h at different longitudinal positions. Side frame, combined stresses.

The as built bottom side girder includes man-holes, "rat"-holes and longitudinal as well as vertical bracings. Different joint classes must therefore be used for fatigue analysis of the different details in the girder. In this report, all stresses in the girder refer to the weld joint between girder web plate and bottom shell plate. This is a typical class F joint, with stress concentrations from "rat"-holes allowed for within the SN-curve.
The lower part of the side frame (position L) could be classified as a E joint while the mid (M) and top (T) positions must be downgraded to class F or G, due to the tripping brackets attached to flange and web, and to the junction of bracket flange and frame flange below top wing tank. The actual relevant classes must, however, be determined by inspection and knowledge of the weld process. This has not been possible to accomplish, and the presented results from fatigue analyses should be regarded as examples.

Figs.6.8 and 6.10 show distributions of cumulative damage ratio D along bottom side girder and in side frames, based on SN mean curves and SN design curves. In the calculations, no local stress concentrations have been applied except for those from the coarse FE-models. It is important to note that the presented damage calculations do not include the effect of speed reduction or non-linearity in the long-term stress distribution.

If the design fatigue strength is coupled to a cumulative damage $D<\eta$, where η is a design usage factor, then the maximum allowed hot-spot stress range can be determined from eq.(6.4)

$$\sigma_{Qmax} = \left(\frac{\eta \, \bar{a}}{n \, \Gamma\left(1+\frac{m}{h}\right)} \right)^{1/m} (\ln n)^{1/h} \qquad (6.6)$$

Comparisons between allowed maximum stresses based on SN design curves, and calculated nominal combined normal stresses are shown in figs. 6.9 and 6.11.

Fig.6.12-6.13 show results from fatigue analysis of side frames at position M with respect only to external pressure induced stresses. This example is applicable for the full load bulk cargo condition, in which Hold 2 and Hold 4 are empty and no counteracting mass forces are present.

The "fatigue life" is generally defined as L_0/D where L_0 is the ship service life time corresponding to the total number of stress cycles n for which the cumulative damage ratio D has been calculated. The fatigue life is coupled to the certain probability of failure incorporated in the used SN curve. For a SN design curve based on mean minus two standard deviations, the probability of fatigue failure is 2,3%. As shown in figs.6.7, 6.9, and 6.12, when comparing damage ratios calculated for SN mean curves and SN design curves, there is a large uncertainty associated with the SN data. For a class F joint, the damage ratio is 2,7 times larger for the SN design curve then for the SN mean curve. Therefore, instead of analysing fatigue lifes, it is more illustrative to analyse the probability of failure during the ship service life.

If a normal distribution of log N for the SN data is assumed, the probability of fatigue failure can be defined as $P_f = \Phi(-\beta)$ where Φ is the normal cumulative probability function and β is the reliability index. The reliability index can be directly calculated from the damage ratio according to eq.(6.7). A fatigue design criterion based on SN design curves and a usage factor η = 1,0 is equal to a reliability index β = 2,0.

$$\beta = -\frac{\log D_{mean}}{\log s} \qquad (6.7)$$

where

β = reliability index
D_{mean} = cumulative damage ratio related to SN mean curve
log s = standard deviation of log N

Reliability index and probabilities of failure at the most critical positions in the studied members are presented in table 6.2 below. When evaluating the results, it must be emphasised that other uncertainties besides the SN data, such as model uncertainty for structure and wave loads, fabrication tolerances, etc. are not incorporated.

Stress position, type, and weld joint class	Damage ratio for SN design curves	Reliability index β	Probability of failure
Bottom side girder position C, Hold 4 Combined stresses, Class F	1,81	0,82	0,21
Side frame Position M Hold 2 Combined stresses, Class F	1,40	1,33	0,09
Side frame Position M Hold 2 Combined stresses, Class G	3,57	-1,08	0,86
Side frame Position M Hold 2 Pressure stresses, Class F	2,82	-0,07	0,53
Side frame Position M Hold 2 Pressure stresses, Class G	7,20	-2,78	0,997

Table 6.2 Condensed results from fatigue analysis at positions exposed to largest dynamic stresses

TABLE 3.3 JOINT CLASSIFICATIONS* (Continued)

Type Number, Description, and Notes on Mode of Failure	Class	Explanatory Comments	Examples, Including Failure Modes
TYPE 6 DETAILS IN WELDED GIRDERS			
Notes on potential modes of failure			
Fatigue cracks generally initiate at weld toes and are especially associated with local stress concentrations at weld ends, short lengths of return welds, and changes of direction. Concentrations are enhanced when these features occur at or near an edge of a part (see notes on joint Type 4)			
General comment			
Most of the joints in this section are also shown, in a more general form, in joint Type 4; they are included here for convenience as being the joints which occur most frequently in welded girders			
6.1 Parent metal at the toe of a weld connecting a stiffener, diaphragm, etc. to a girder flange		Edge distance refers to distance from a free, i.e. unwelded, edge. In this example, therefore, it is not relevant	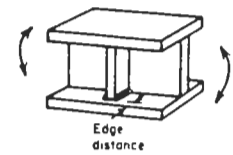
(a) Edge distance ≥ 10 mm (see joint Type 4.2)	F	as far as the (welded) edge of the web plate is concerned. For reason for edge	
(b) Edge distance < 10 mm	G	distance see note on joint Type 2	
6.2 Parent metal at the end of a weld connecting a stiffener, diaphragm, etc. to a girder web in a region of combined bending and shear	E	This classification includes all attachments to girder webs	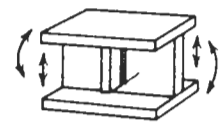
6.3 Parent metal adjacent to welded shear connectors			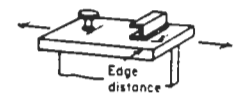
(a) Edge distance ≥ 10 mm	F		
(b) Edge distance < 10 mm (see Type 4.2)	G		
6.4 Parent metal at the end of a partial length welded cover plate, regardless of whether the plate has square or tapered ends and whether or not there are welds across the ends	G	This Class includes cover plates which are wider than the flange. However, such a detail is not recommended because it will almost inevitably result in undercutting of the flange edge where the transverse weld crosses it, as well as involving a longitudinal weld terminating on the flange edge and causing a high stress concentration	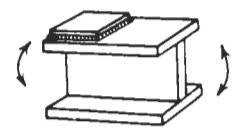
6.5 (a) Parent metal adjacent to the ends of discontinuous welds, e.g. intermittent web/flange welds, tack welds unless subsequently buried in continuous runs	E	This also includes tack welds which are not subsequently buried in a continuous weld. This may be particularly relevant in tack welded backing strips	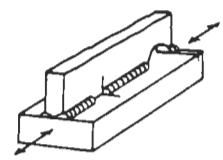
(b) Same as (a) but adjacent to cope holes	F	Note that the existence of the cope hole is allowed for in the joint classification; it should not be regarded as an additional stress concentration	

Fig.6.7 Examples of different weld joints classes, from [10]

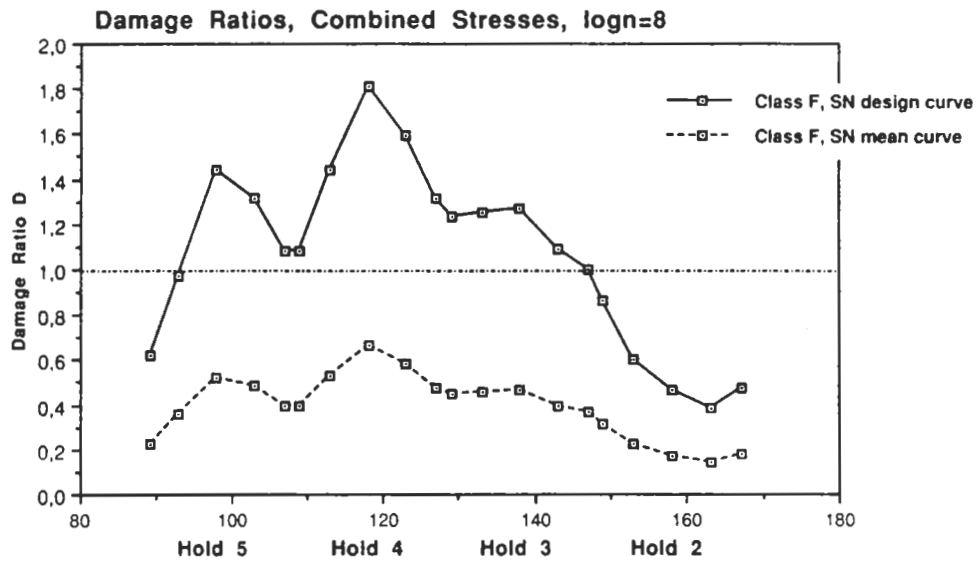

Fig.6.8 Cumulative damage ratios along the bottom side girder

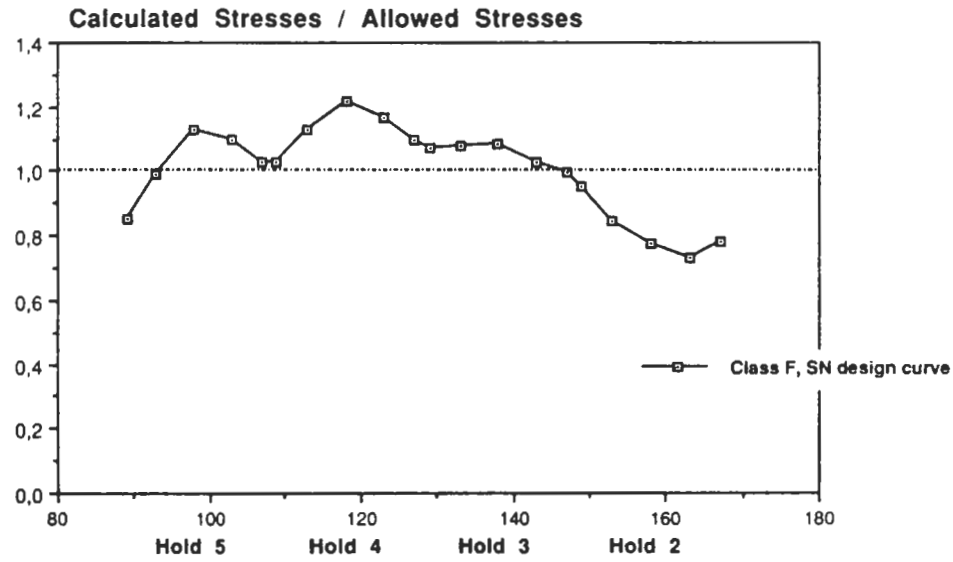

Fig.6.9 Distribution of maximum allowable stresses compared with calculated nominal normal stresses. Bottom side girder. Usage factor $\eta = 1$

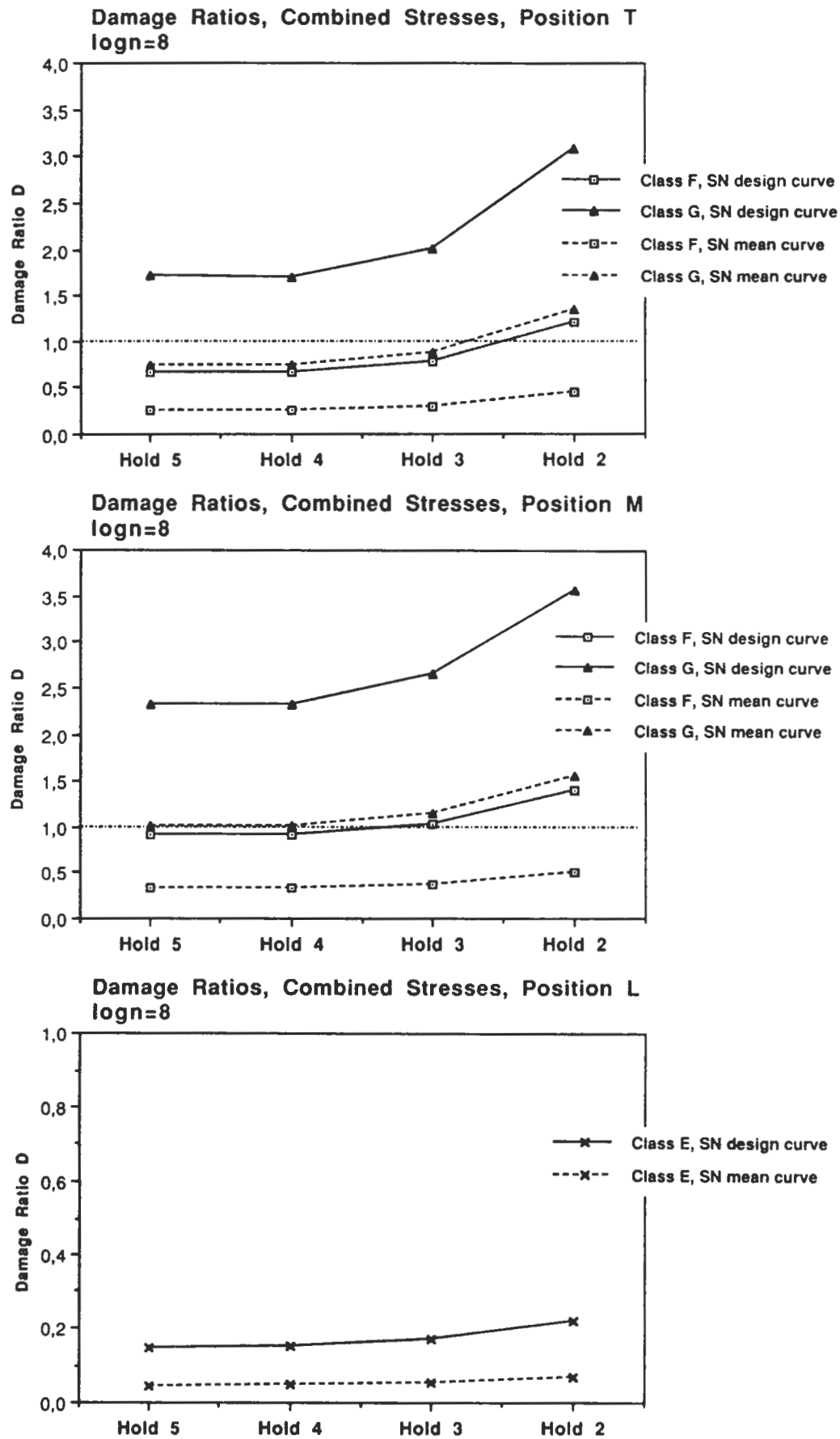

Fig.6.10 Cumulative damage ratios in side frames

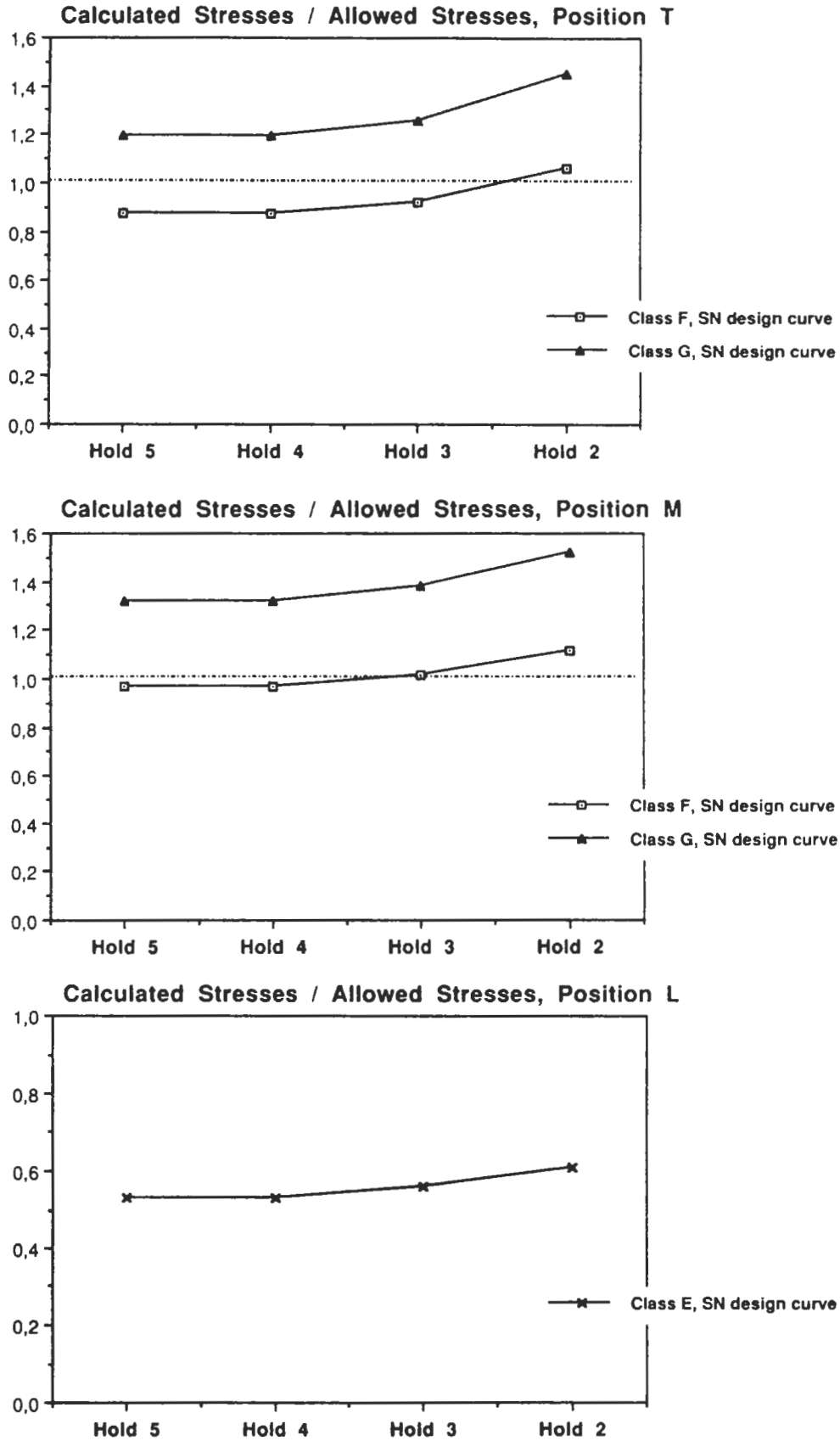

Fig.6.11 Distribution of maximum allowable stresses compared with calculated nominal normal stresses. Side frames. Usage factor $\eta = 1$

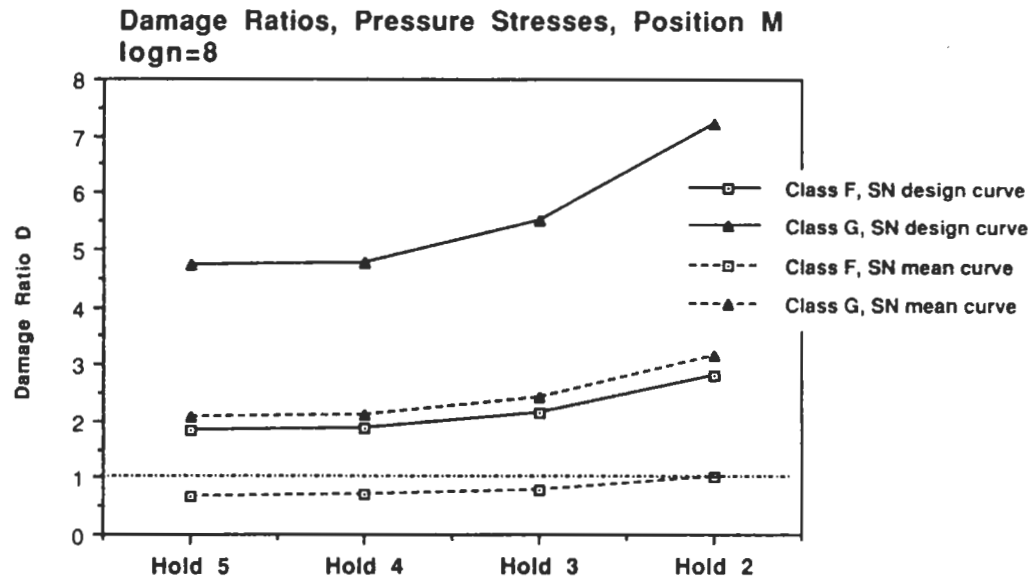

Fig.6.12 Cumulative damage ratios in side frames, position M. Pressure induced stresses only.

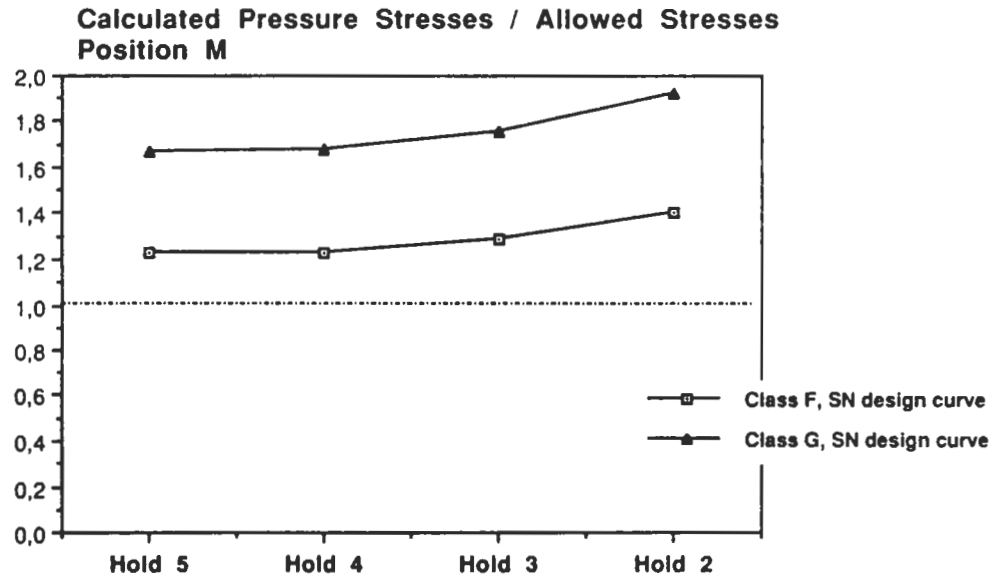

Fig.6.13 Distribution of maximum allowable stresses compared with calculated nominal normal stresses. Side frames, position M, Usage factor $\eta = 1$ Pressure induced stresses only.

6.2 *Influence of speed reduction*

Voluntary or involuntary speed reduction is generally a function of the sea state and can therefore directly be taken into account in the long-term stress distribution by using stress response functions for different speeds according to the sea state. Figs.6.16-6.17 illustrate the influence of speed reduction. For simplicity it is here assumed that the speed is reduced to zero at all sea states with significant wave heights above 6m and 9m respectively, independent of the mean periods. For the bottom side girder at position C in Hold 4, the damage ratio is reduced 2% if the speed is reduced at 9m and 10% if the speed is reduced at 6m significant wave height. For the side frame at position M in Hold 2, the damage ratio is reduced 5% and 21% respectively. From this example, it is obvious that speed reduction will not necessarily in any dramatic way increase the fatigue life of the structures.

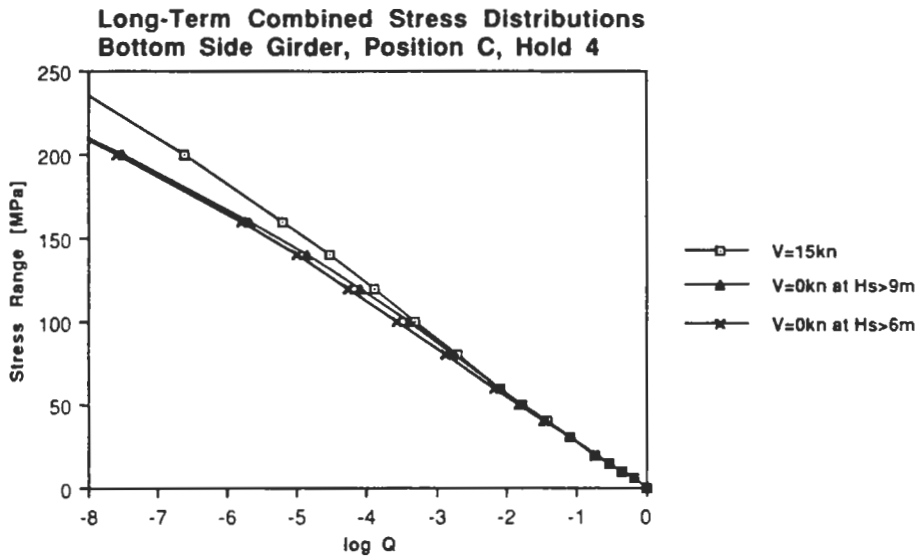

Fig.6.14 Influence of speed reduction on long-term stress distribution Bottom side girder

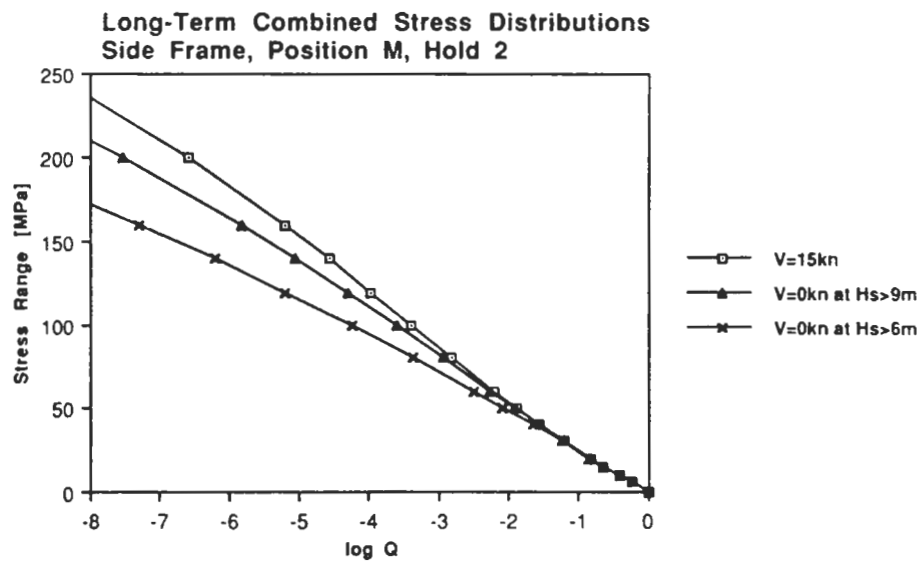

Fig.6.17 Influence of speed reduction on long-term stress distribution Side frame

6.3 Influence of non-linearity

As shown in figs.5.18 and 5.19, the non-linear pressure variation at ship sides will reduce the stress response even at rather moderate wave heights. The actual stress probability function in a short-term irregular sea will not follow a Rayleigh distribution, and hence the influence of non-linearity on the long-term stress distribution cannot be taken into account directly. It must be evaluated from time simulations in different irregular seas. A rough estimate of the influence of non-linearity might be made by corrections of the long-term stress distribution based on the long-term distribution of single wave heights. For the side frame at position M in Hold 2, reductions of long-term stress ranges by: 14% at $Q=10^{-1}$, 24% at 10^{-2}, 32% at 10^{-3}, and 37% at 10^{-4}, follow approximately the reductions shown in fig.5.8 for headings 180° and -135°. If these reductions are applied in a fatigue calculation, the damage ratio will be reduced by approximately 50%. This will increase the reliability index β from 1,33 as shown in table 6.2, to 2,7 for joint class F, and from -1,08 to 0,6 for class G.
If a similar test on the non-linear influence is made for pressure induced stresses only, as in the bulk load condition, stress reductions become: 12% at $Q=10^{-1}$, 21% at 10^{-2}, 29 % at 10^{-3}, and 33 % at 10^{-4}. The damage ratio will be reduced by 44%, and the reliability index β increased from -0,07 to 1,1 for class F, and from -2,78 to -1,4 for class G.

6.4 Hot-spot stresses from combination of nominal normal- and shear stresses

The actual local stress e.g. at the edge of a hole, is a function of both nominal shear and normal stress but generally with different stress concentration factors. If the hot-spot stress is uniaxial as in the case of a free edge, then the short-term local stress response can be calculated directly with use of correlation coefficients for nominal stresses

$$\bar{\sigma}_{hs\ 1/3} = (SCF_\sigma^2\ \bar{\sigma}_{1/3}^2 + SCF_\tau^2\ \bar{\tau}_{1/3}^2 + \rho_{\sigma\tau}\ 2\ SCF_\sigma\ SCF_\tau\ \bar{\sigma}_{1/3}\ \bar{\tau}_{1/3})^{1/2} \qquad (6.8)$$

where

$\bar{\sigma}_{hs\ 1/3}$	=	significant hot–spot stress in an irregular sea
$\bar{\sigma}_{1/3}$	=	significant nominal normal stress
$\bar{\tau}_{1/3}$	=	significant nominal shear stress
SCF_σ	=	stress concentration factor, hot–spot stress/nominal normal stress
SCF_τ	=	hot–spot stress/nominal shear stress
$\rho_{\sigma\tau}$	=	short term correlation coefficient normal – shear stress

In the third part of this report series, a more detailed fatigue analysis of the bottom side girder will be presented. The planned report will also assess the possibility of optimising the position of structural details with respect to fatigue damage from both combined normal and shear stresses.

7 CONCLUSIVE COMMENTS ON CALCULATION PROCEDURE AND RESULTS

7.1 Direct calculations for improved structural design

This report focus on showing the additional information that can be achieved with a direct method for calculation of wave induced dynamic stresses in comparison with ordinary quasi-static stress calculations. The present calculation procedure was introduced in [1]. Results from stress response calculations for regular waves and short-term irregular seas in primary members of the midship hold structure in a lo/lo containership were presented. From the pilot study the following conclusions were drawn :

The major advantages of the direct procedure in comparison with an ordinary "design load" procedure are:

* The relative importance of different load components can be evaluated
* The actual correlation between load components is taken into account
* Nominal and hot-spot stresses can be determined at any probability level in the long-term stress history

In this report the procedure has been extended to include long-term stress calculations and fatigue analysis. The conclusions above are verified by the results in this report. Examples of new information obtained from the direct dynamic calculations is the important, each other counteracting effect of internal mass force and external pressure induced stress components in the side frame, and the correlation between local and global stress components along the bottom side girder. None of these effects could have been established by a static stress analysis. Estimated fatigue damages also demonstrate the possibility of increasing structural safety by a better optimization of the detail design with respect to the distribution of wave induced stresses.

The calculated stress levels cannot directly be compared with stress criteria established by the classification rules. For instance, in DnV rules for ships, [19], maximum allowable combined normal stress levels obtained by direct strength calculations are specified for longitudinal girders to 190 MPa, and for transverse girders to 160 MPa for normal strength structural steel. Calculations are to be based on "the most severe realistic load condition", and "realistic combinations of external and internal dynamic loads at design level". According to the specifications in the rules, this means combinations of most severe static still water condition, global hull girder bending moments at probability level 10^{-8} divided by 1,7, and dynamic local loads corresponding to a probability level of 10^{-4}. Hence the specified loads are not related to a certain most severe sea condition, but rather to empirical knowledge of acceptable safety levels.
The maximum long-term wave induced stresses presented in this report should only be combined with still water stresses from the actual load cases used in the calculations. These are not necessarily the worst possible conditions. Since still water stresses are of large importance for the structural design, a combination of static calculations for determination of most severe conditions, and direct dynamic calculations for these conditions, is required. Acceptable stress levels obtained by this approach should preferable be established from comparative calculations with the procedure specified by the rules, to ascertain an equal and acceptable level of structural reliability.

There are no explicit criteria for fatigue design in the ship rules today. The direct dynamic approach provides a basis for establishing such criteria. A calculation of damage ratio distribution in a certain structural member can further be used to concentrate efforts to improve detail design in areas where dynamic stresses are significantly higher. As example, fig.6.8 clearly shows that a more balanced distribution of fatigue safety can be achieved by improve the detail design of the junction between bottom girder and bottom plate in the middle of Hold 5 and Hold 4, while the design is not at all critical in Hold 2.

7.2 *Model uncertainty and sources of error*

The outlined method for calculation of low-frequency wave induced stresses is - although based on statistical distributions of sea spectra - in principal deterministic. A probabilistic analysis needs assumptions of all the main statistical distributions of loads (still water- and sea loads) and strength (scantlings, fabrication quality and material properties), and of the model uncertainties incorporated in the calculation procedure. Extensive summaries of status and reliability of wave load models is given by Lewis in [20], and by Soares in [21]. Strip calculations of vertical motions and hull girder bending moments are generally considered satisfactory although different results can be found among the large number of published comparisons between calculated responses and measurements on models or full-scale ships. The vertical bending moment in large waves is proved to be non-linear with larger sagging moments than hogging moments, especially for slender ships, but the peak-to-trough range is still close to linear with respect to the wave height. The calculation of hydrodynamic pressure distribution in moderate waves is also shown to be in good agreement with measurements. However, quoted from [20]: *"clarification is needed of the local pressure distribution around a section between the still water level and a wave crest, as well as the modified distribution just below a wave hollow"*. The suggested method introduced in this study for estimate of non-linear pressure induced stresses close to SWL, has not been verified by tests.

Errors in the calculation procedure due to the representation of structural response by a limited number of influence coefficients can be kept low or insignificant if the division of the hull into "load areas" is made with some care and with respect to the structural arrangement.

In addition to the low frequency wave induced loads, the effect of transient, impulsive loads from slamming and whipping should be considered. For ultimate strength estimates it is important to establish both the magnitude of the transient loads and the phase relationships between transient loads and low frequency loads. Theoretical models for calculation of stresses induced by transient loads become however quite different from models for static or low frequency loads and are therefore difficult to incorporate in the same calculation procedure.

A survey over the most important sources of uncertainties and errors in fatigue life estimates of mobile offshore rigs is reported in [22]. The by far most important uncertainty is declared to be the scattering in SN-data. This is probably also applicable to fatigue analyses of ships with the addition that different load cases and different areas for wave statistics might contribute significantly to the overall uncertainty.

7.3 *Application in an ordinary design process*

The first version of the WAIST program, [2], was used for studies of the validity of the method, and for studies of the importance of different wave load components. It can be regarded as a "pilot" program hardly suitable for routine calculations. The experience from the first version was used when the new present system was constructed.

The new version of WAIST is divided into three independent parts which can be separately executed. The first part performs strip calculations of transfer functions for motions, hull girder loads, and hydrodynamic pressures at arbitrary sections along the hull. The second part performs calculation of stress transfer functions based on results from strip calculations and on structural data stored on separate files. This second part also includes the optional time-step procedure for calculation of non-linear pressure induced stresses . The third part is an interactive post-processor where results from part two can be processed, printed, and plotted. The post-processor includes short-term responses, long-term statistics for optional ocean areas, calculation of correlation coefficients between

any components, and fatigue analysis with the possibility of adding individual stress concentration factors to the different stress components.

The division of the program in separate parts makes it is easy to perform systematic studies of different parameters. Different load cases can be executed without changing the structural data, and several stress points can be analysed for the same strip calculation.

In the design process of ships today, strip calculations and FE-analyses of primary structural members under static loads, have become routine. The only extra work necessary to perform a complete direct dynamic analysis is that several loadcases have to be analysed with the structural models to obtain influence coefficients. This work is usually not large in comparison to the work of modelling large complicated structures. It therefore appears realistic to perform routine calculations of dynamic stresses in critical parts of the structure.

The rationally-based calculation method described here is a possible instrument for better control over the dynamic stresses and can be utilized for optimizing the ship structure both with respect to ultimate strength and to fatigue. It is a well known fact that minor fatigue damages rarely leads to major failure of primary members, but this is no excuse for not taking the fatigue resistance into consideration both for safety and for economical reasons. The very same day that this report is summed up, the following small note is found in The Scandinavian Shipping Gazette, [23]:
"CRACKS: ... classification society ... is now to increase the control of modern VLCC built after 1985. The ships are designed with 20-25 percent lower steel weight and a number of serious cracks have been discovered."

ACKNOWLEDGEMENTS

The study presented in this report started in 1986, when the structural FE-analysis and calculations of influence coefficients were performed by my colleague Anders Olander at the Department of Naval Architecture, KTH. He also performed systematic calculations of wave induced stresses with the previous WAIST program. Due to some problems with the main frame computer based program, and due to other assignments, the work was not taken up until 1989 when the WAIST program was totally re-programmed for a mini-computer and coupled to the strip program SGENS. Anders Olander is acknowledged for his substantial contribution and for his patience with seeing the results in print.

I also wish to thank my colleague Jianbo Hua for his assistance with adjusting the SGENS strip program to fit the requirements of the new WAIST program.

The work has been performed under the supervision of professor Erik Steneroth. The contribution from his experience is highly appreciated.

Uddevallavarvet AB has kindly supported the study by making all structural plans of the OBO carrier available.

This research project is to a major part financed with funds from the National Swedish Board for Technical Development (STU) and the Swedish Shipyard Association (SVF).

REFERENCES

[1] Huss M.,
COMBINED WAVE INDUCED STRESSES IN A LO/LO CONTAINER SHIP; APPLICATION OF A RATIONALLY BASED DIRECT CALCULATION METHOD, PART 1
Royal Inst. of Technology, Dep. of Naval Architecture, Report TRITA-SKP 1059, Stockholm 1987

[2] Huss M.,
WAIST, PROGRAM FOR CALCULATION OF WAVE INDUCED STRESSES IN SHIPS DESCRIPTION AND USERS MANUAL (In Swedish)
Royal Inst. of Technology, Dep. of Naval Architecture, Report TRITA-SKP 1058, Stockholm 1986

[3] Hua J.,
SGENS, USERS MANUAL (In Swedish)
Royal Inst. of Technology, Dep. of Naval Architecture, Report TRITA-SKP 1064, Stockholm 1990

[4] Salvesen N., Tuck E.O., Faltinsen O.,
SHIP MOTIONS AND SHIP LOADS
SNAME Transactions Vol. 78, 1970

[5] Kaplan P., Raff A.I.,
EVALUATION AND VERIFICATION OF COMPUTER CALCULATIONS OF WAVE-INDUCED SHIP STRUCTURAL LOADS
Ship Structure Committee, Report SSC-229, 1972

[6] Raff A.I.,
PROGRAM SCORES - SHIP STRUCTURAL RESPONSE IN WAVES
Ship Structure Committee, Report SSC-230, 1972

[7] de Jong B.,
COMPUTATION OF THE HYDRODYNAMIC COEFFICIENTS OF OSCILLATING CYLINDERS
Netherlands Ship Research Centre TNO, Report 145 S, Delft 1973

[8] Hogben N., Dacunha N.M.C., Olliver G.F.,
GLOBAL WAVE STATISTICS
Brittish Marine Technology Limited 1986

[9] Munse W.H., Wilbur T.W., Tellialian M.L., Nicoll K., Wilson K.,
FATIGUE CHARACTERIZATION OF FABRICATED SHIP DETAILS FOR DESIGN
Ship Structure Committee, Report SSC-318, 1982

[10] Gurney T.R.,
FATIGUE DESIGN RULES FOR WELDED STEEL JOINTS
The Welding Institute Research Bulletin, Vol 17 (5), 1976

[11] UK Department of Energy
OFFSHORE INSTALLATIONS: GUIDANCE ON DESIGN AND CONSTRUCTION, NEW FATIGUE DESIGN GUIDANCE FOR STEEL WELDED JOINTS IN OFFSHORE STRUCTURES, Issue N., 1983

[12] Det norske Veritas
FATIGUE STRENGTH ANALYSIS FOR MOBILE OFFSHORE UNITS
Classification Notes No.30.2, 1984

[13] Little R.S., Lewis E.V.,
A STATISTICAL STUDY OF WAVE-INDUCED BENDING MOMENTS ON LARGE OCEANGOING TANKERS AND BULK CARRIERS
SNAME Transactions Vol. 79, 1971

[14] Hoffman D., van Hooff R., Lewis E.V.,
EVALUATION OF METHODS FOR EXTRAPOLATION OF SHIP BENDING STRESS DATA
Ship Structure Committee, Report SSC-234, 1972

[15] Kjellander S.L., Persson B.G.,
HULL DAMAGES ON LARGE SWEDISH-BUILT SHIPS
Swedish Board for Technical Development STU, Report No.70-1272/U 981, 1972

[16] Antaniou A.C.,
A SURVEY ON CRACKS IN TANKERS UNDER REPAIRS
Int. Symposium on Practical Design in Shipbuilding PRADS, Tokyo 1977

[17] LARGE OIL TANKER STRUCTURAL SURVEY EXPERIENCE
Position Paper EXXON Corp., 1982

[18] Svensson C.A.T.,
A CRITICAL SURVEY OF LONG-TERM DISTRIBUTION FORMULATIONS OF OCEAN WAVE INDUCED LOAD EFFECTS OF SHIP STRUCTURES - WITH REFERENCE TO APPLICATION IN FATIGUE ANALYSIS
Chalmers Univ. of Technology, Dep. of Naval Architecture and Ocean Engineering Report CHA/NAV/R-90/0003, Göteborg 1990

[19] Det norske Veritas
HULL STRUCTURAL DESIGN; SHIPS WITH LENGTH 100 METERS AND ABOVE
Rules for Classification of Steel Ships, Part 3 Chapter 1, 1988

[20] Lewis E.V.,
THE STATUS OF COMMERSIAL SEAKEEPING RESEARCH
SNAME Technical and Research Bulletine No.1-39, 1982

[21] Soares C.G.,
PROBABILISTIC MODELS FOR LOAD EFFECTS IN SHIP STRUCTURES
The Norwegian Institute of Technology, Report UR-84-38, 1984

[22] Carlsen C.A., Gundersen H.B., Gran S.,
ENVIRONMENTAL DATA IN OPERATION & DESIGN CASE - MOBILE RIGS
DnV Paper Series No.81 P017, 1981

[23] The Scandinavian Shipping Gazette No.34, 1990

NOTATION

First apperance in text or equations is indicated. (A few symbols that only occur temporary, or are directly understood by the connection are not listed below).

a	Parameter of the SN mean curve. The intercept of the log N axis for a SN mean curve, eq.(6.2)
a	Parameter of the SN design curve, the intercept of the log N axis for a mean minus two standard deviations SN design curve, eq.(6.3)
A,B,C,D,E	Positions along bottom side girder for stress response calculations, figs.2.2-2.3
B	Parameter of Weibull distribution, eq.(5.6)
BM_y	Hull girder vertical bending moment, fig.3.1, eq.(4.2)
BM_z	Hull girder horizontal bending moment, fig.3.1, eq.(4.2)
CA	Combined total stress (in figures), fig.5.2
CG	Combined global stress (in figures), fig.5.3. (Centre of gravity, fig.3.1)
CL	Combined local stress (in figures), fig.5.3
C_{Mx},C_{My},C_{Mz}	Normal stress coefficients for global hull girder moments, eq.(4.2)
C_m	Mass force influence coefficient, p.10, eq.(4.5)
C_{posx},C_{posy}	Internal normalized tank coordinates, eq.(3.7)
C_p	Pressure influence coefficient, eq.(4.4)
C_{Tx},C_{Ty},C_{Tz}	Shear stress coefficients for global torsional moment and shear forces,eq.(4.3)
D	Cumulative damage ratio, eq.(6.1)
F_{mx},F_{my},F_{mz}	Mass force components in x, y, z, directions, eq.(3.4-6)
g	Acceleration of gravity, eq.(3.4)
h	Parameter of Weibull distribution, eq.(5.6)
H	Wave height (double amplitude), p.15
$\bar{H}_{1/3}$	Significant wave height, mean value of the upper third fractile of wave height distribution, eq.(5.1). (In figures also denoted H_S)
H_S	Significant wave height (in figures), fig.5.23
HB	Hull girder horizontal bending stress (in figures), fig.5.3
I_y	Midship vertical moment of inertia, p.3

I_z	Midship horizontal moment of inertia, p.3
i	Position for calculation of stress response, eq.(4.1)
j	Position for calculation of hydrodynamic pressure, eq.(4.4)
k	Position for calculation of mass force influence coefficients, eq.(3.1)
L,M,T	Positions along side frames for stress response calculations, fig.2.2
L_{pp}	Ship length between perpendiculars, p.18
m	Parameter of the SN-curve. The negative inverse slope of the SN-curve, eq.(6.2)
MF	Internal mass force induced stress (in figures), fig.5.4
m_x, m_y, m_z	"Active" mass components in x, y, z, directions, eq.(3.4-6)
n	Number of cycles, p.29, eq.(5.8)
N	Total number of cycles to fatigue failure at constant stress range (SN-curve), eq.(6.1)
p	Hydrodynamic pressure, eq.(4.4)
p( )	Discrete probability, eq.(5.5)
PR	External hydrodynamic pressure induced stress (in figures), fig.5.4
Q	Probability of exceedance, = 1-F, where F is cumulative probability distribution function, eq.(5.3)
R_σ	Parameter of the Rayleigh distribution of stress amplitudes, eq.(5.3)
RMS	Root mean square, i.e $[(\Sigma(x^2/n)-\Sigma(x/n)^2]^{1/2}$, where x are time step values and n are number of time steps, p.15
s	log s is standard deviation of log N in the SN-curve, eq.(6.3)
S_0	Cut-off stress level (fatigue limit) of the SN-curve at $N=2\cdot10^8$, table 6.1
$S_w(\omega)$	Wave spectrum, eq.(5.1)
$S_\sigma(\omega)$	Stress spectrum, eq.(5.2)
SCF	Stress concentration factor, eq.(6.8)
SWL	Still water line, p.8
t	Time variable, eq.(3.1-3)
T	Regular wave period, fig.5.25

$\bar{T}$	Mean zero uppcrossing wave period of a stationary irregular sea, eq.(5.1)
T_y	Hull girder horizontal shear force, fig.3.1, eq.(4.3)
T_z	Hull girder vertical shear force, fig.3.1, eq.(4.3)
$T_\sigma(\omega)$	Stress transfer function, eq.(5.2)
TM_x	Hull girder torsional moment, fig.3.1, eq.(4.2)
V	Ship speed, fig.3.1
VB	Hull girder vertical bending stress (in figures), fig.5.3
x	Coordinate, surge motion, fig.3.1, eq.(3.1)
y	Coordinate, sway motion, fig.3.1, eq.(3.1)
z	Coordinate, heave motion, fig.3.1, eq.(3.1)
β	Reliability index, eq.(6.7). (Wave heading angle, eq.5.5)
ε	Phase lag relative the encountering wave elevation, eq.(3.1-3)
ϕ	Roll motion, fig.3.1, eq.(3.2)
η	Usage factor, eq.(6.6)
λ	Wave length, table 5.1
θ	Pitch motion, fig.3.1, eq.(3.1)
ρ	Correlation coefficient in a short-term irregular sea, eq.(5.4)
ρ_Q	Correlation coefficient in a long-term calculation, eq.(5.7)
σ	Stress in general, especially normal stress, eq.(4.1), eq.(4.2)
$\bar{\sigma}_{1/3}$	Significant stress, mean value of the upper third fractile of stress amplitude distribution, eq.(5.3)
τ	Shear stress, eq.(4.3)
ω	Wave frequency, Table 5.1
ω_e	Wave frequency of encounter eq.(3.1)
ψ	Yaw motion, fig.3.1, eq.(3.1)

APPENDIX 1 STRESS RESPONSE IN REGULAR WAVES

TABLE OF CONTENTS:

Response curves (transfer functions) are presented as stress per wave height. This means double amplitude stress if double amplitude wave height is refered to, or single amplitude stress if single wave amplitude is refered to.

The figures are based on stress calculations for 50 regular wave frequencies ω, ranging from 0,15 rad/s to 2,60 rad/s with intervals of 0,05 rad/s. The corresponding regular wave lengths are $\lambda = 2\pi g/\omega^2$. The wave length equal to the ship Lpp, 200m, has a frequency of 0,55 rad/s.

For the side frame, also non-linear combined stress responses are presented. Non-linear, non-harmonic stresses are represented by equivalent harmonic amplitudes calculated as $\sqrt{2}$*RMS of the time step values.

Bottom Side Girder, Position C Hold 4
Normal Stress Components

0°

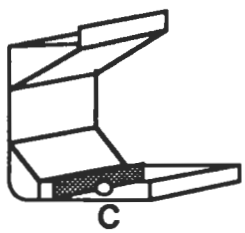

1: Vertical Bending
2: Horizontal Bending
3: Pressure
4: Mass Force
5: Combined

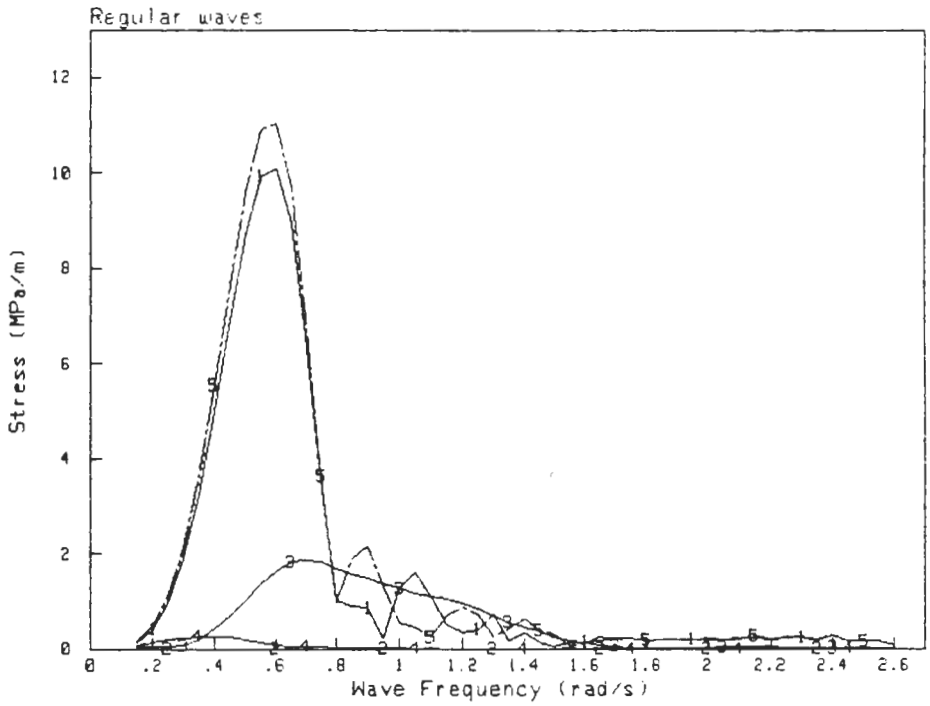

Bottom Side Girder, Position C Hold 4
Normal Stress Components

45°

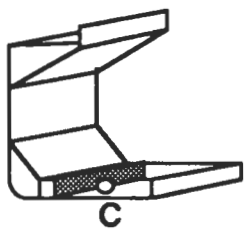

1: Vertical Bending
2: Horizontal Bending
3: Pressure
4: Mass Force
5: Combined

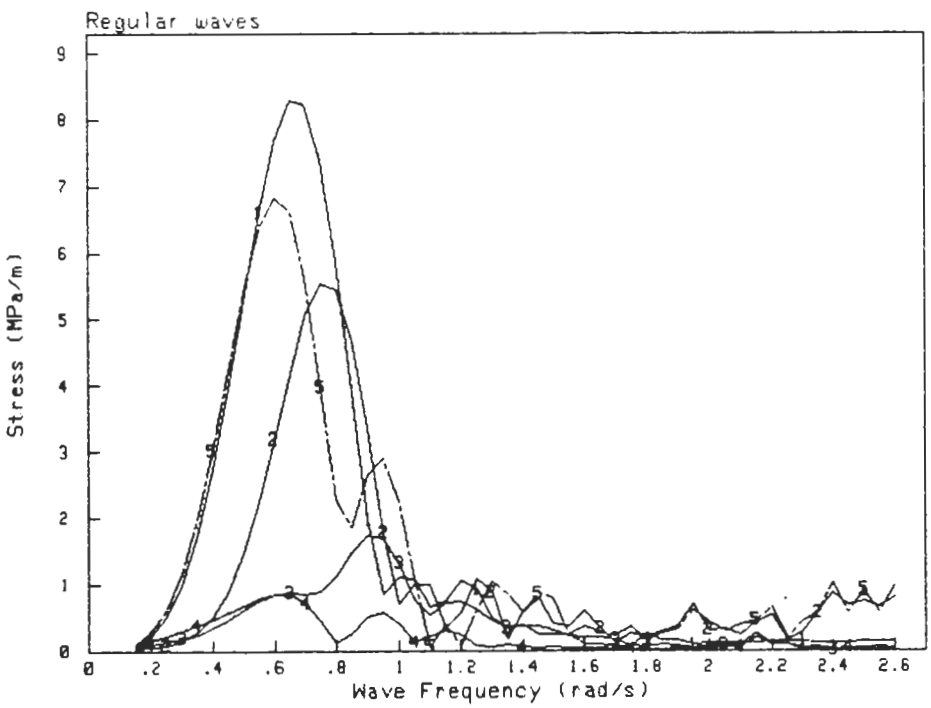

Bottom Side Girder, Position C Hold 4
Normal Stress Components

90°

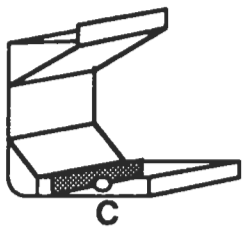

1: Vertical Bending
2: Horizontal Bending
3: Pressure
4: Mass Force
5: Combined

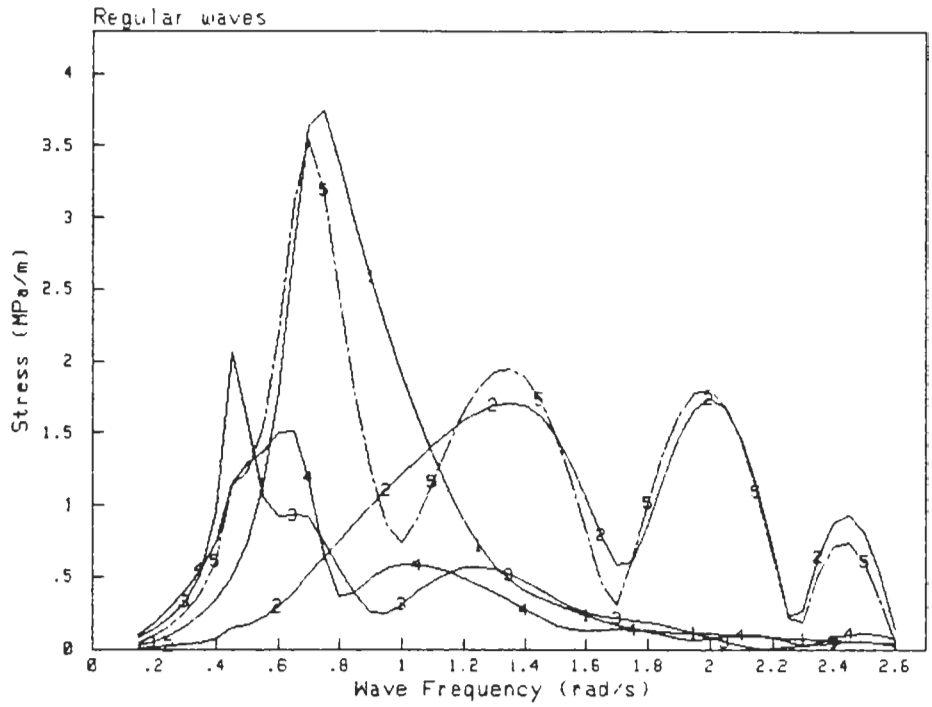

Bottom Side Girder, Position C Hold 4
Normal Stress Components

135°

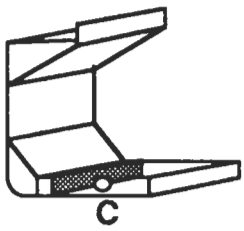

1: Vertical Bending
2: Horizontal Bending
3: Pressure
4: Mass Force
5: Combined

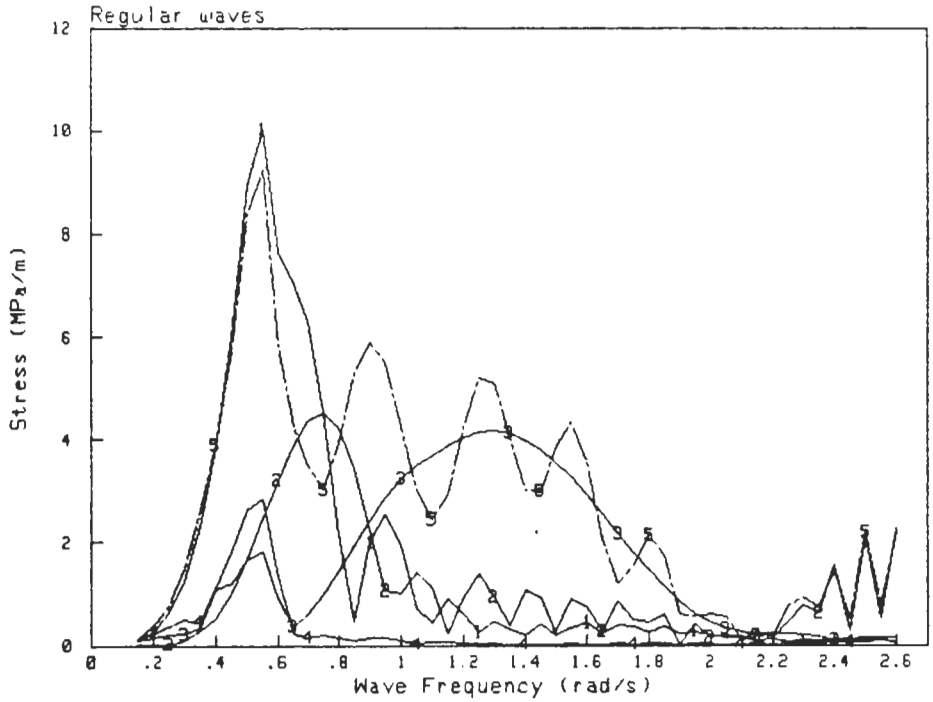

Bottom Side Girder, Position C Hold 4
Normal Stress Components

180°

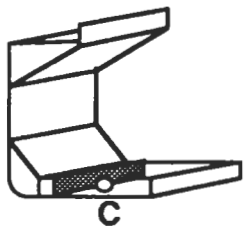

1: Vertical Bending
2: Horizontal Bending
3: Pressure
4: Mass Force
5: Combined

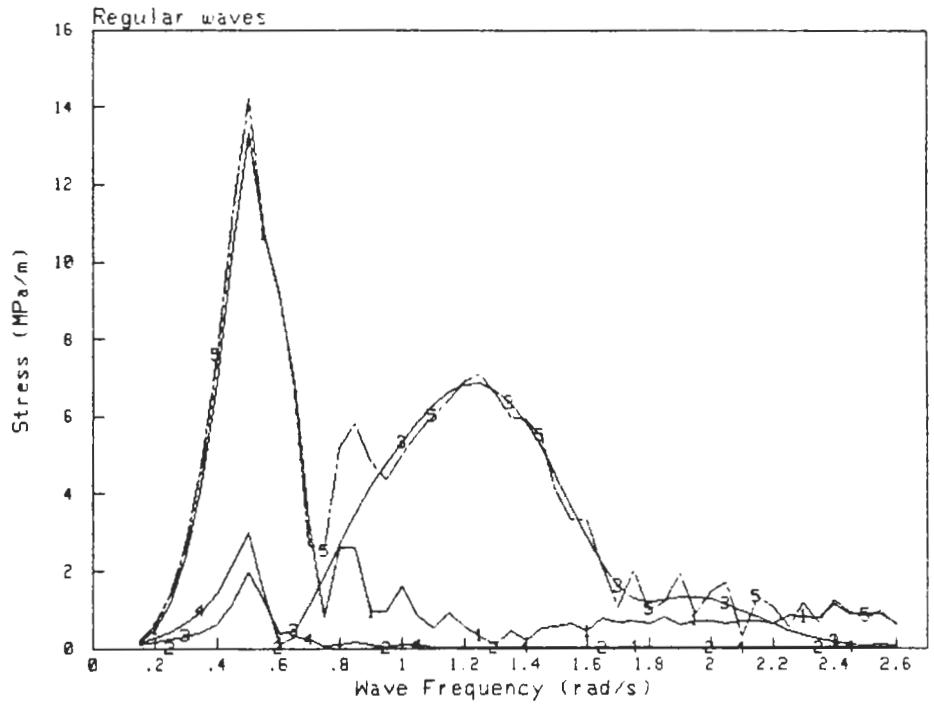

Bottom Side Girder, Position C Hold 4
Normal Stress Components

-135°

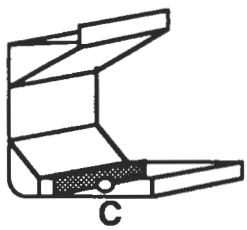

1: Vertical Bending
2: Horizontal Bending
3: Pressure
4: Mass Force
5: Combined

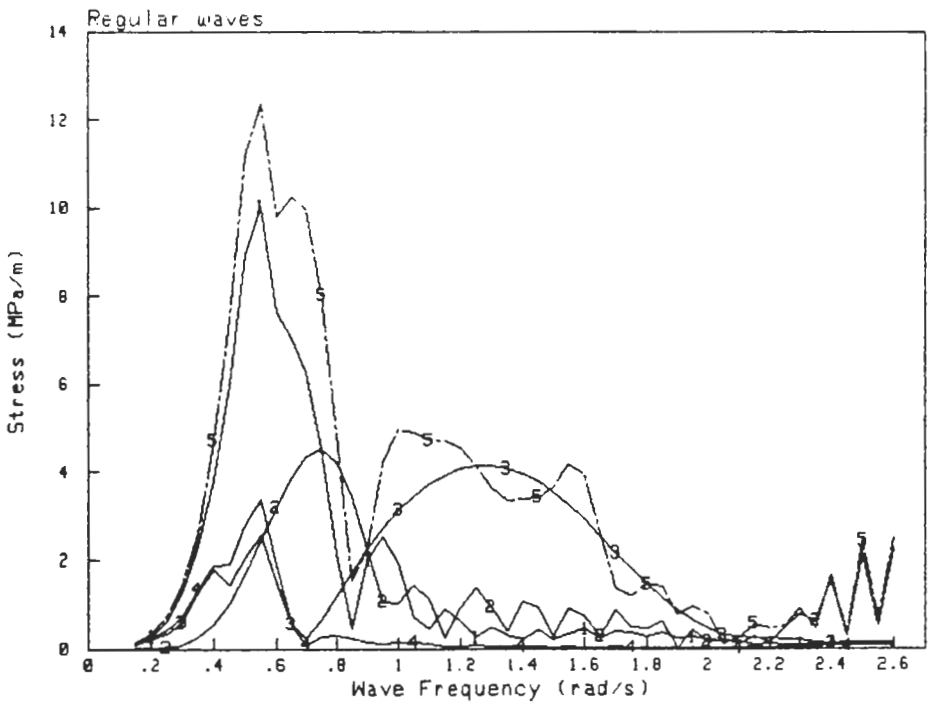

Bottom Side Girder, Position C Hold 4
Normal Stress Components

-90°

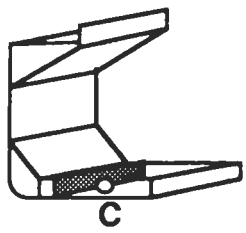

1: Vertical Bending
2: Horizontal Bending
3: Pressure
4: Mass Force
5: Combined

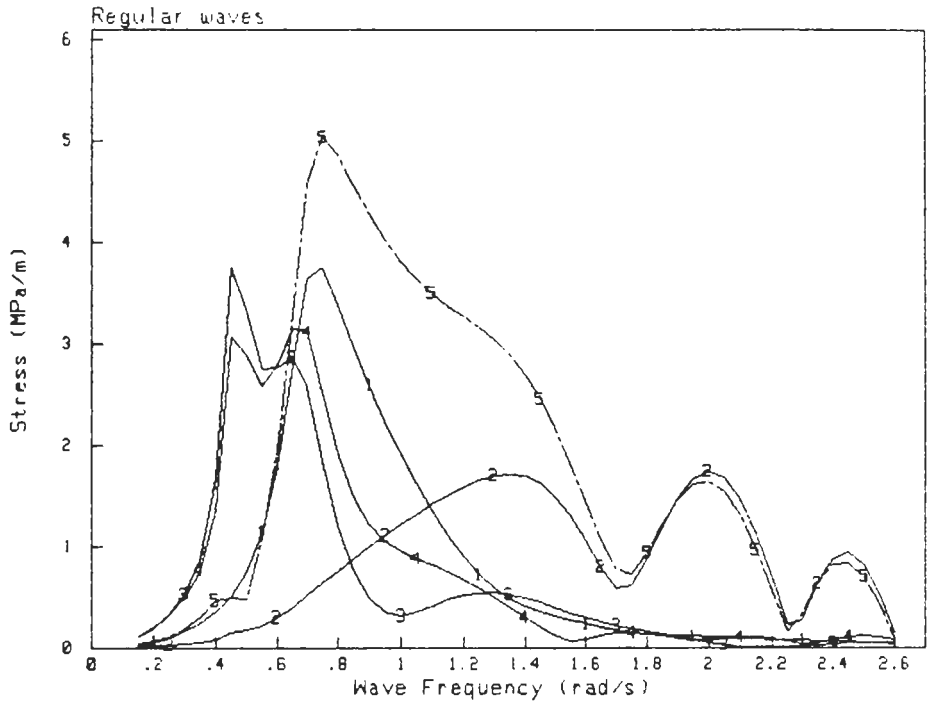

Bottom Side Girder, Position C Hold 4
Normal Stress Components

-45°

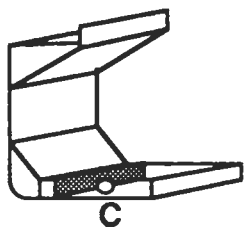

1: Vertical Bending
2: Horizontal Bending
3: Pressure
4: Mass Force
5: Combined

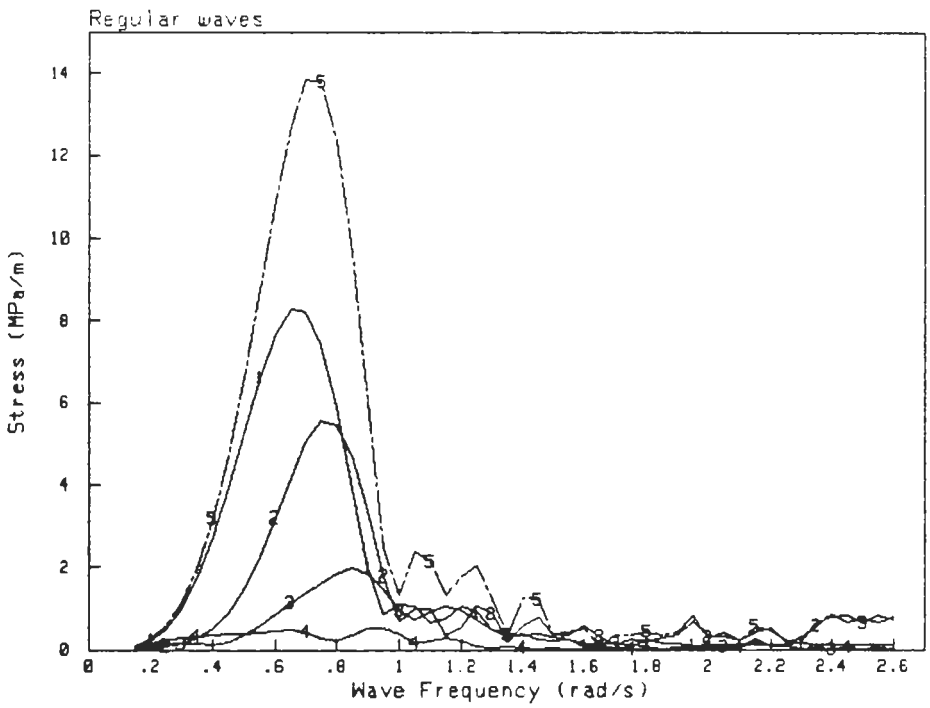

Side Frame, Position M Hold 2
Normal Stress Components

0°

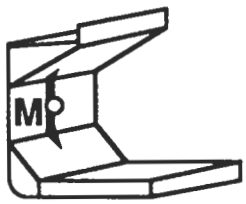

1: Pressure
2: Mass Force
3: Combined linear
4: Combined n-l, H=8m
5: Combined n-l, H=16m

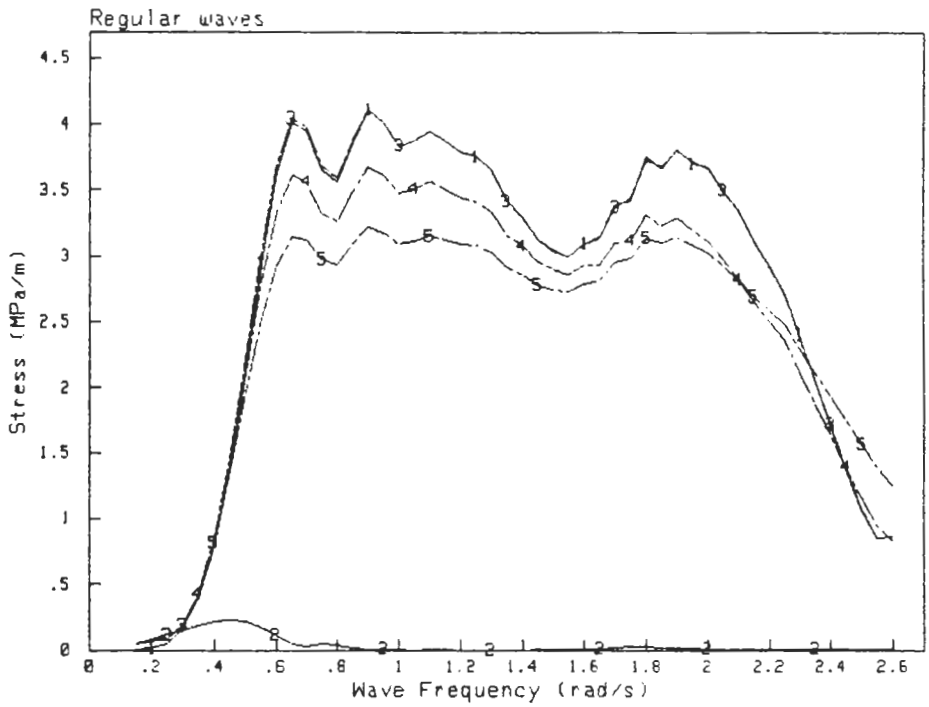

Side Frame, Position M Hold 2
Normal Stress Components

45°

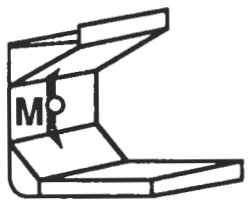

1: Pressure
2: Mass Force
3: Combined linear
4: Combined n-l, H=8m
5: Combined n-l, H=16m

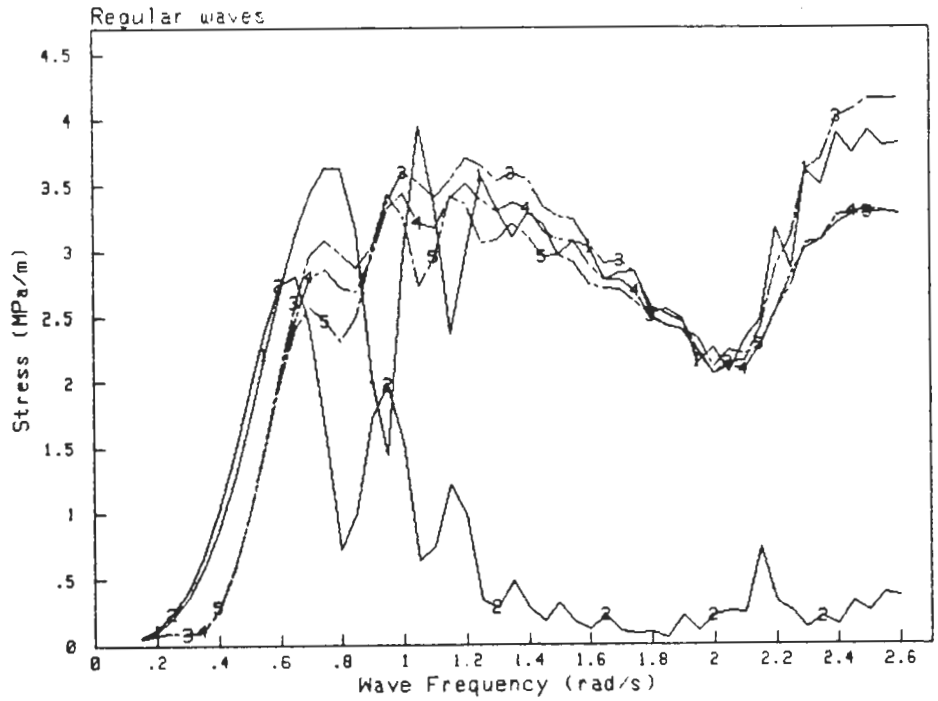

Side Frame, Position M Hold 2
Normal Stress Components

90°

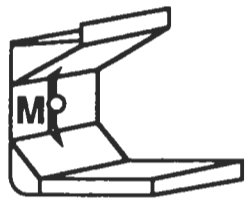

1: Pressure
2: Mass Force
3: Combined linear
4: Combined n-l, H=8m
5: Combined n-l, H=16m

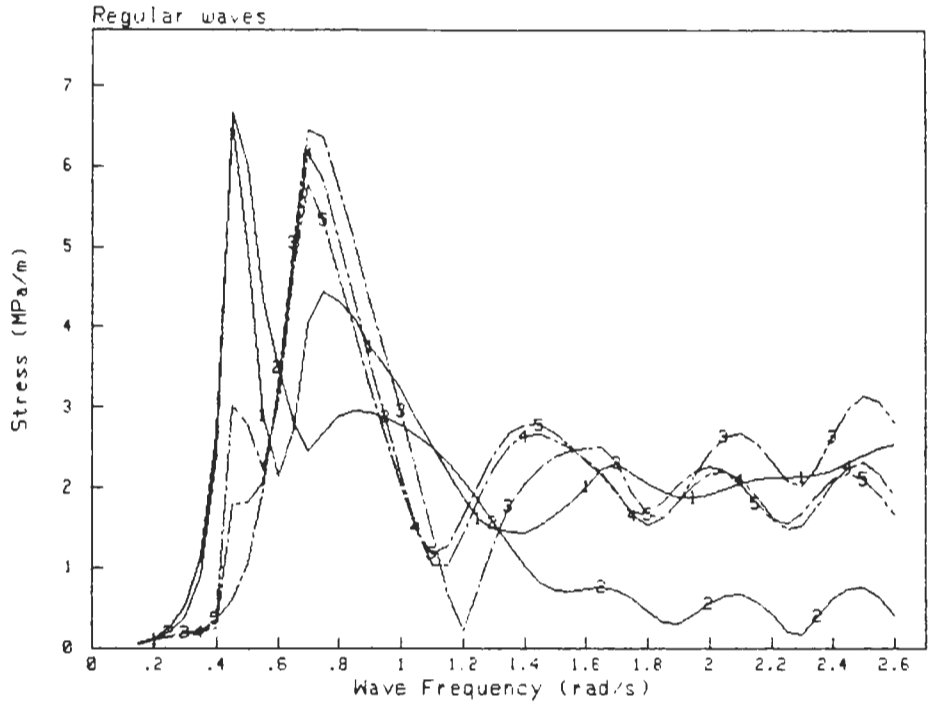

Side Frame, Position M Hold 2
Normal Stress Components

135°

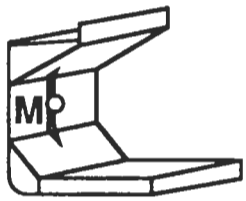

1: Pressure
2: Mass Force
3: Combined linear
4: Combined n-l, H=8m
5: Combined n-l, H=16m

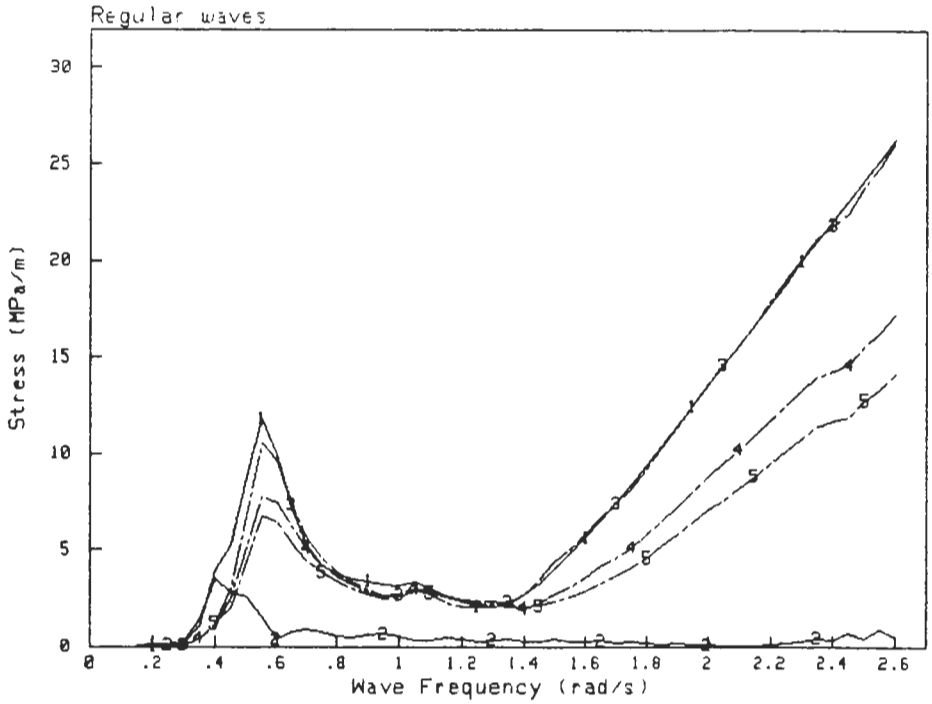

Side Frame, Position M Hold 2
Normal Stress Components

180°

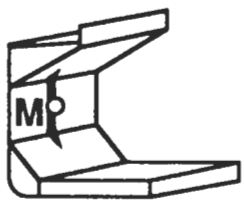

1: Pressure
2: Mass Force
3: Combined linear
4: Combined n-l, H=8m
5: Combined n-l, H=16m

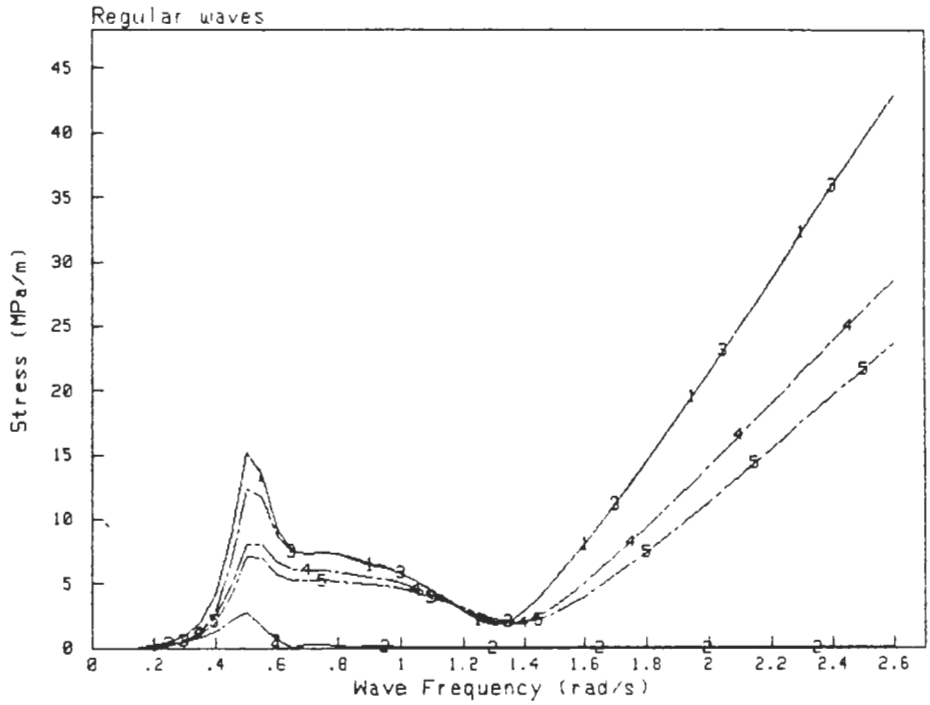

Side Frame, Position M Hold 2
Normal Stress Components

-135°

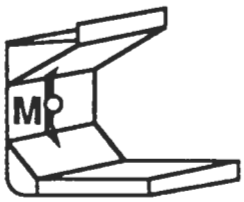

1: Pressure
2: Mass Force
3: Combined linear
4: Combined n-l, H=8m
5: Combined n-l, H=16m

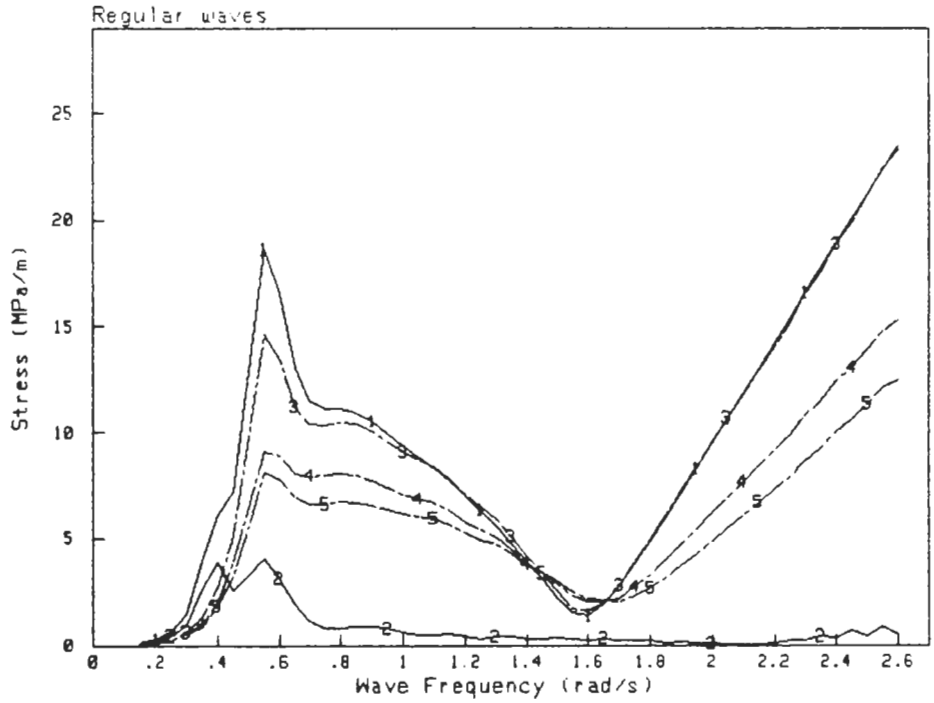

Side Frame, Position M Hold 2
Normal Stress Components

-90°

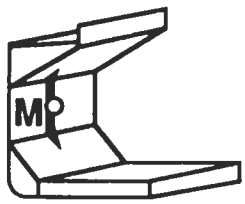

1: Pressure
2: Mass Force
3: Combined linear
4: Combined n-l, H=8m
5: Combined n-l, H=16m

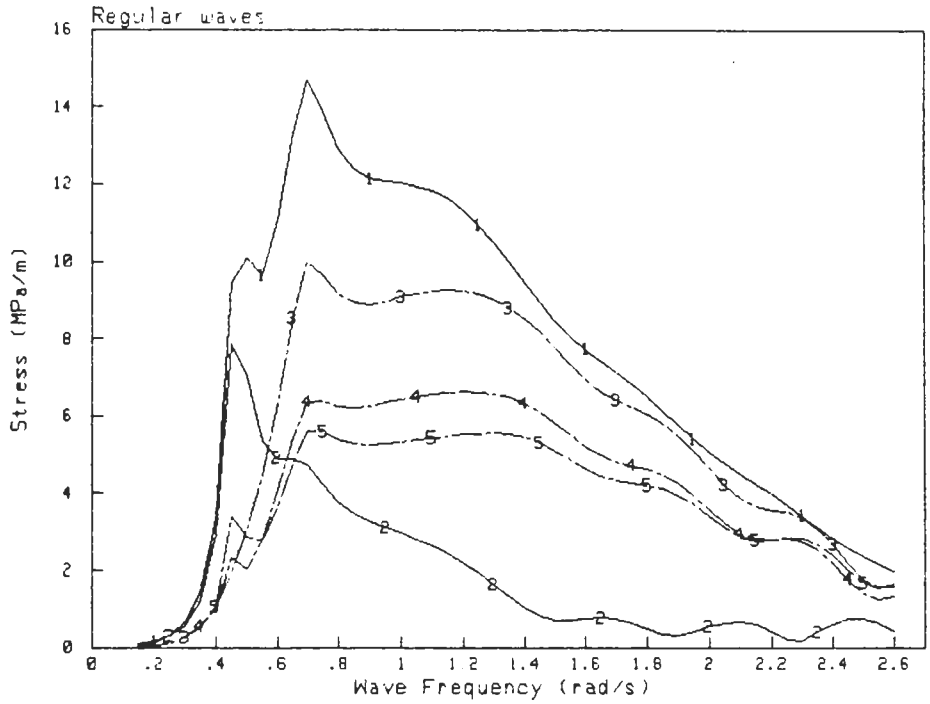

Side Frame, Position M Hold 2
Normal Stress Components

-45°

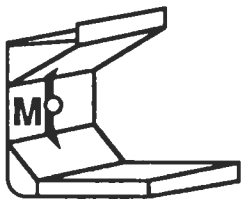

1: Pressure
2: Mass Force
3: Combined linear
4: Combined n-l, H=8m
5: Combined n-l, H=16m

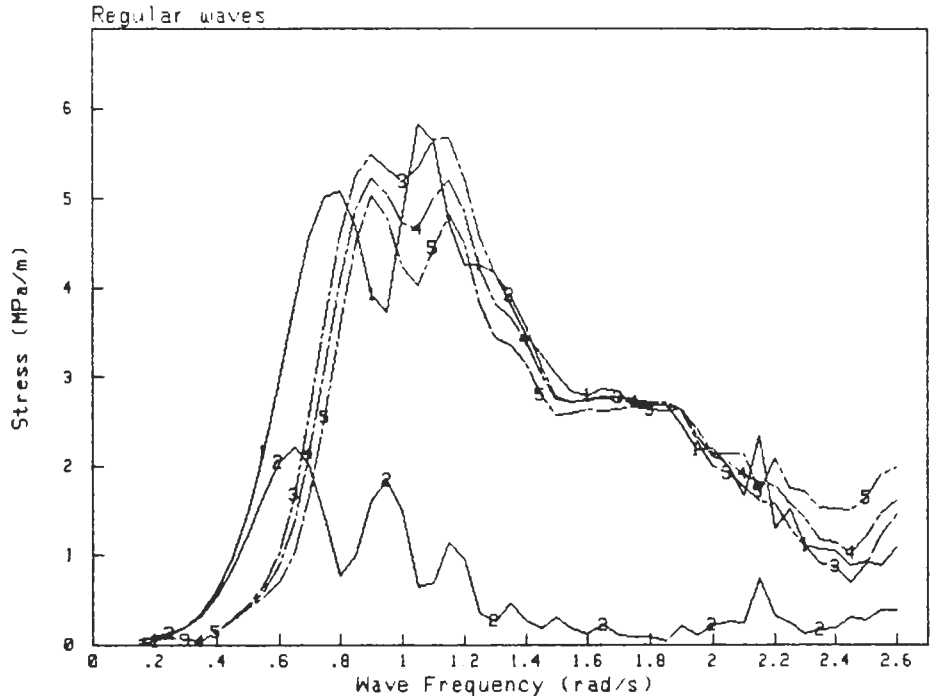

APPENDIX 2 STRESS RESPONSE IN LONGCRESTED IRREGULAR SEAS

TABLE OF CONTENTS:

Response curves are presented as significant stress per significant wave height. This means double amplitude stress if the ordinary double amplitude significant wave height, $\bar{H}_{1/3}$ is refered to.

Figures are based on results from linear spectrum analysis using ordinary 2-parameter Pierson-Moskowitz wave spectra according to eq.(5.1). Correlation coefficients are defined according to eq.(5.4).

Bottom Side Girder, Position A Hold 4
Normal Stress Components

0°

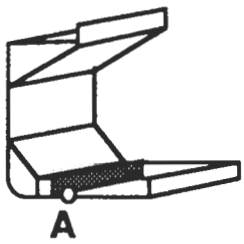

1: Vertical Bending
2: Horizontal Bending
3: Pressure
4: Mass Force
5: Combined

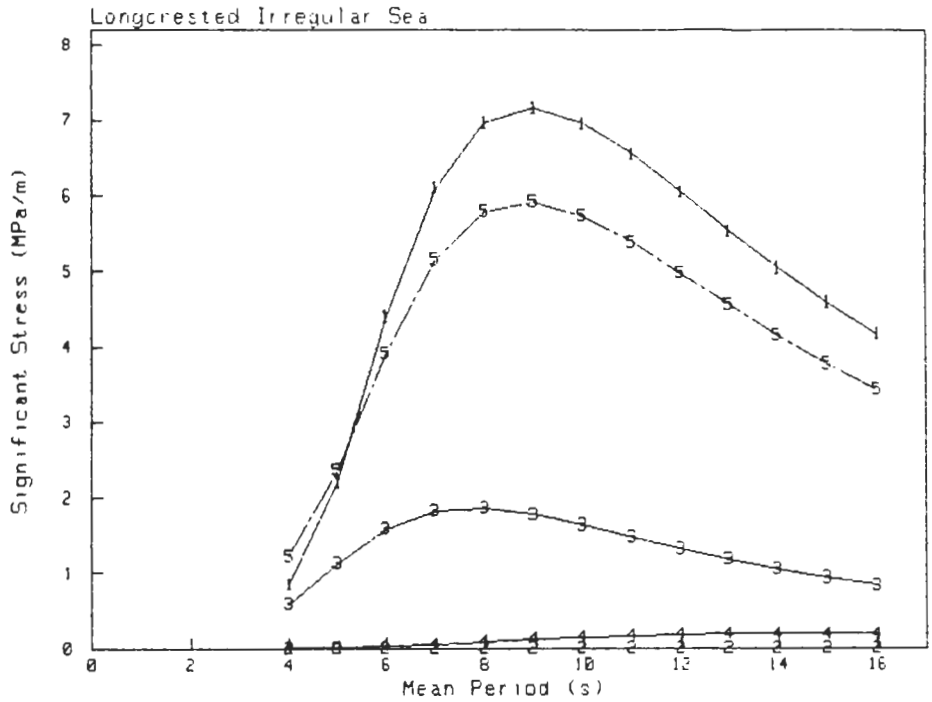

Bottom Side Girder, Position A Hold 4
Shear Stress Components

0°

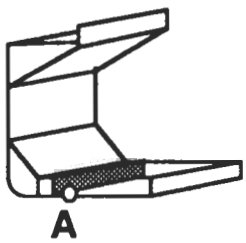

1: Pressure
2: Mass Force
3: Combined
4: Correlation Coefficient Shear/Normal Stress

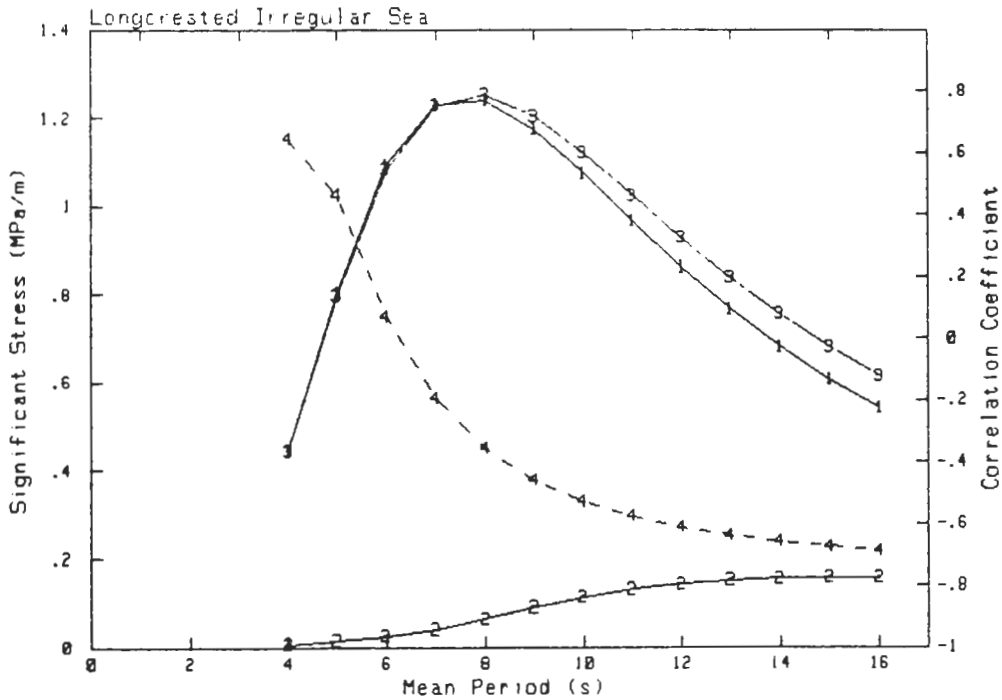

Bottom Side Girder, Position A Hold 4
Normal Stress Components

45°

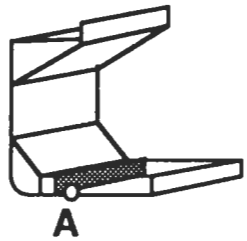

1: Vertical Bending
2: Horizontal Bending
3: Pressure
4: Mass Force
5: Combined

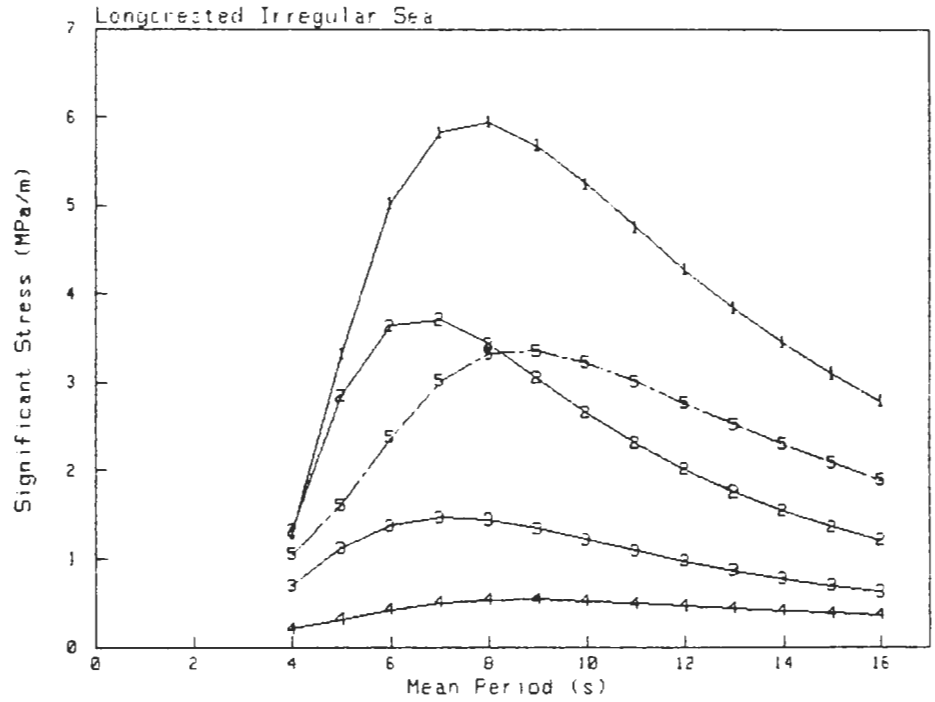

Bottom Side Girder, Position A Hold 4
Shear Stress Components

45°

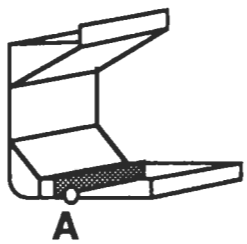

1: Pressure
2: Mass Force
3: Combined
4: Correlation Coefficient
Shear/Normal Stress

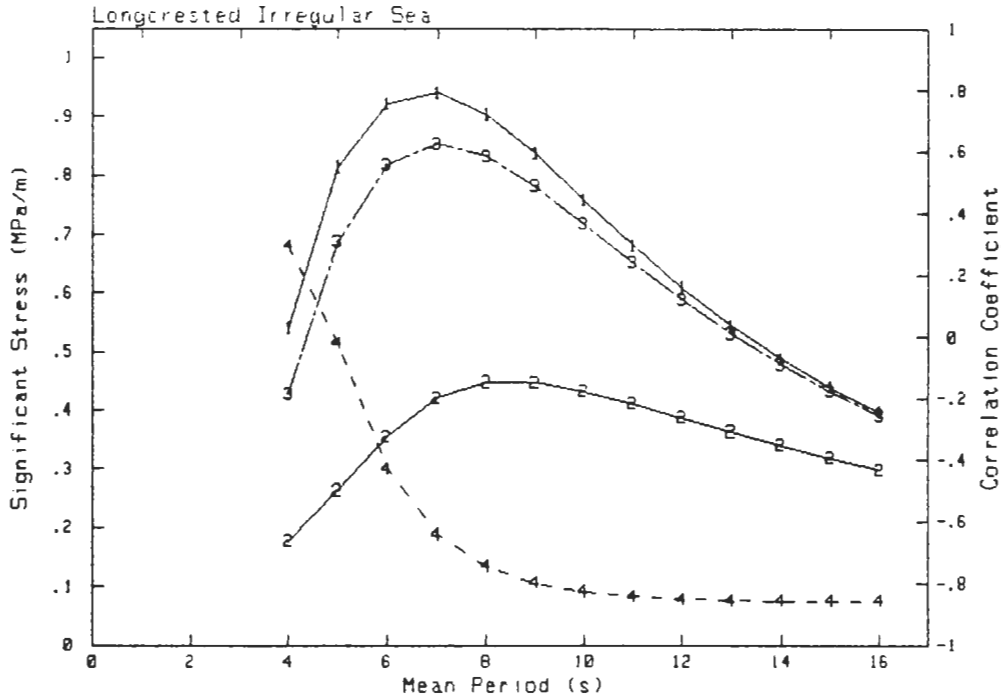

Bottom Side Girder, Position A Hold 4
Normal Stress Components

90°

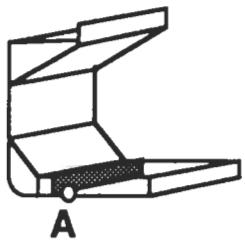

1: Vertical Bending
2: Horizontal Bending
3: Pressure
4: Mass Force
5: Combined

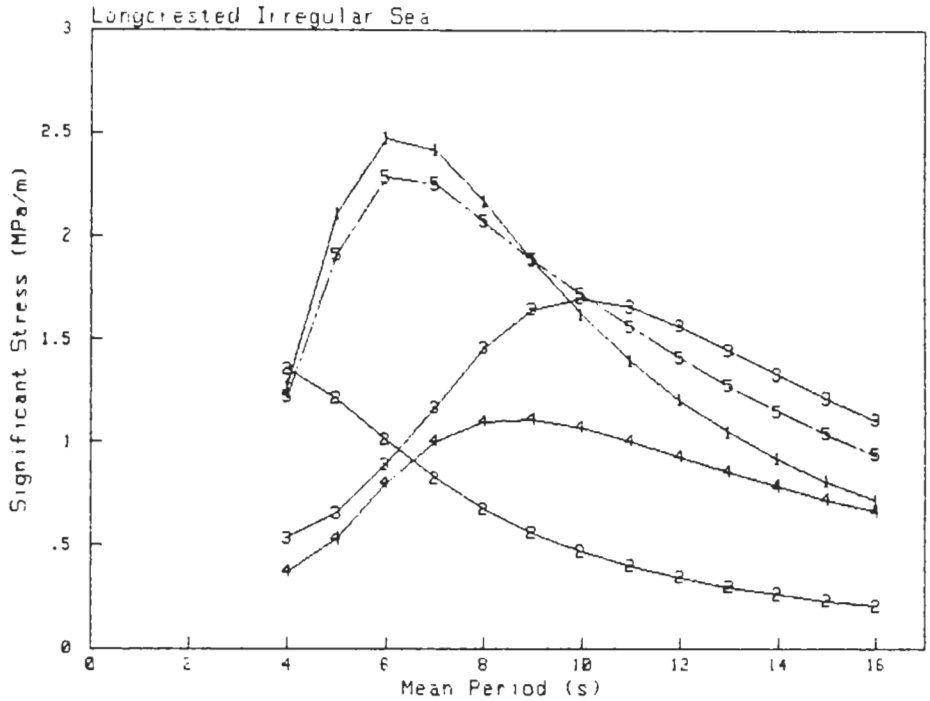

Bottom Side Girder, Position A Hold 4
Shear Stress Components

90°

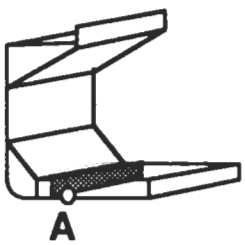

1: Pressure
2: Mass Force
3: Combined
4: Correlation Coefficient Shear/Normal Stress

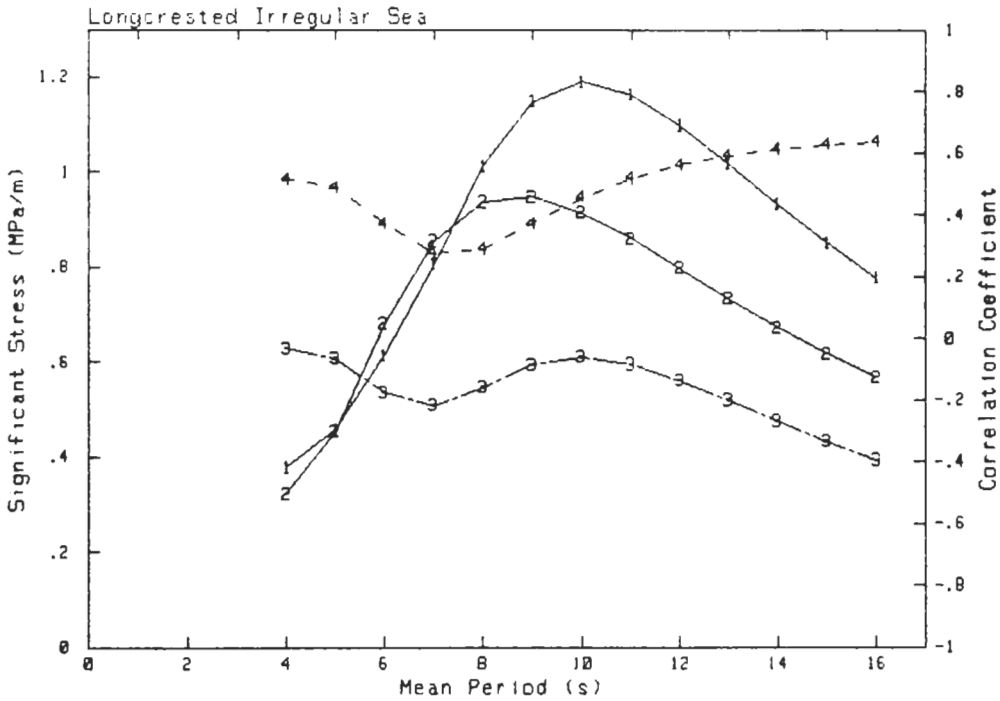

Bottom Side Girder, Position A Hold 4
Normal Stress Components

135°

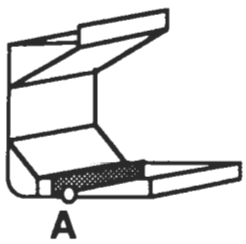

1: Vertical Bending
2: Horizontal Bending
3: Pressure
4: Mass Force
5: Combined

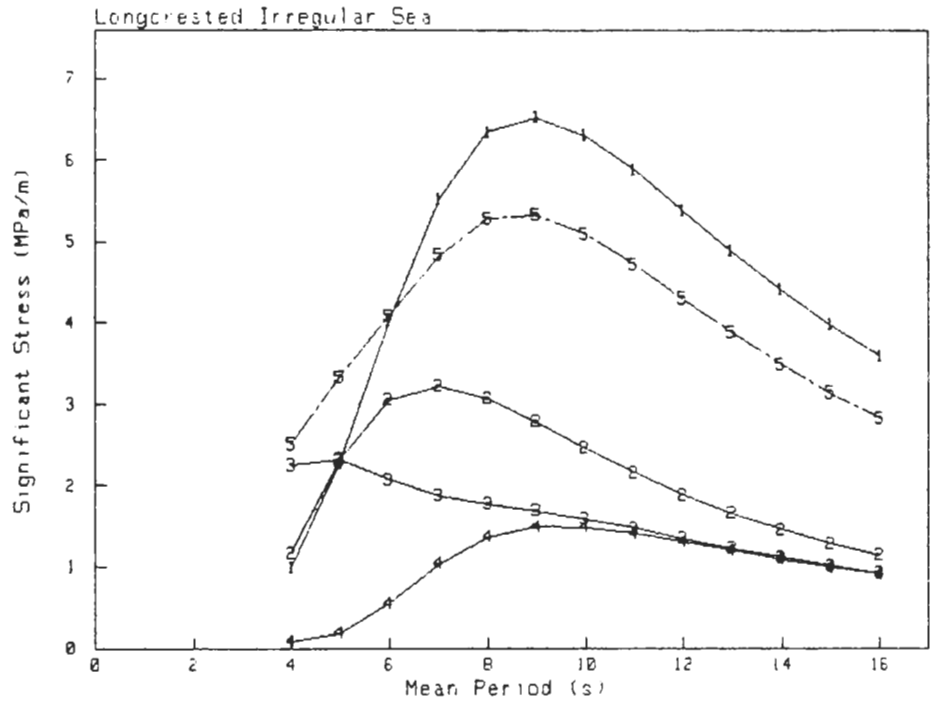

Bottom Side Girder, Position A Hold 4
Shear Stress Components

135°

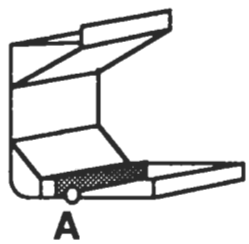

1: Pressure
2: Mass Force
3: Combined
4: Correlation Coefficient
Shear/Normal Stress

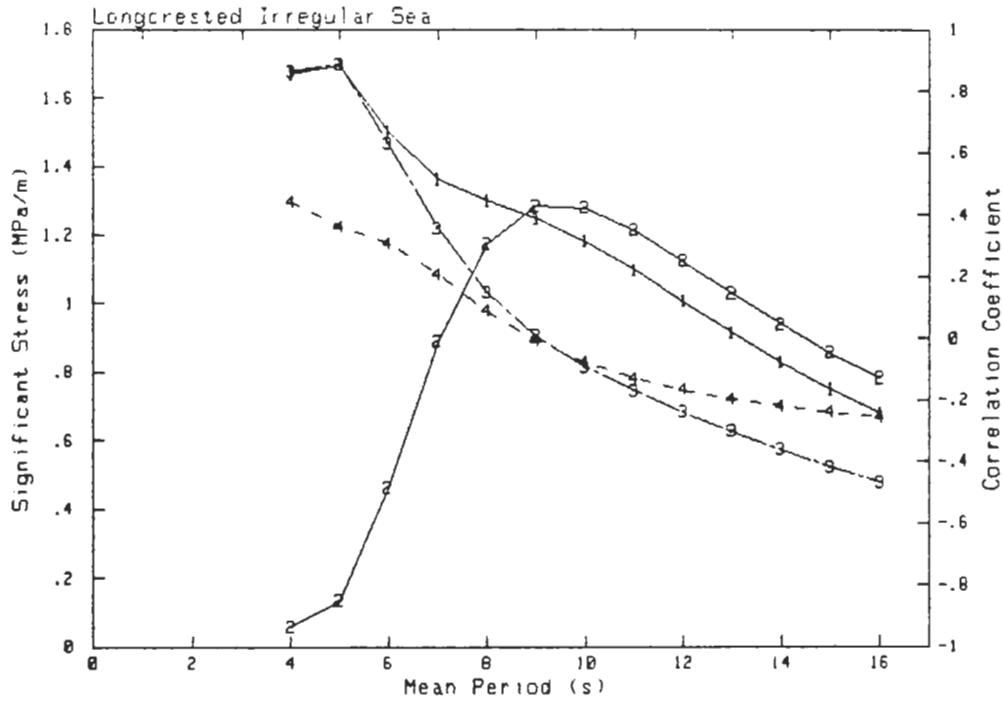

Bottom Side Girder, Position A Hold 4
Normal Stress Components

180°

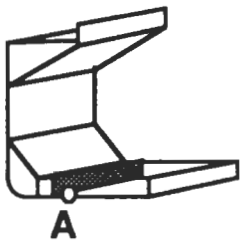

1: Vertical Bending
2: Horizontal Bending
3: Pressure
4: Mass Force
5: Combined

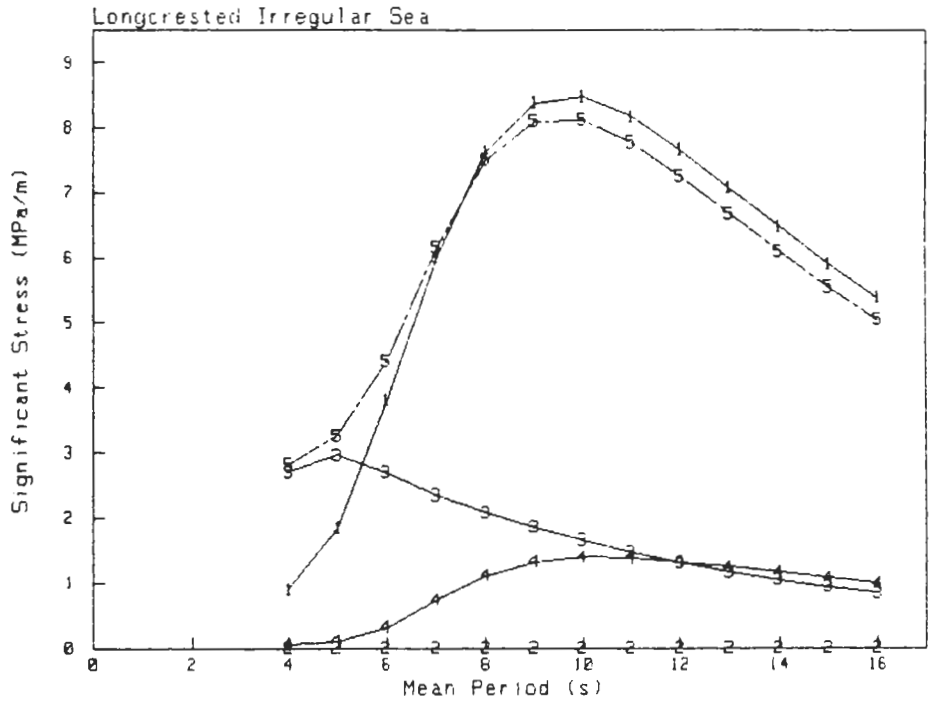

Bottom Side Girder, Position A Hold 4
Shear Stress Components

180°

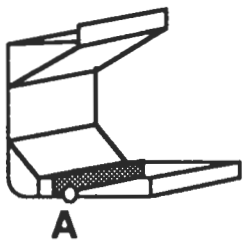

1: Pressure
2: Mass Force
3: Combined
4: Correlation Coefficient
Shear/Normal Stress

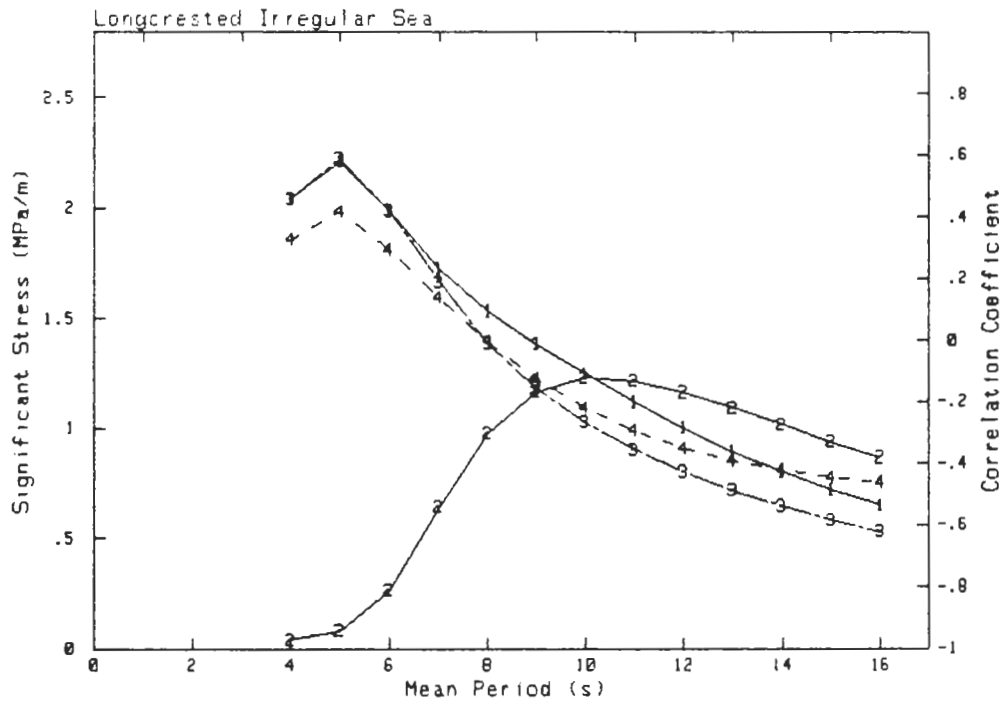

Bottom Side Girder, Position A Hold 4
Normal Stress Components

-135°

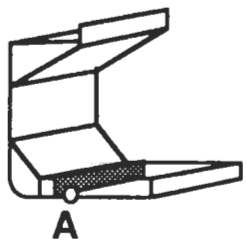

1: Vertical Bending
2: Horizontal Bending
3: Pressure
4: Mass Force
5: Combined

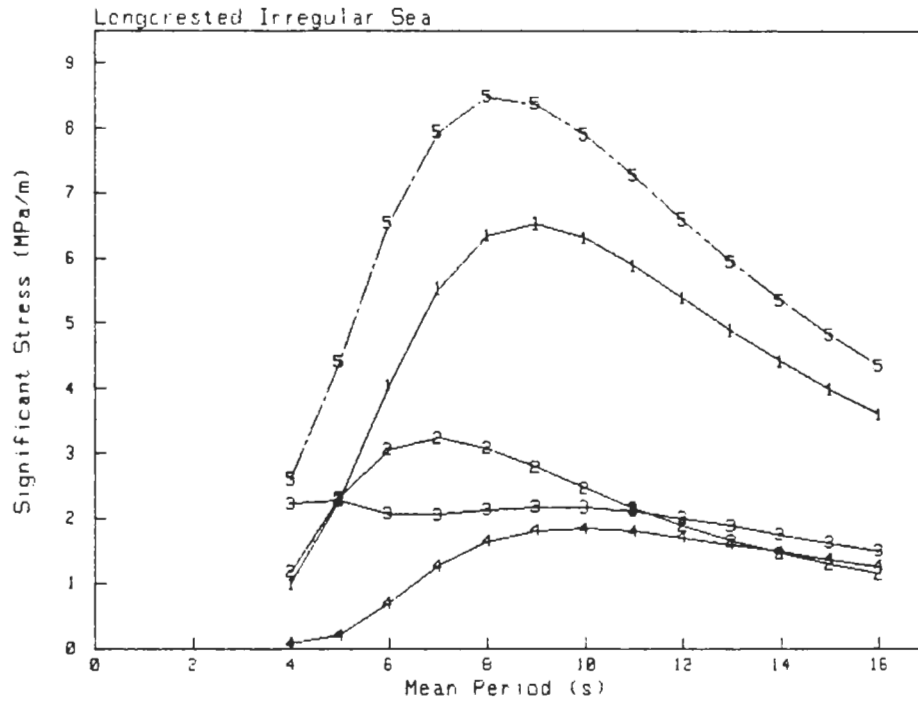

Bottom Side Girder, Position A Hold 4
Shear Stress Components

-135°

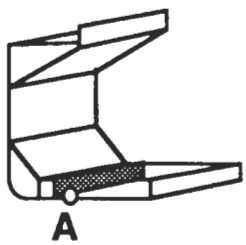

1: Pressure
2: Mass Force
3: Combined
4: Correlation Coefficient
Shear/Normal Stress

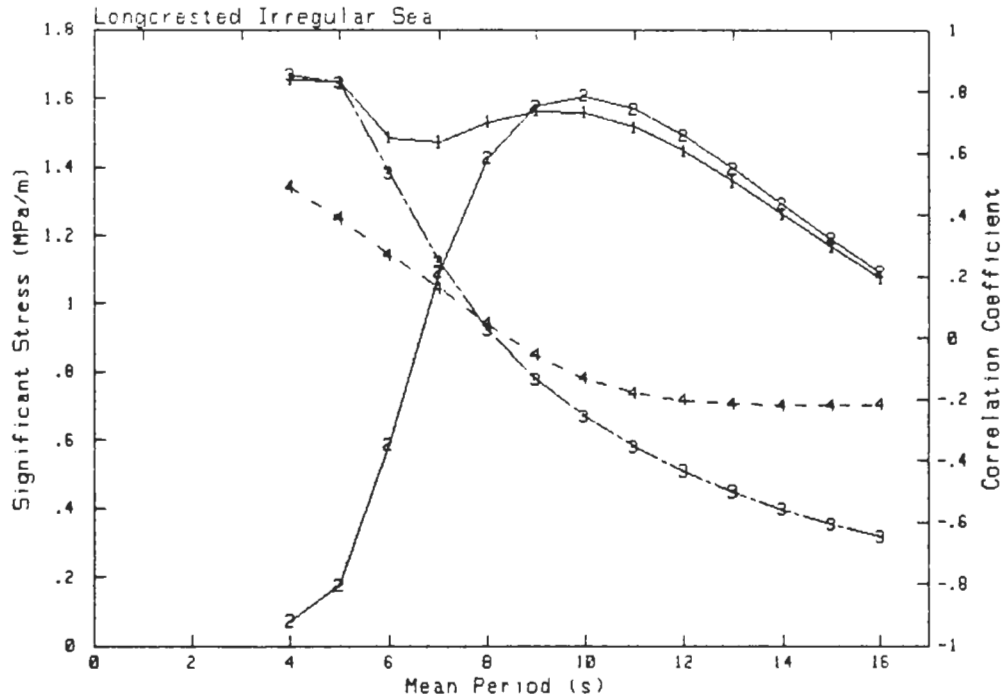

Bottom Side Girder, Position A Hold 4
Normal Stress Components

-90°

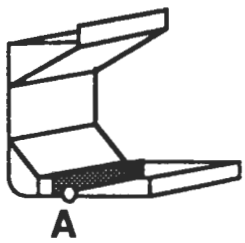

1: Vertical Bending
2: Horizontal Bending
3: Pressure
4: Mass Force
5: Combined

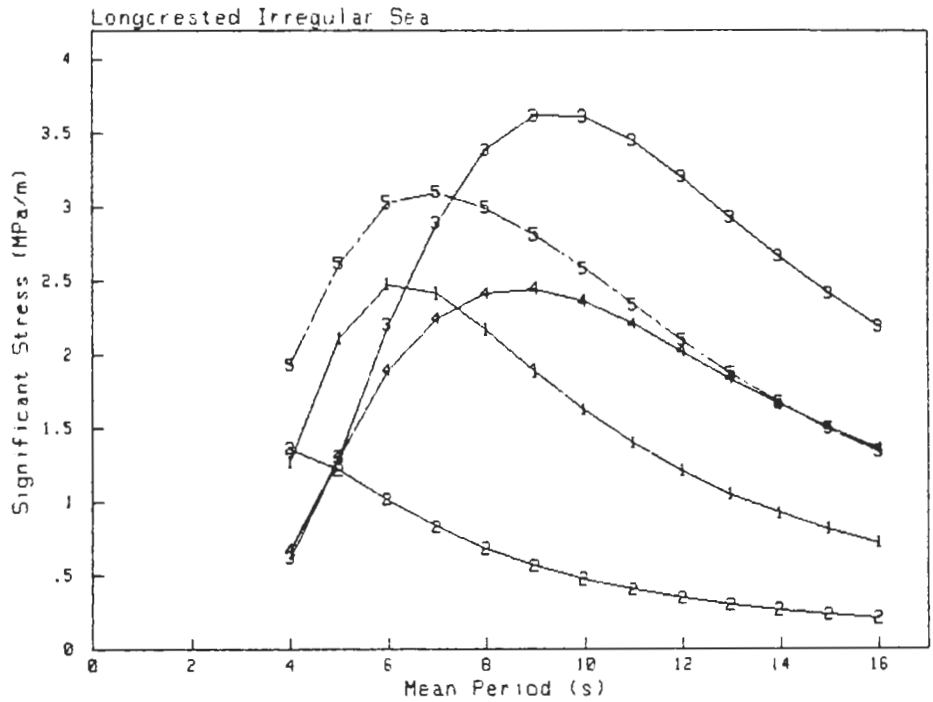

Bottom Side Girder, Position A Hold 4
Shear Stress Components

-90°

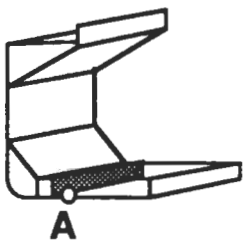

1: Pressure
2: Mass Force
3: Combined
4: Correlation Coefficient Shear/Normal Stress

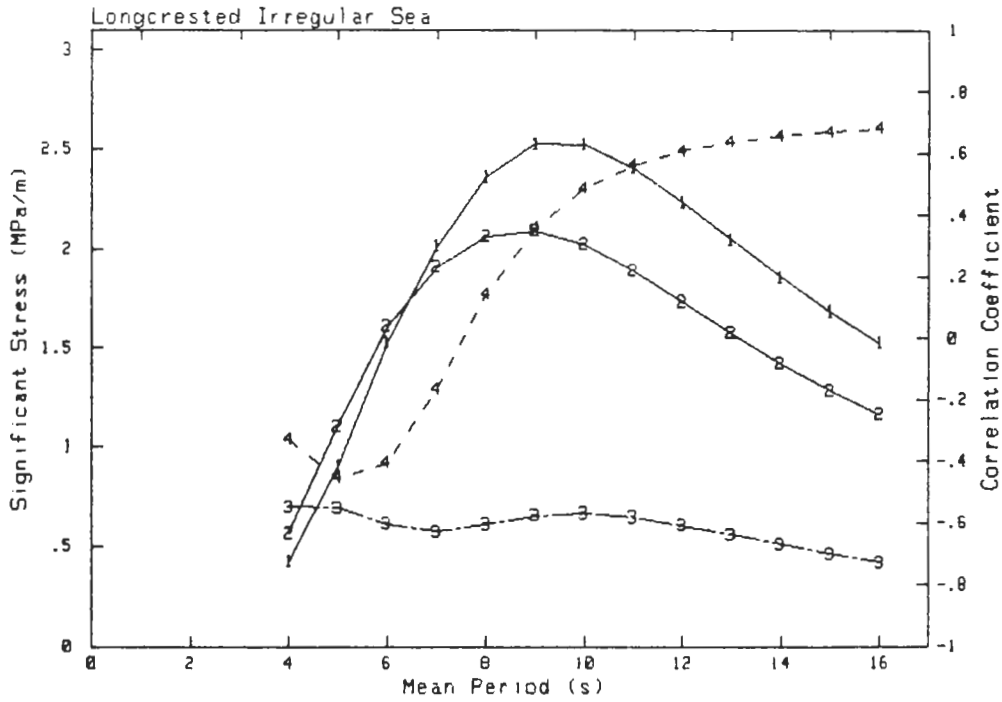

Bottom Side Girder, Position A Hold 4
Normal Stress Components

-45°

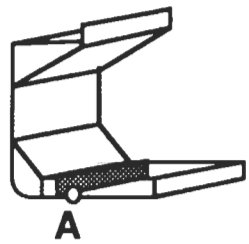

1: Vertical Bending
2: Horizontal Bending
3: Pressure
4: Mass Force
5: Combined

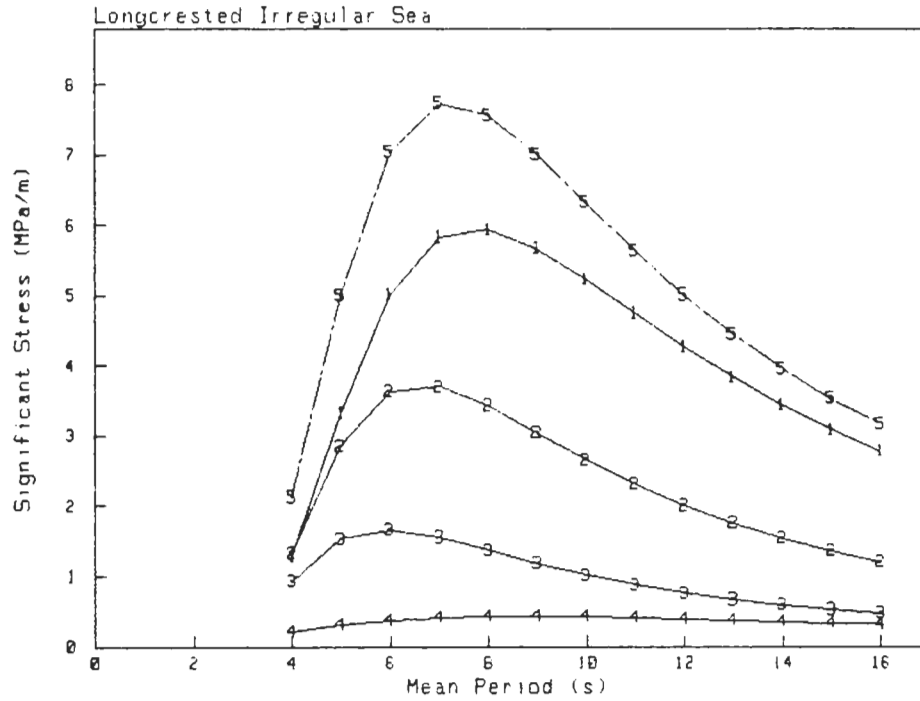

Bottom Side Girder, Position A Hold 4
Shear Stress Components

-45°

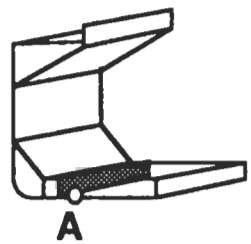

1: Pressure
2: Mass Force
3: Combined
4: Correlation Coefficient
Shear/Normal Stress

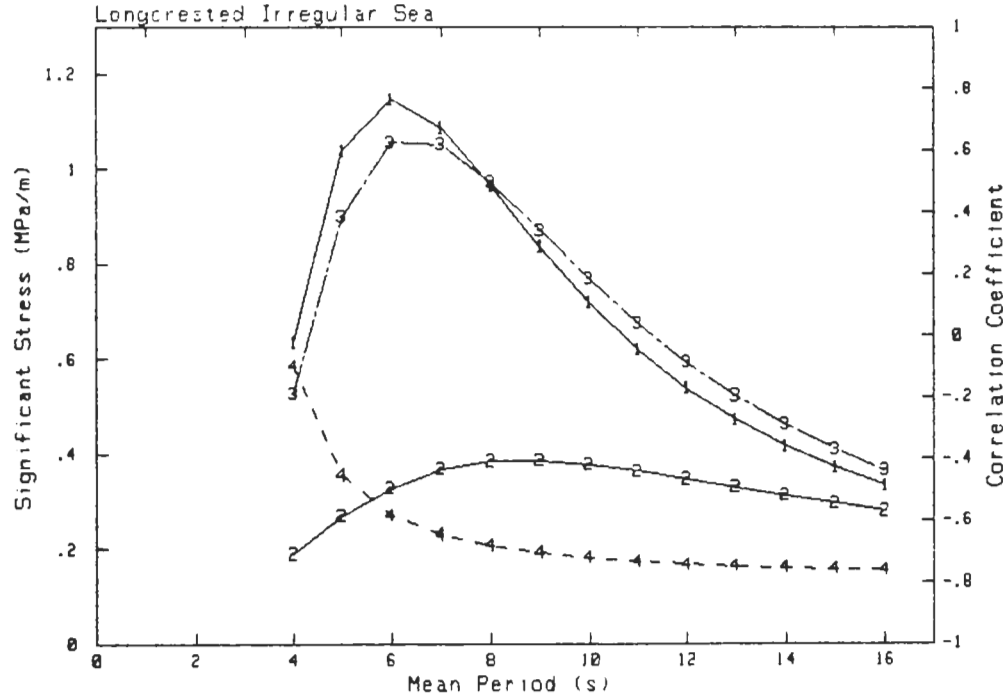

Bottom Side Girder, Position C Hold 4
Normal Stress Components

0°

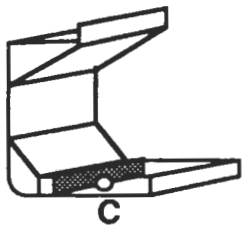

1: Vertical Bending
2: Horizontal Bending
3: Pressure
4: Mass Force
5: Combined

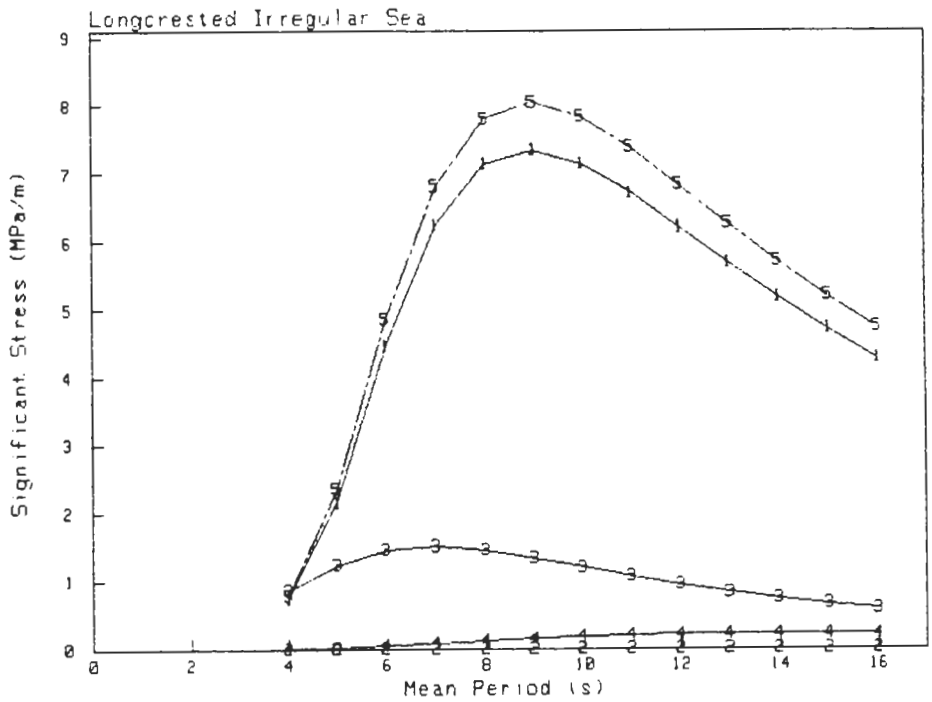

Bottom Side Girder, Position C Hold 4
Normal Stress Correlation Coefficients

0°

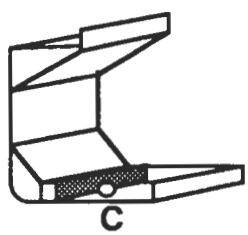

1: Global / Local
2: Pressure / Mass Force

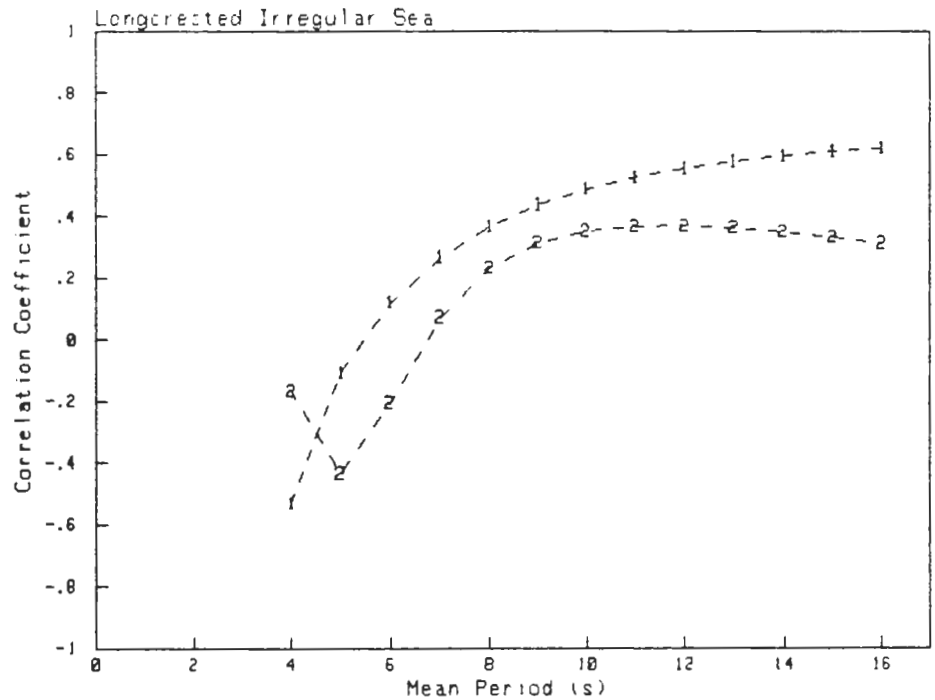

Bottom Side Girder, Position C Hold 4
Normal Stress Components

45°

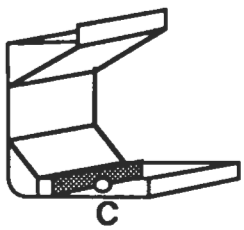

1: Vertical Bending
2: Horizontal Bending
3: Pressure
4: Mass Force
5: Combined

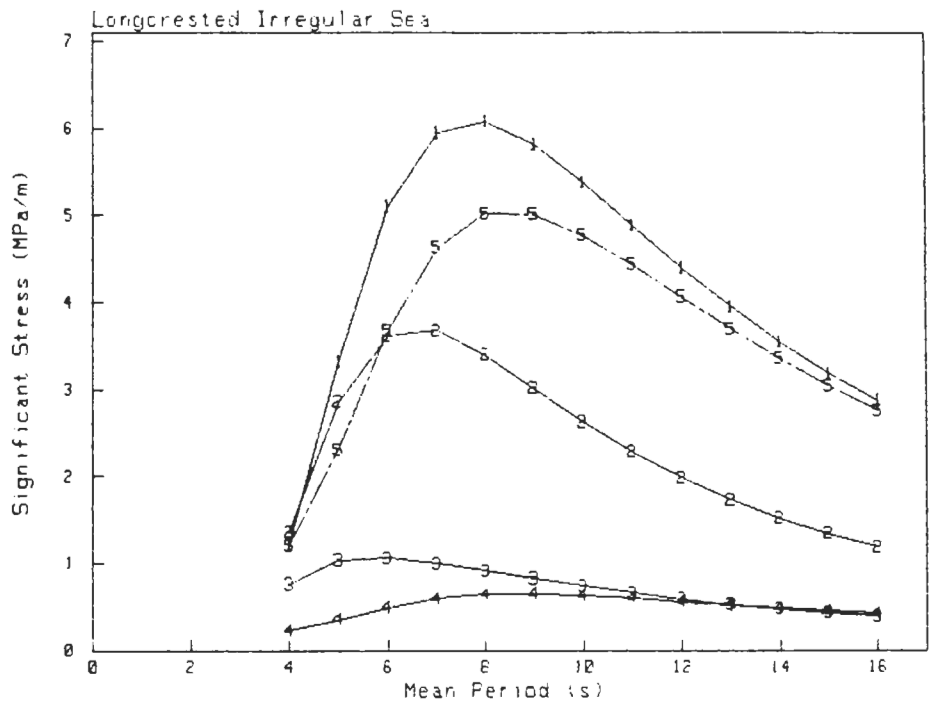

Bottom Side Girder, Position C Hold 4
Normal Stress Correlation Coefficients

45°

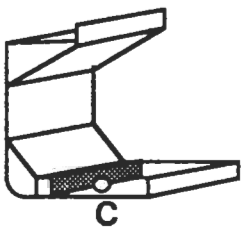

1: Global / Local
2: Pressure / Mass Force
3: Vertical Bending / Horizontal Bending

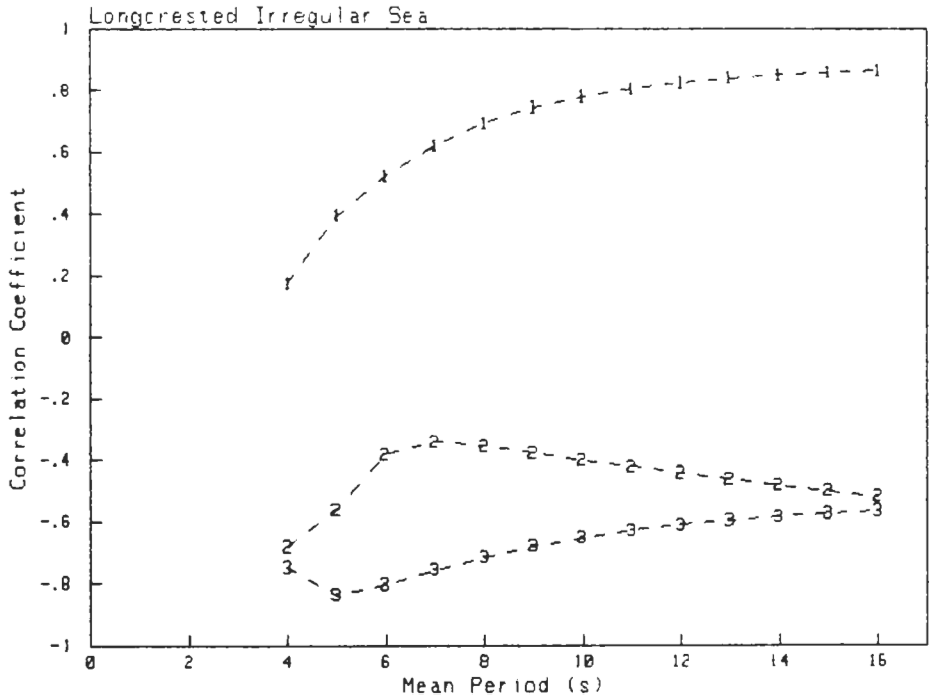

Bottom Side Girder, Position C Hold 4
Normal Stress Components

90°

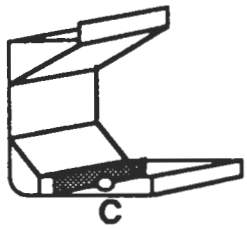

1: Vertical Bending
2: Horizontal Bending
3: Pressure
4: Mass Force
5: Combined

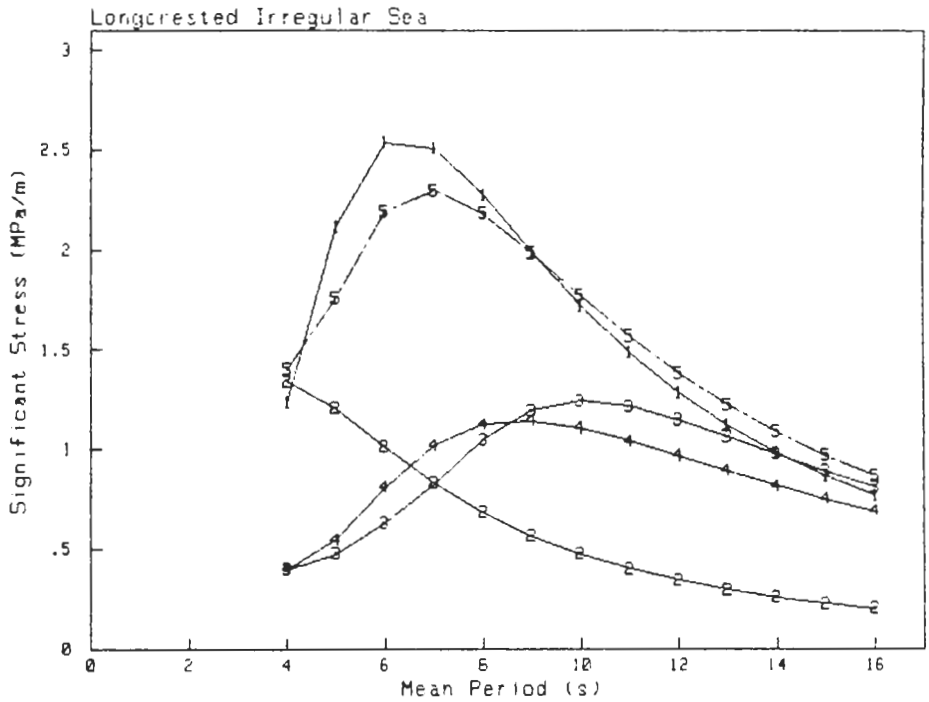

Bottom Side Girder, Position C Hold 4
Normal Stress Correlation Coefficients

90°

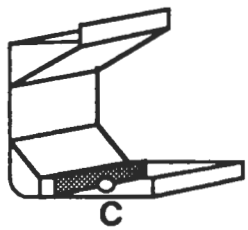

1: Global / Local
2: Pressure / Mass Force
3: Vertical Bending / Horizontal Bending

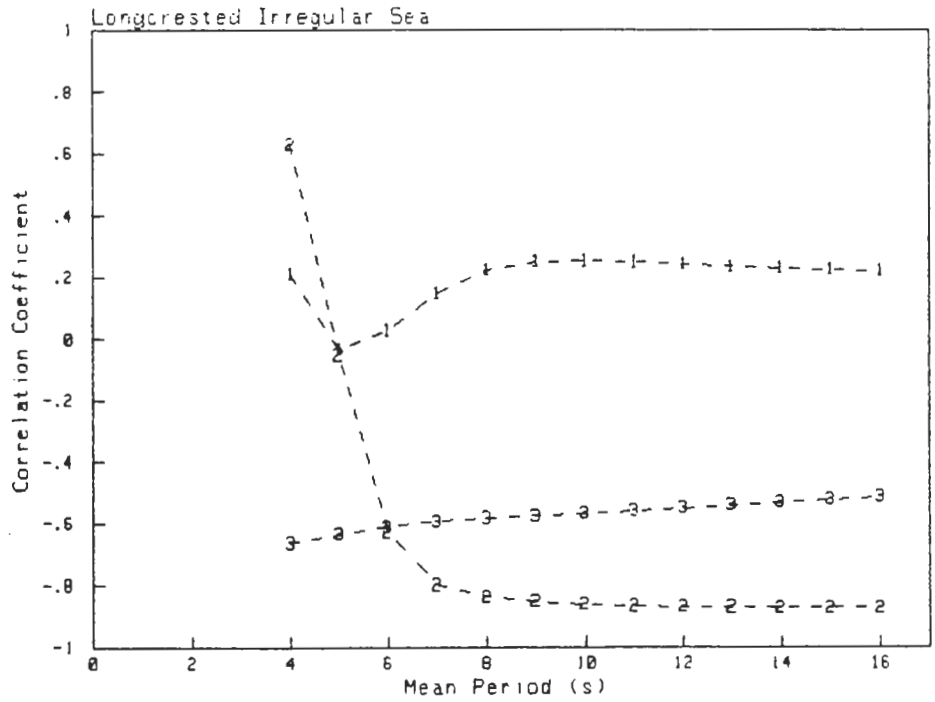

Bottom Side Girder, Position C Hold 4
Normal Stress Components

135°

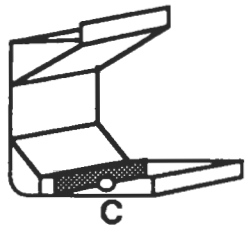

1: Vertical Bending
2: Horizontal Bending
3: Pressure
4: Mass Force
5: Combined

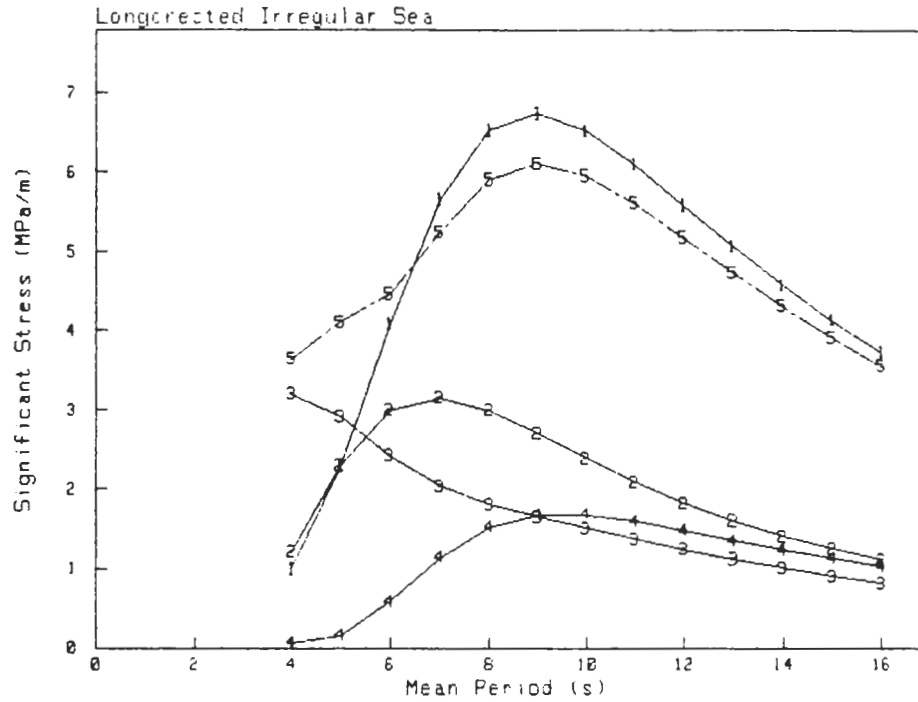

Bottom Side Girder, Position C Hold 4
Normal Stress Correlation Coefficients

135°

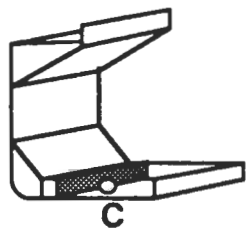

1: Global / Local
2: Pressure / Mass Force
3: Vertical Bending / Horizontal Bending

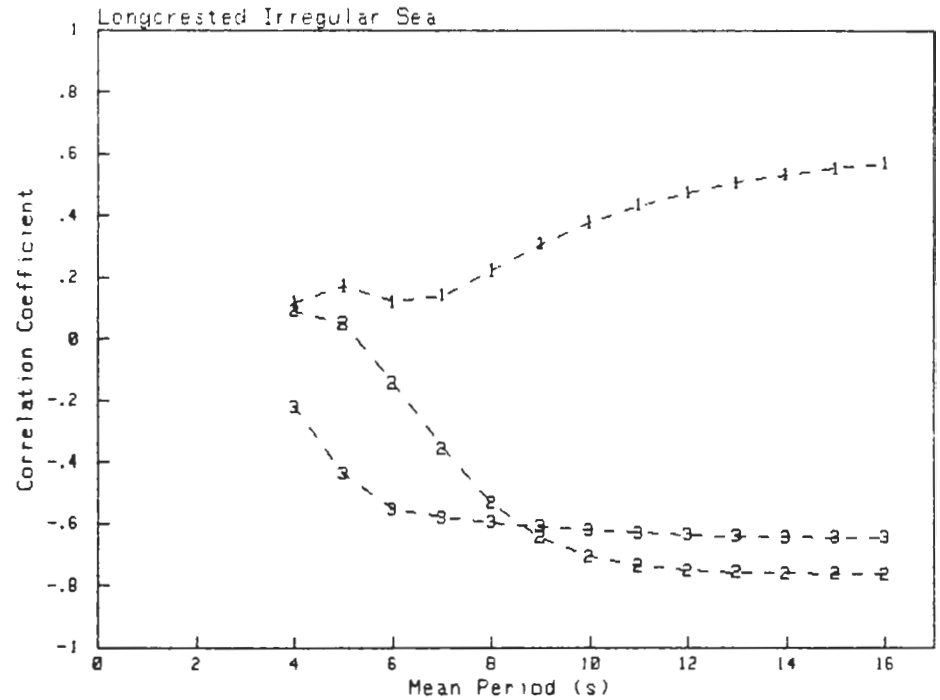

Bottom Side Girder, Position C Hold 4
Normal Stress Components

180°

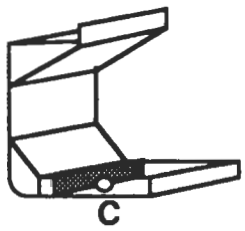

1: Vertical Bending
2: Horizontal Bending
3: Pressure
4: Mass Force
5: Combined

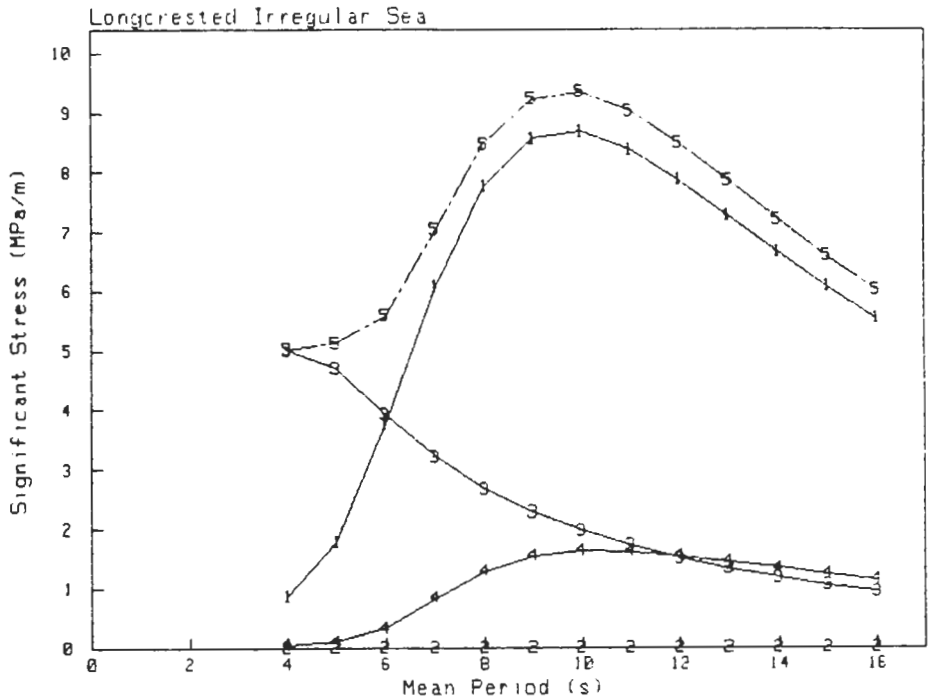

Bottom Side Girder, Position C Hold 4
Normal Stress Correlation Coefficients

180°

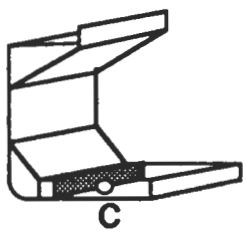

1: Global / Local
2: Pressure / Mass Force

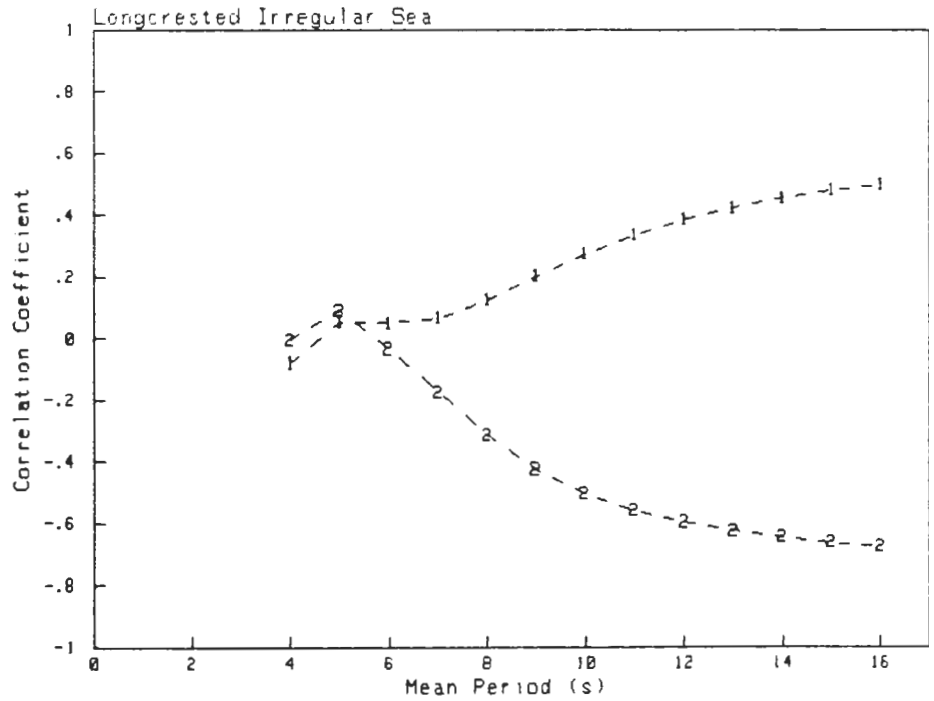

Bottom Side Girder, Position C Hold 4
Normal Stress Components

-135°

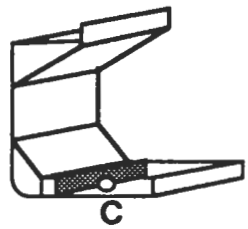

1: Vertical Bending
2: Horizontal Bending
3: Pressure
4: Mass Force
5: Combined

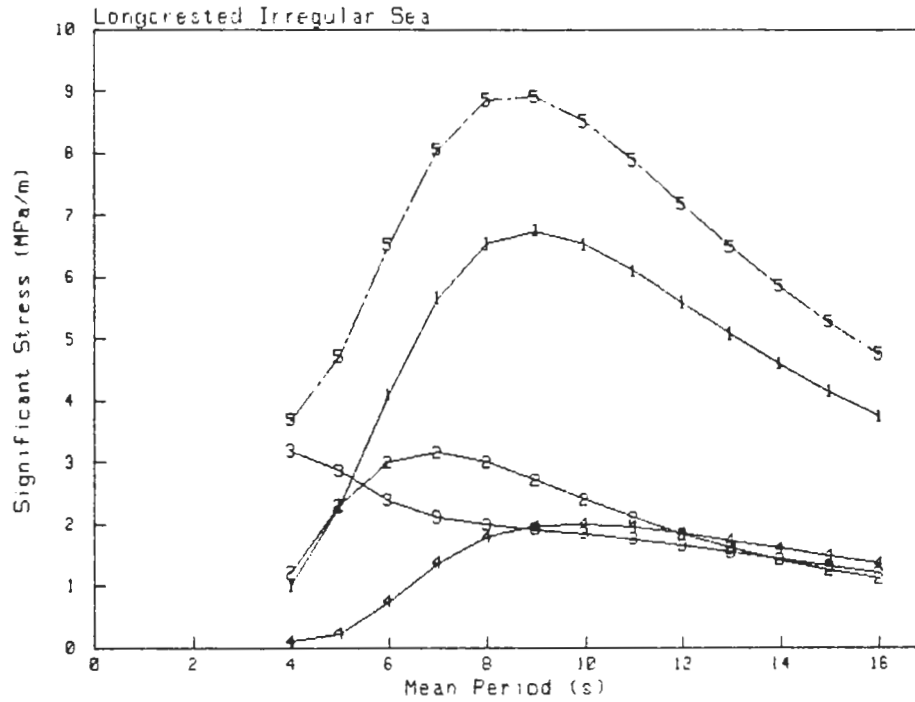

Bottom Side Girder, Position C Hold 4
Normal Stress Correlation Coefficients

-135°

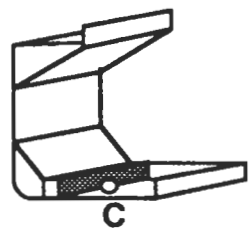

1: Global / Local
2: Pressure / Mass Force
3: Vertical Bending / Horizontal Bending

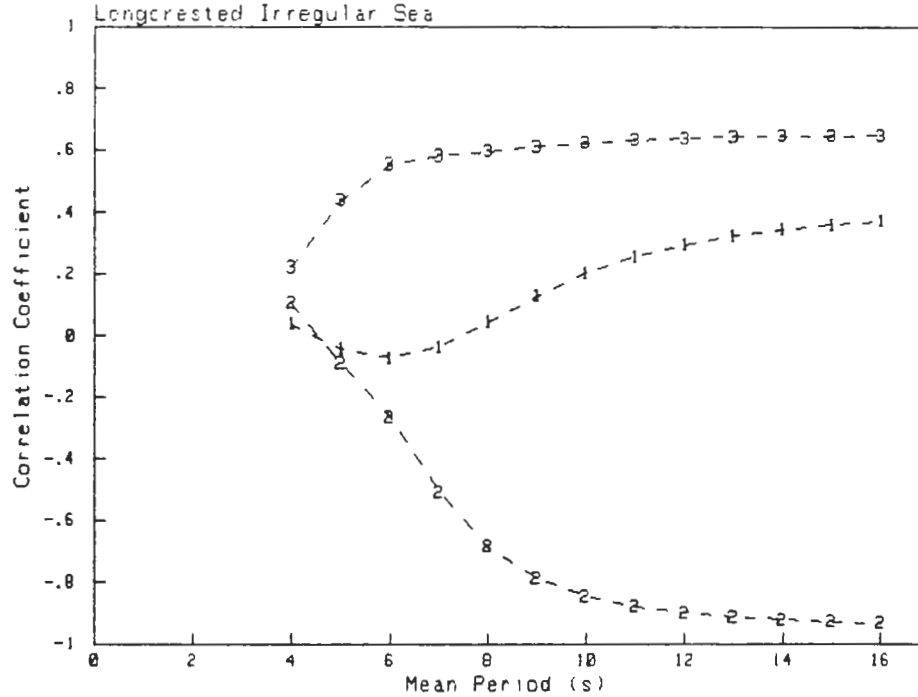

Bottom Side Girder, Position C Hold 4
Normal Stress Components

-90°

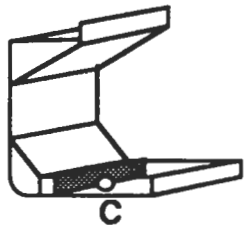

1: Vertical Bending
2: Horizontal Bending
3: Pressure
4: Mass Force
5: Combined

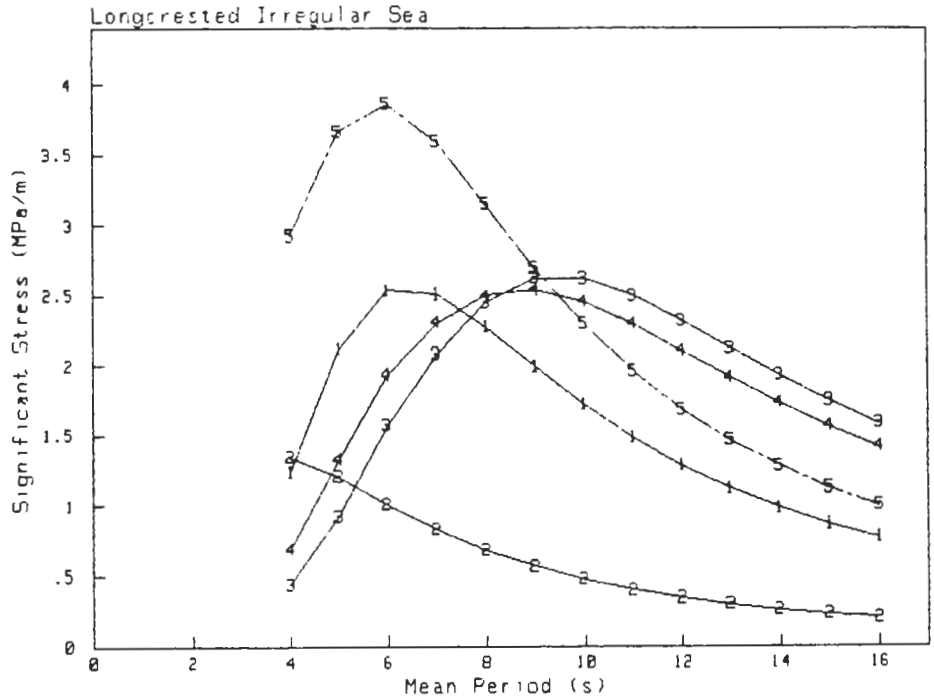

Bottom Side Girder, Position C Hold 4
Normal Stress Correlation Coefficients

-90°

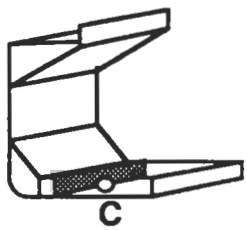

1: Global / Local
2: Pressure / Mass Force
3: Vertical Bending / Horizontal Bending

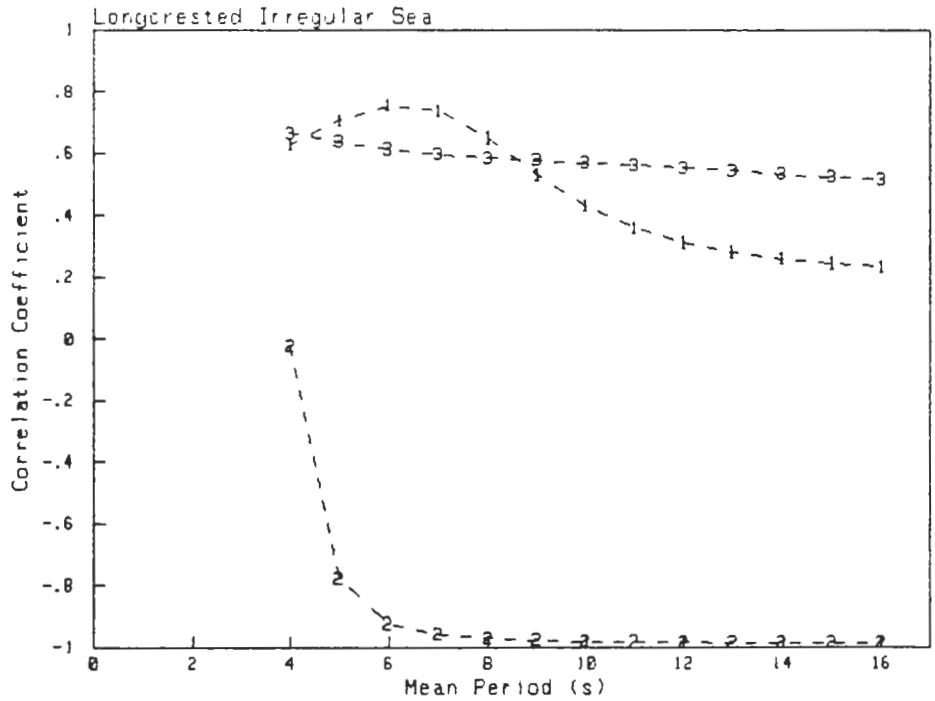

Bottom Side Girder, Position C Hold 4
Normal Stress Components

-45°

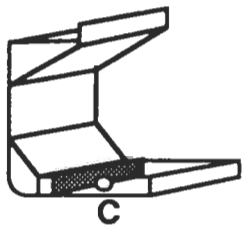

1: Vertical Bending
2: Horizontal Bending
3: Pressure
4: Mass Force
5: Combined

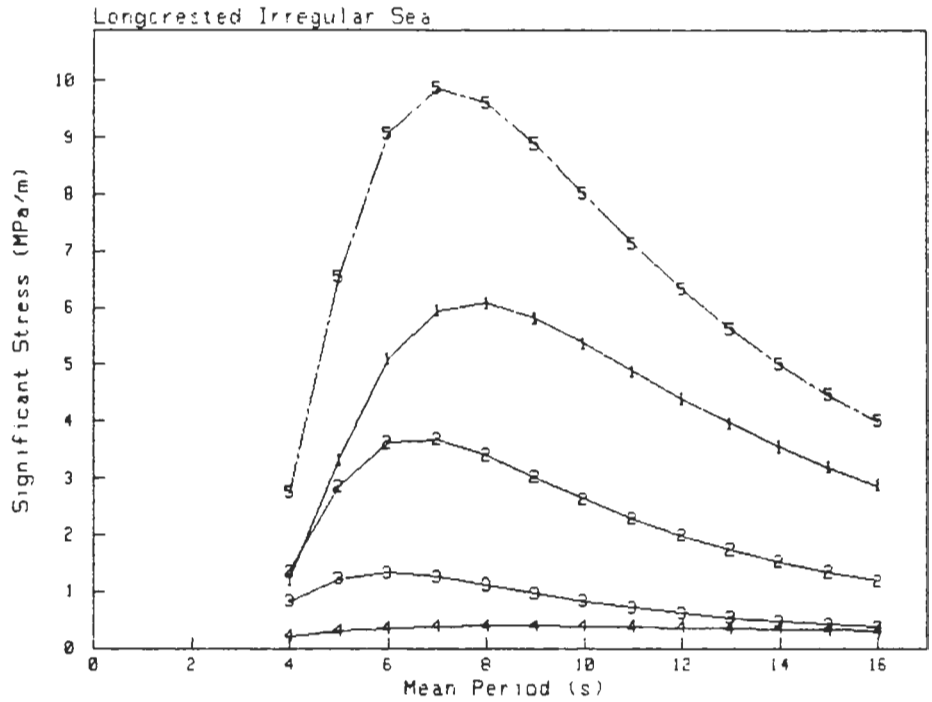

Bottom Side Girder, Position C Hold 4
Normal Stress Correlation Coefficients

-45°

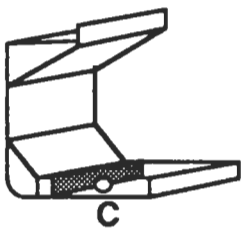

1: Global / Local
2: Pressure / Mass Force
3: Vertical Bending / Horizontal Bending

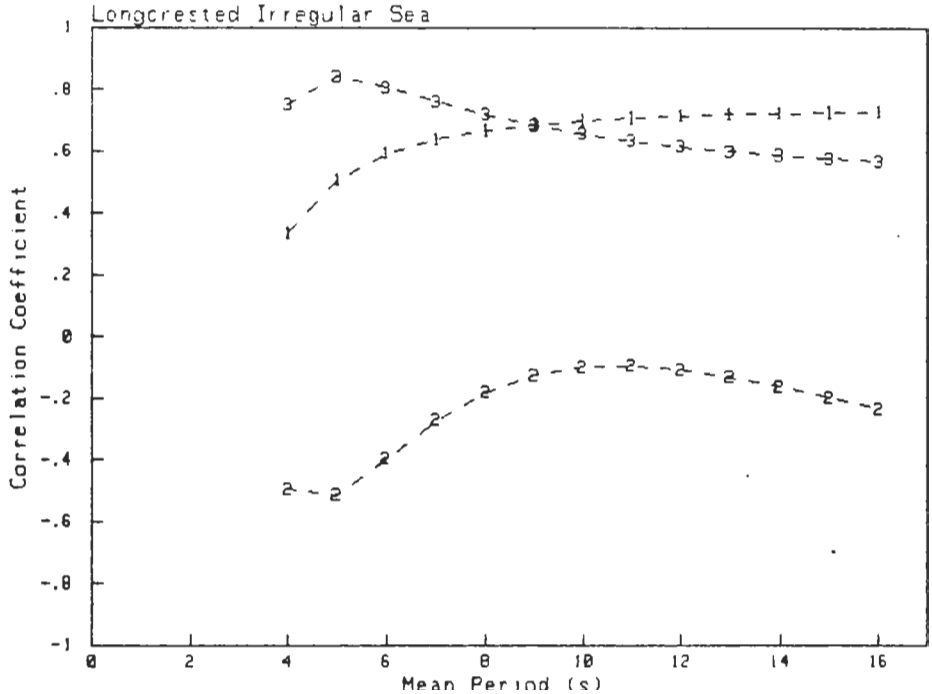

Side Frame, Position L Hold 2
Normal Stress Components

0°

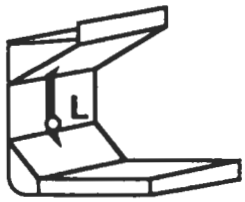

1: Pressure
2: Mass Force
3: Combined linear
4: Correlation Coefficient
Pressure/Mass Force

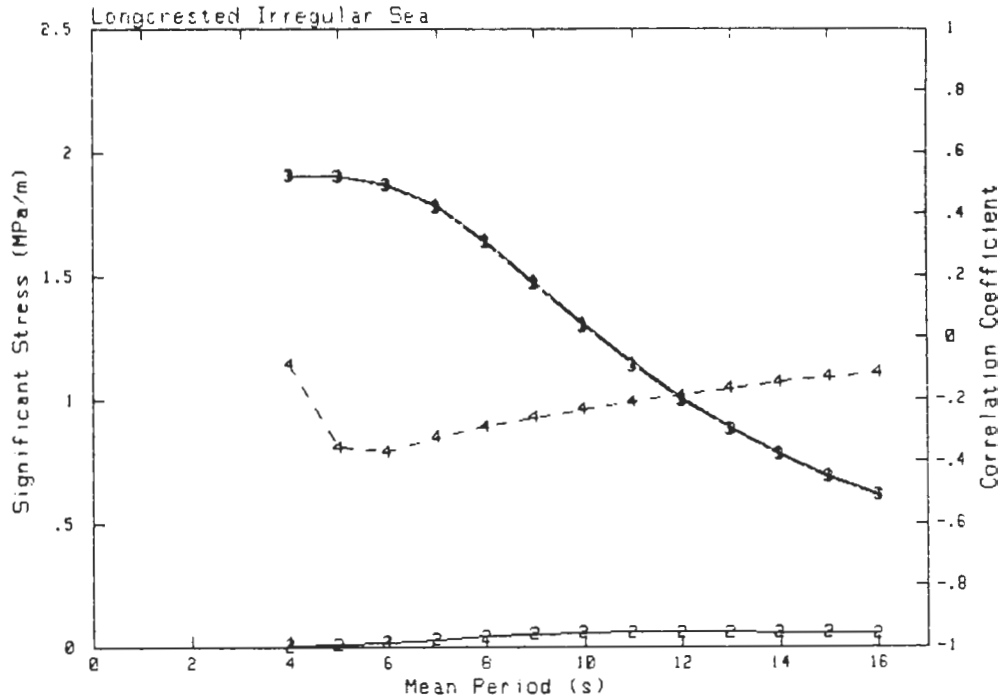

Side Frame, Position L Hold 2
Normal Stress Components

45°

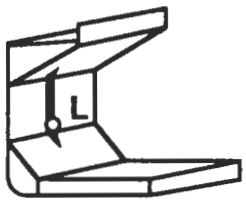

1: Pressure
2: Mass Force
3: Combined linear
4: Correlation Coefficient
Pressure/Mass Force

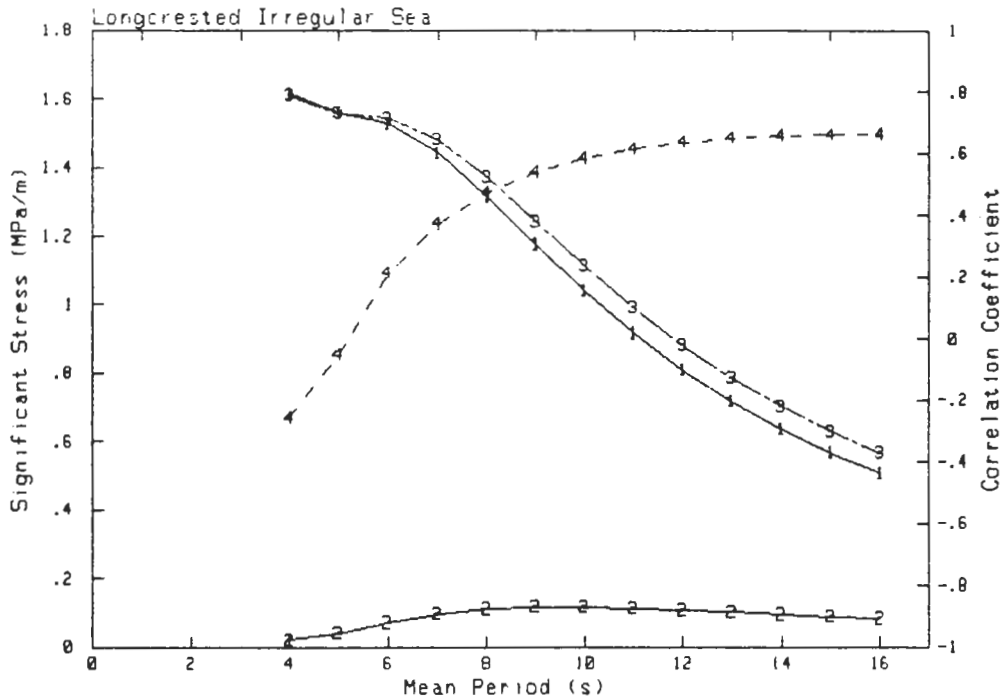

Side Frame, Position L Hold 2
Normal Stress Components

90°

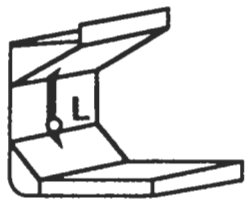

1: Pressure
2: Mass Force
3: Combined linear
4: Correlation Coefficient
Pressure/Mass Force

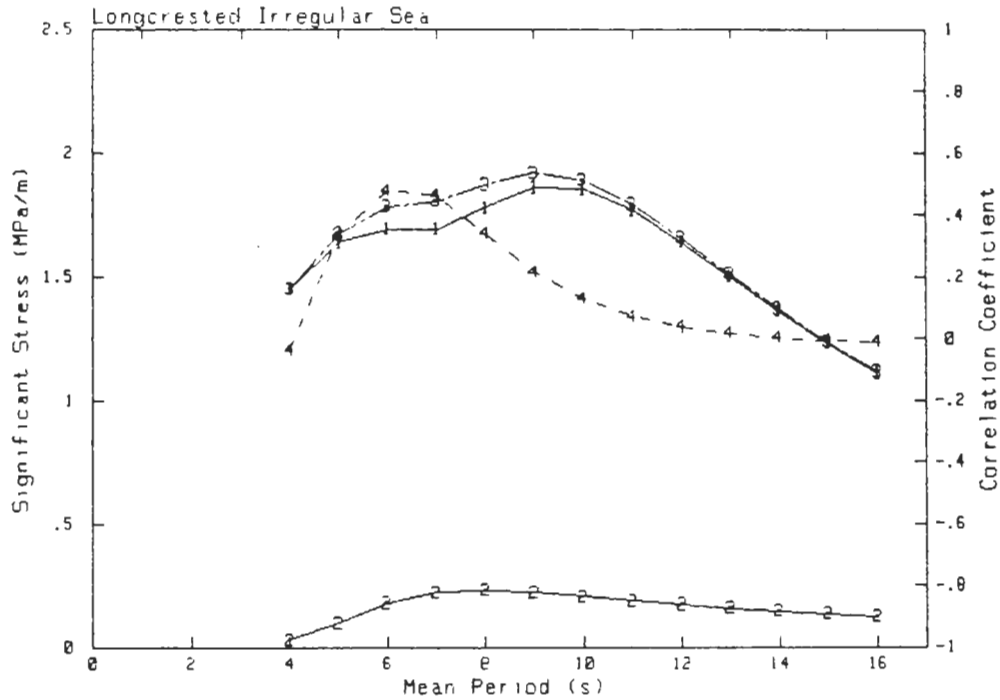

Side Frame, Position L Hold 2
Normal Stress Components

135°

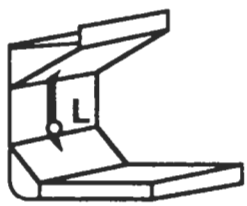

1: Pressure
2: Mass Force
3: Combined linear
4: Correlation Coefficient
Pressure/Mass Force

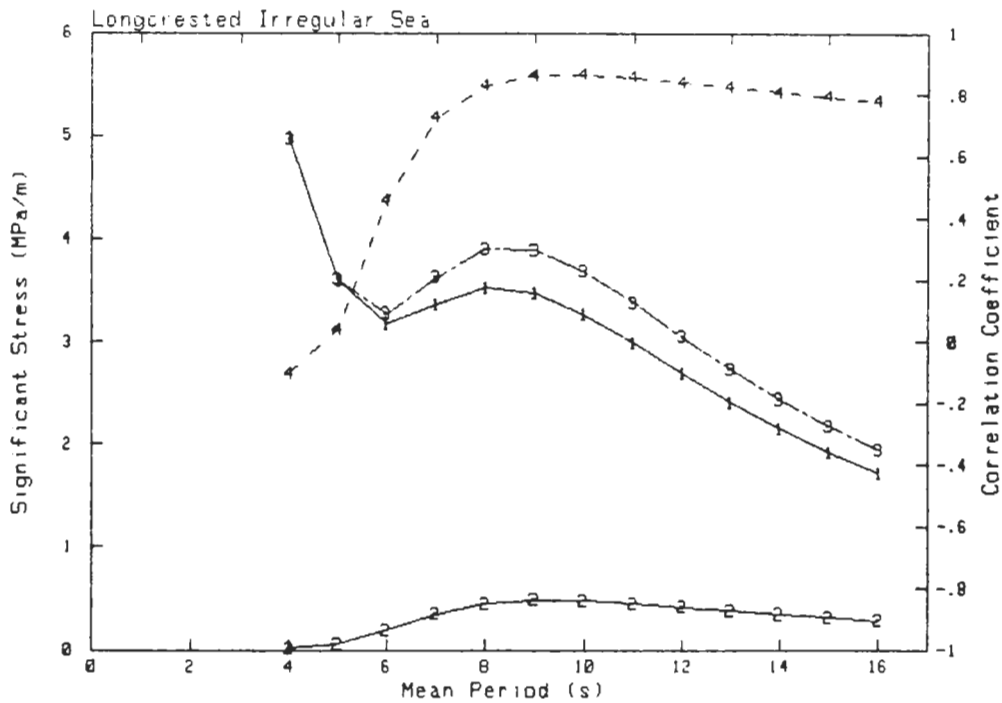

Side Frame, Position L Hold 2
Normal Stress Components

180°

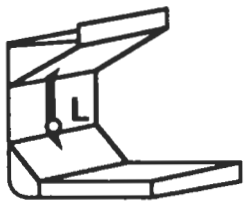

1: Pressure
2: Mass Force
3: Combined linear
4: Correlation Coefficient
Pressure/Mass Force

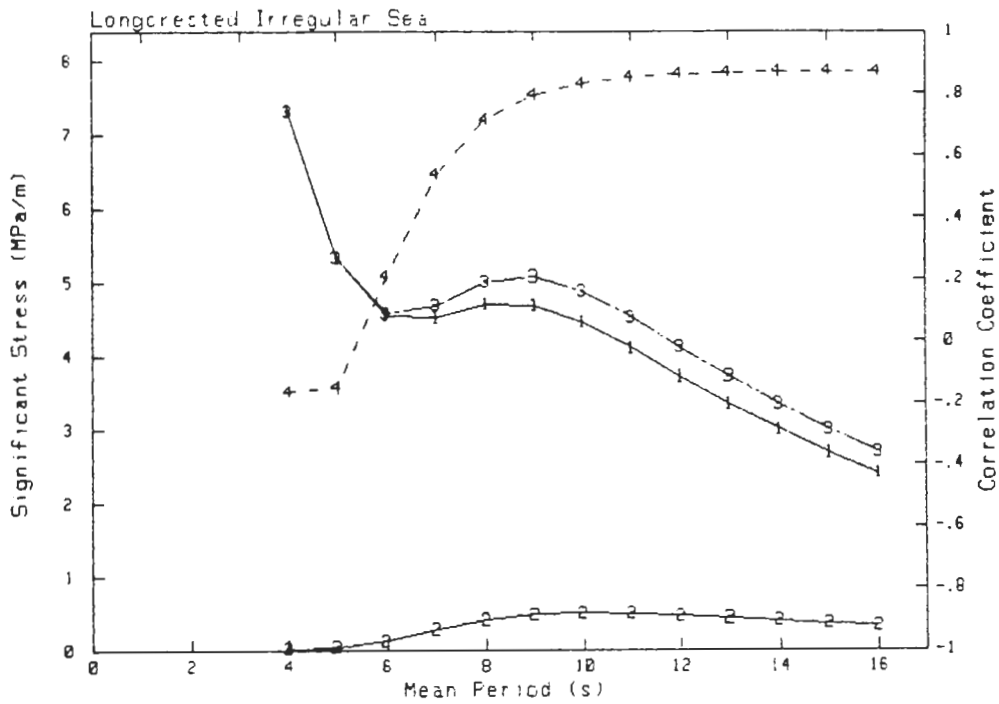

Side Frame, Position L Hold 2
Normal Stress Components

-135°

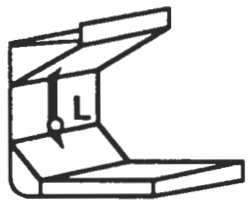

1: Pressure
2: Mass Force
3: Combined linear
4: Correlation Coefficient
Pressure/Mass Force

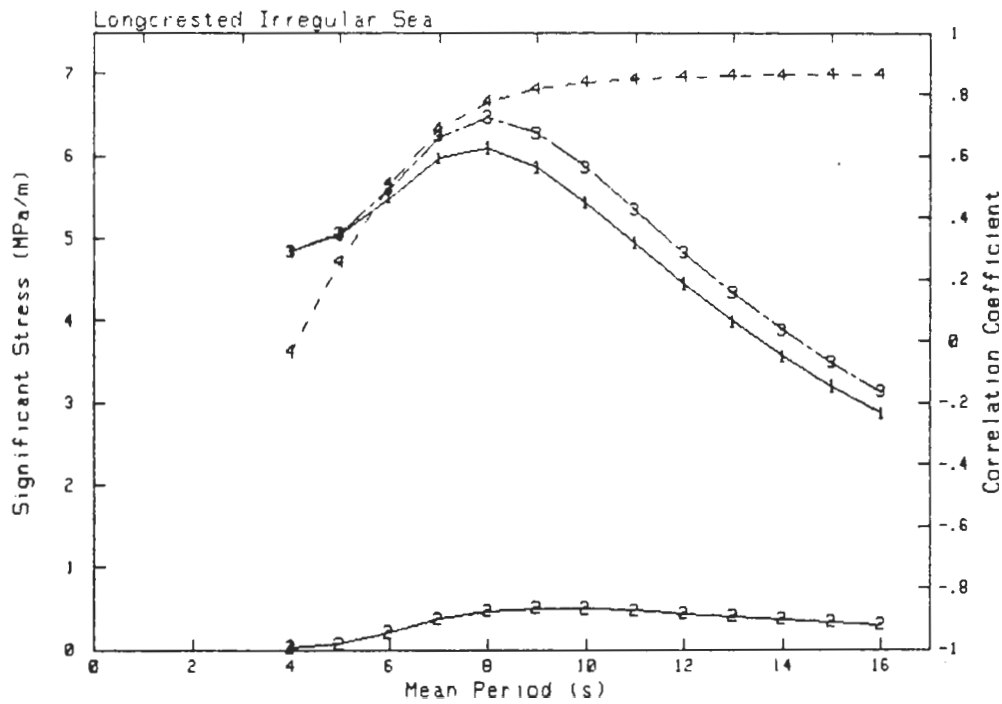

Side Frame, Position L Hold 2
Normal Stress Components

-90°

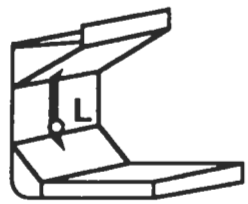

1: Pressure
2: Mass Force
3: Combined linear
4: Correlation Coefficient
Pressure/Mass Force

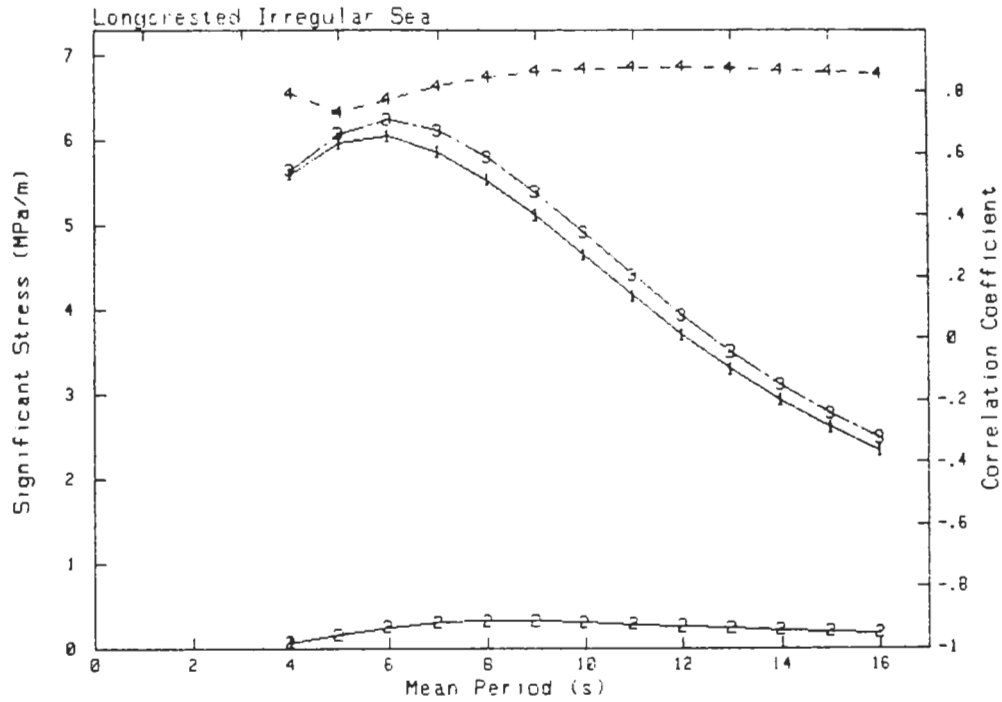

Side Frame, Position L Hold 2
Normal Stress Components

-45°

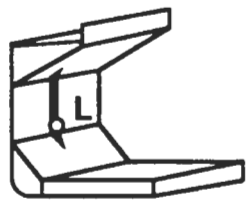

1: Pressure
2: Mass Force
3: Combined linear
4: Correlation Coefficient
Pressure/Mass Force

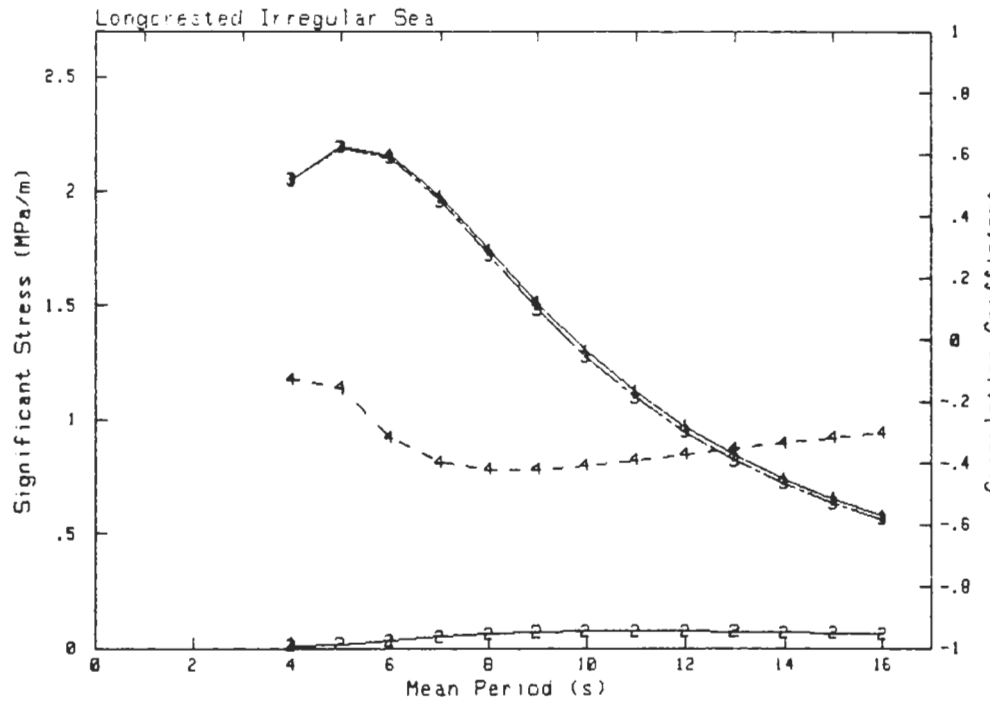

Side Frame, Position M Hold 2
Normal Stress Components

0°

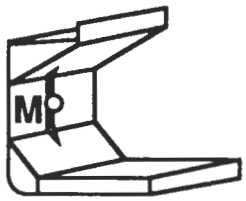

1: Pressure
2: Mass Force
3: Combined linear
4: Correlation Coefficient
Pressure/Mass Force

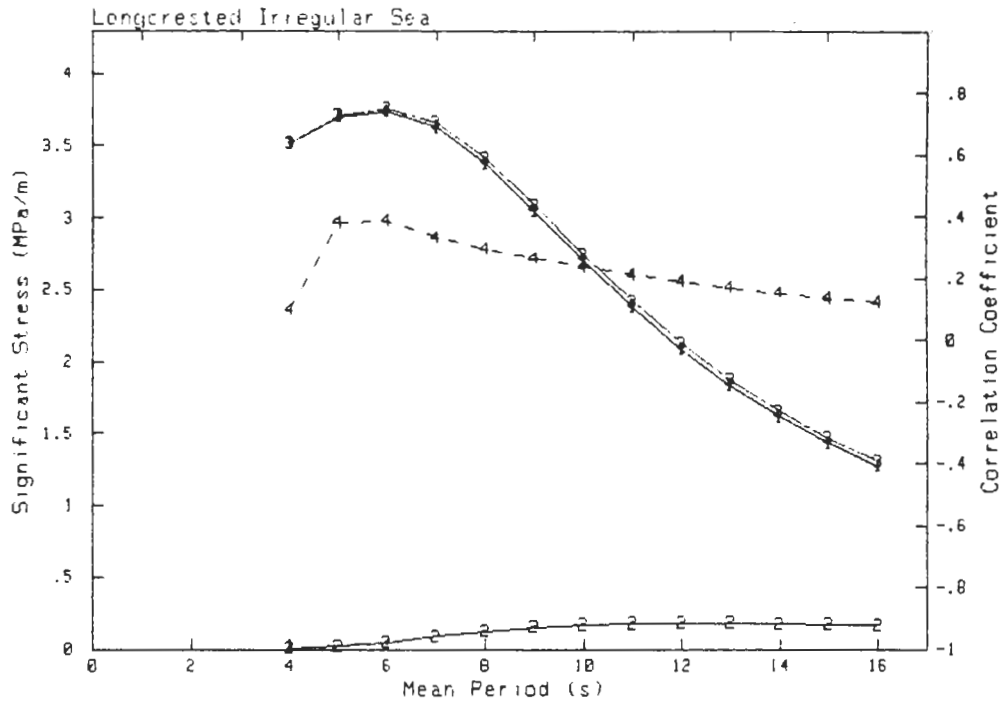

Side Frame, Position M Hold 2
Normal Stress Components

45°

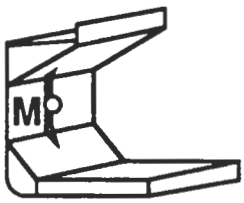

1: Pressure
2: Mass Force
3: Combined linear
4: Correlation Coefficient
Pressure/Mass Force

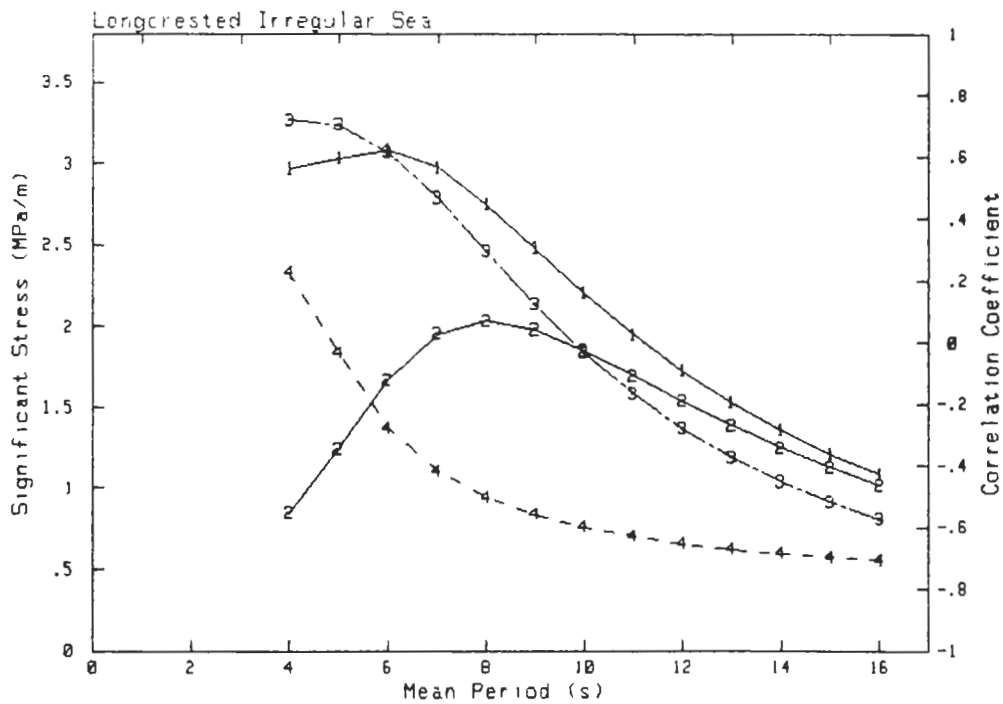

Side Frame, Position M Hold 2
Normal Stress Components

90°

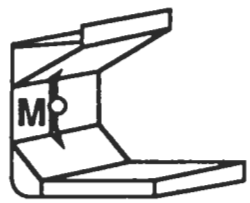

1: Pressure
2: Mass Force
3: Combined linear
4: Correlation Coefficient
Pressure/Mass Force

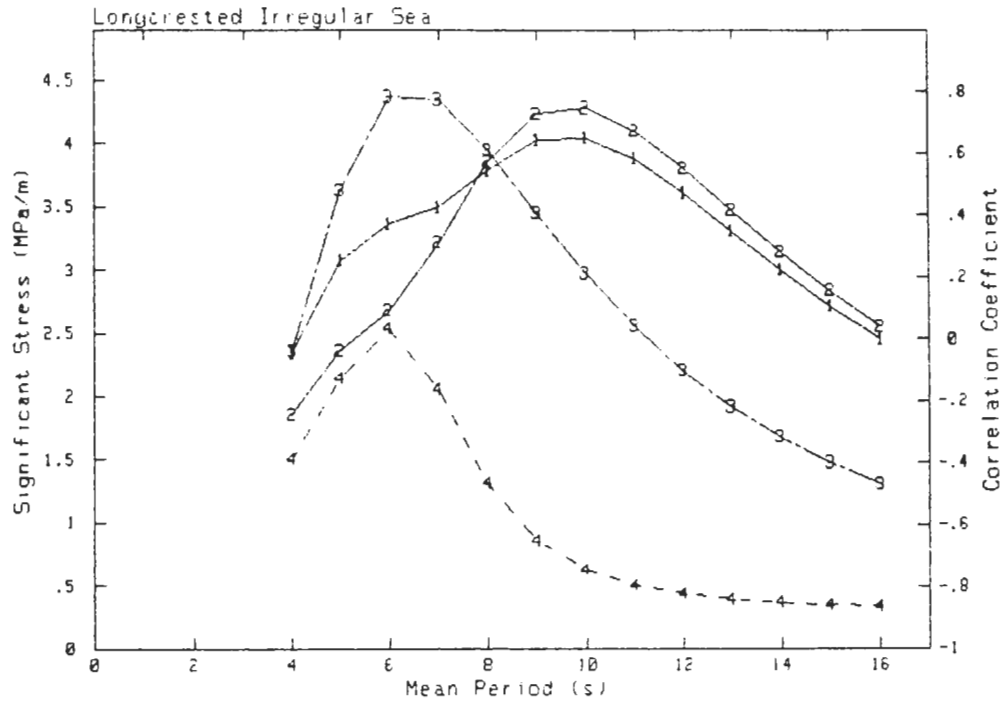

Side Frame, Position M Hold 2
Normal Stress Components

135°

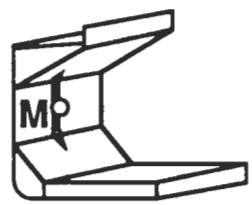

1: Pressure
2: Mass Force
3: Combined linear
4: Correlation Coefficient
Pressure/Mass Force

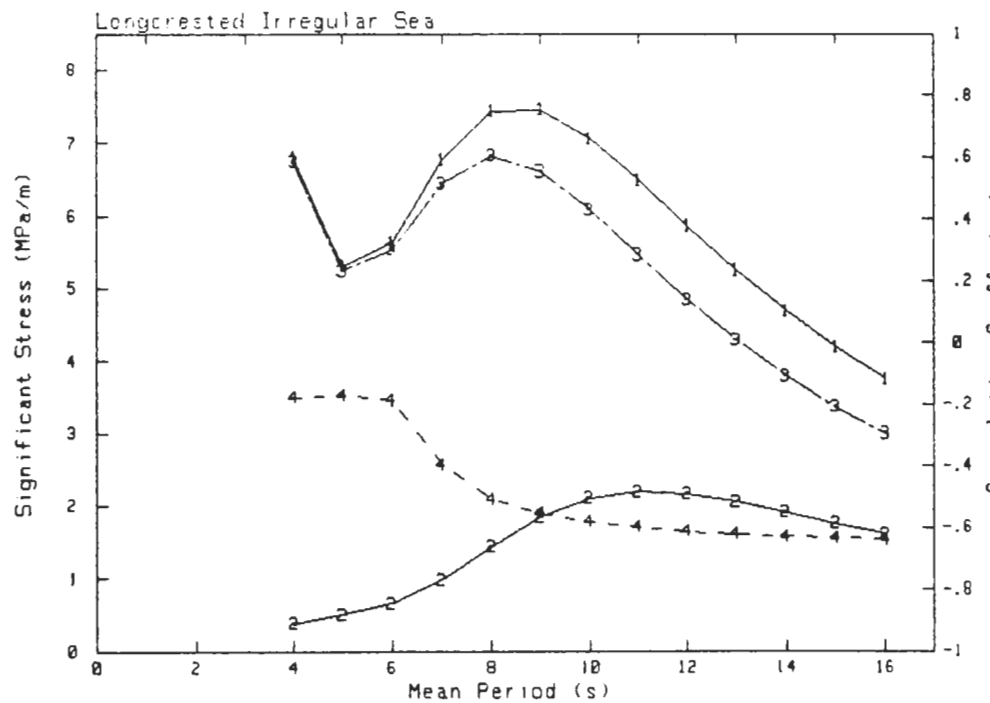

Side Frame, Position M Hold 2
Normal Stress Components

180°

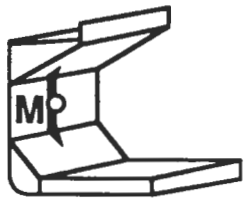

1: Pressure
2: Mass Force
3: Combined linear
4: Correlation Coefficient Pressure/Mass Force

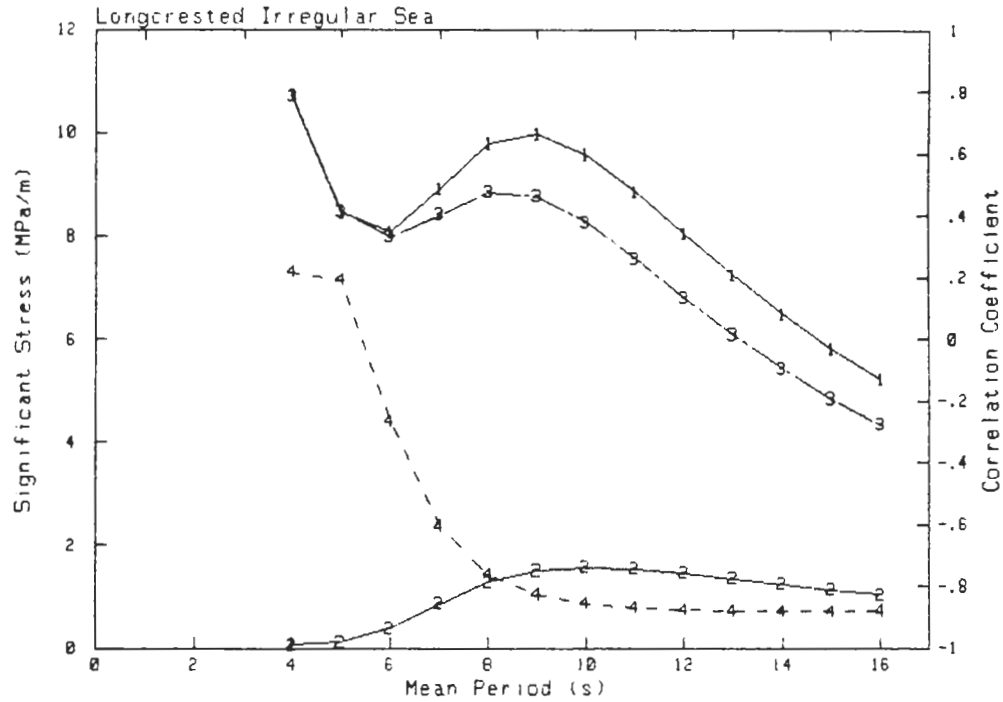

Side Frame, Position M Hold 2
Normal Stress Components

-135°

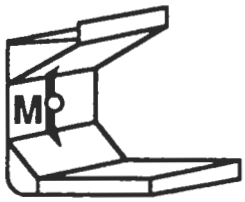

1: Pressure
2: Mass Force
3: Combined linear
4: Correlation Coefficient Pressure/Mass Force

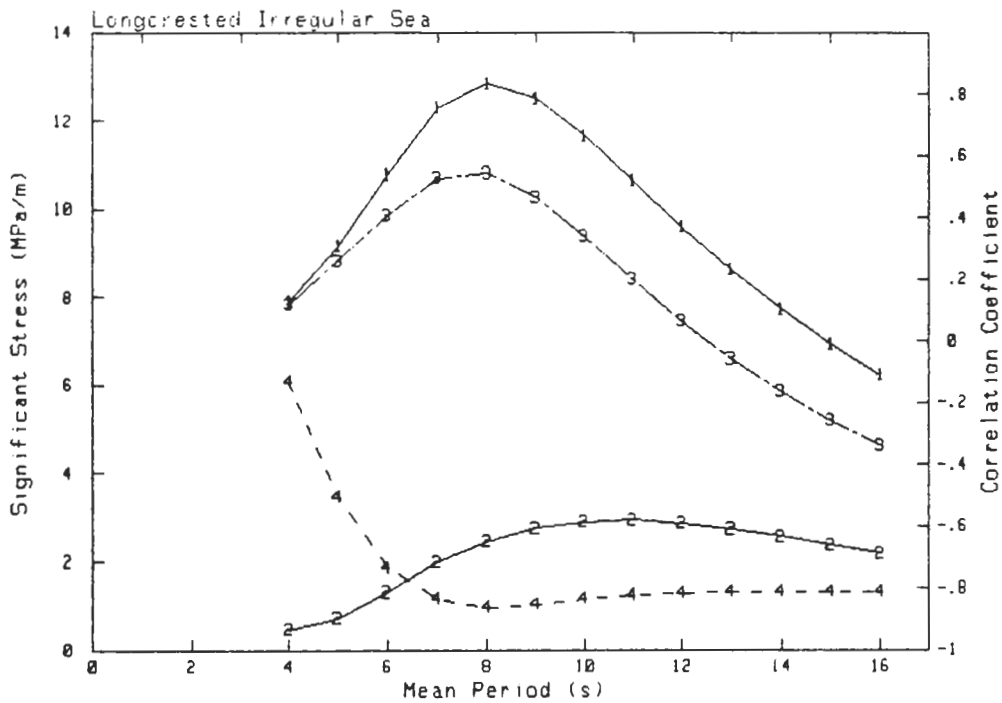

Side Frame, Position M Hold 2
Normal Stress Components

-90°

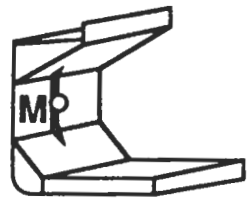

1: Pressure
2: Mass Force
3: Combined linear
4: Correlation Coefficient Pressure/Mass Force

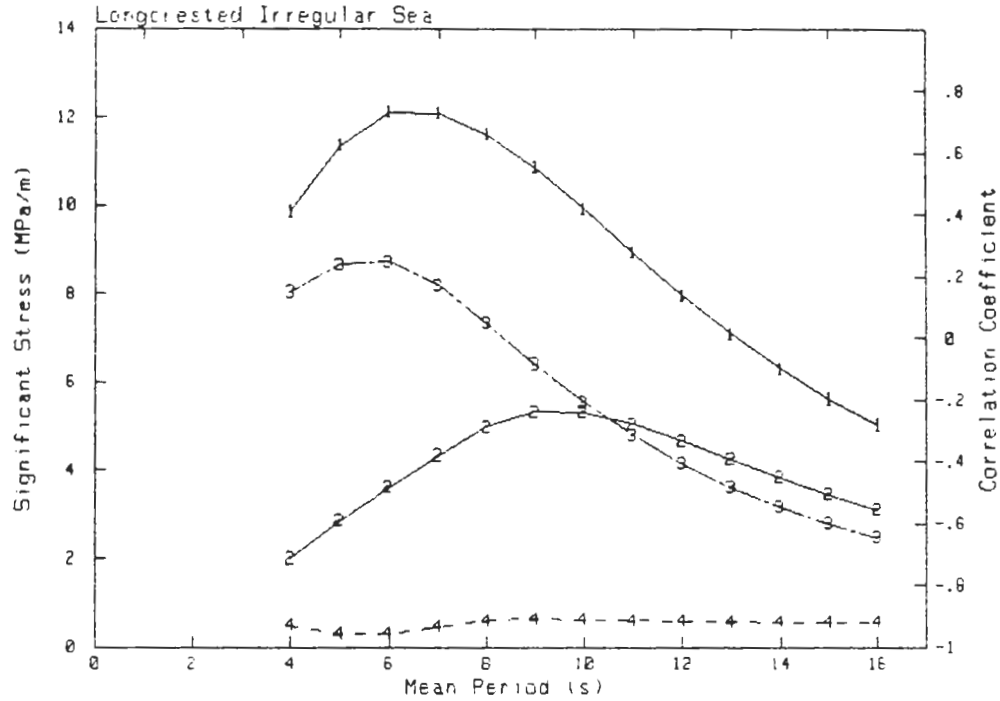

Side Frame, Position M Hold 2
Normal Stress Components

-45°

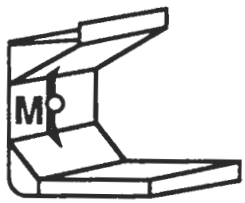

1: Pressure
2: Mass Force
3: Combined linear
4: Correlation Coefficient Pressure/Mass Force

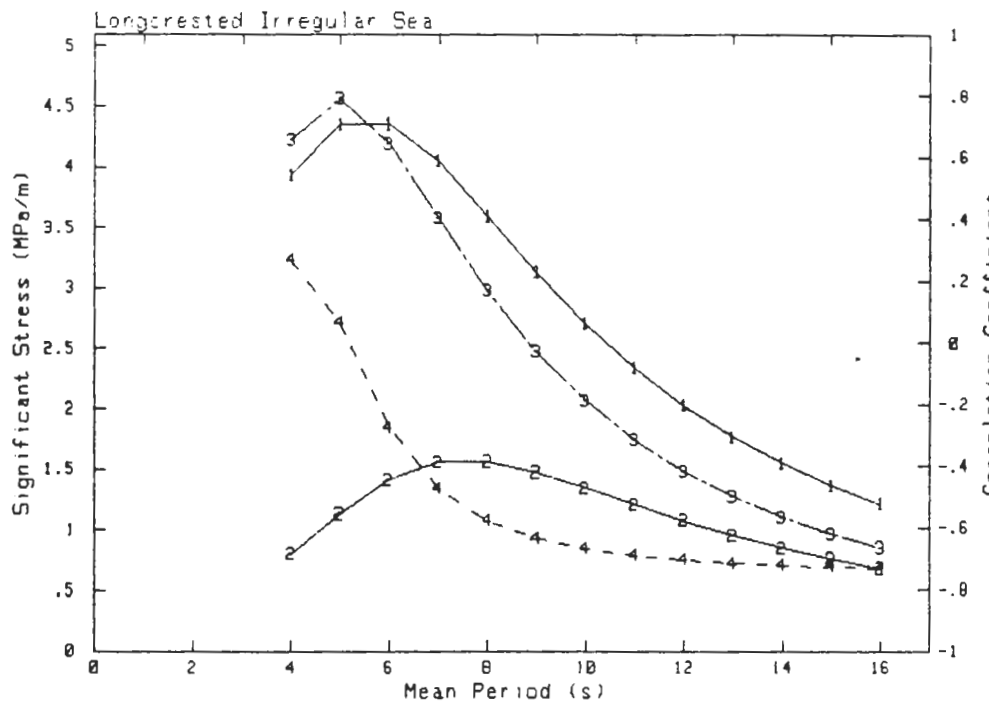

Side Frame, Position T Hold 2
Normal Stress Components

0°

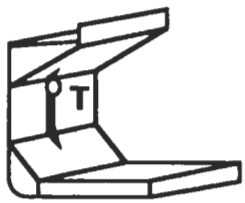

1: Pressure
2: Mass Force
3: Combined linear
4: Correlation Coefficient Pressure/Mass Force

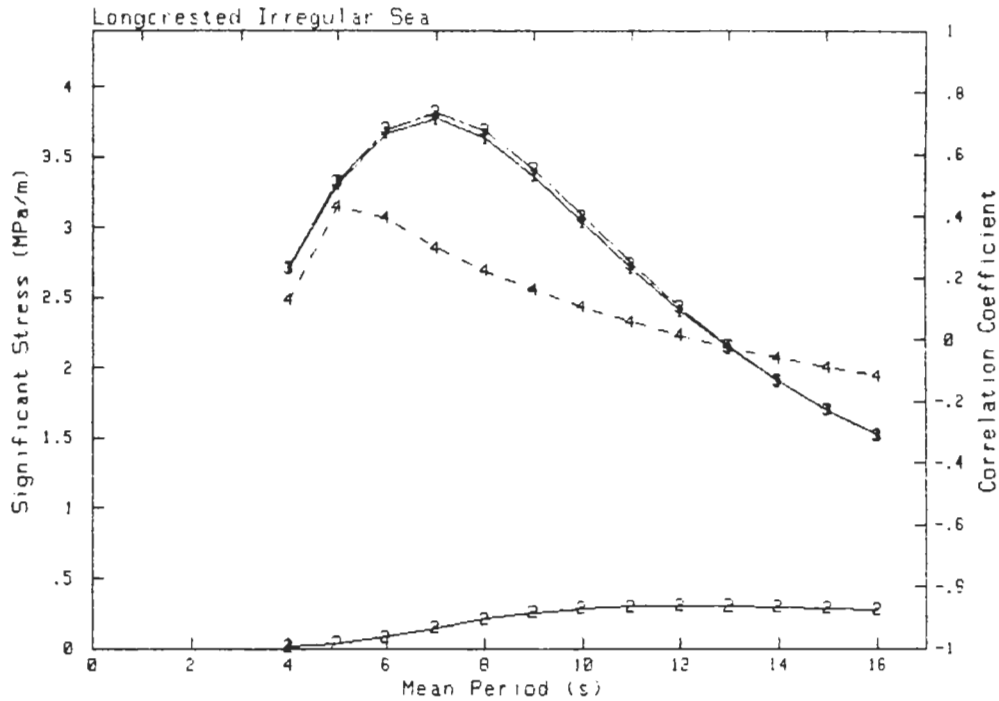

Side Frame, Position T Hold 2
Normal Stress Components

45°

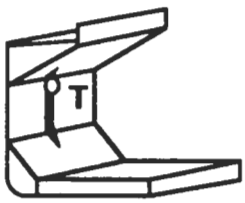

1: Pressure
2: Mass Force
3: Combined linear
4: Correlation Coefficient Pressure/Mass Force

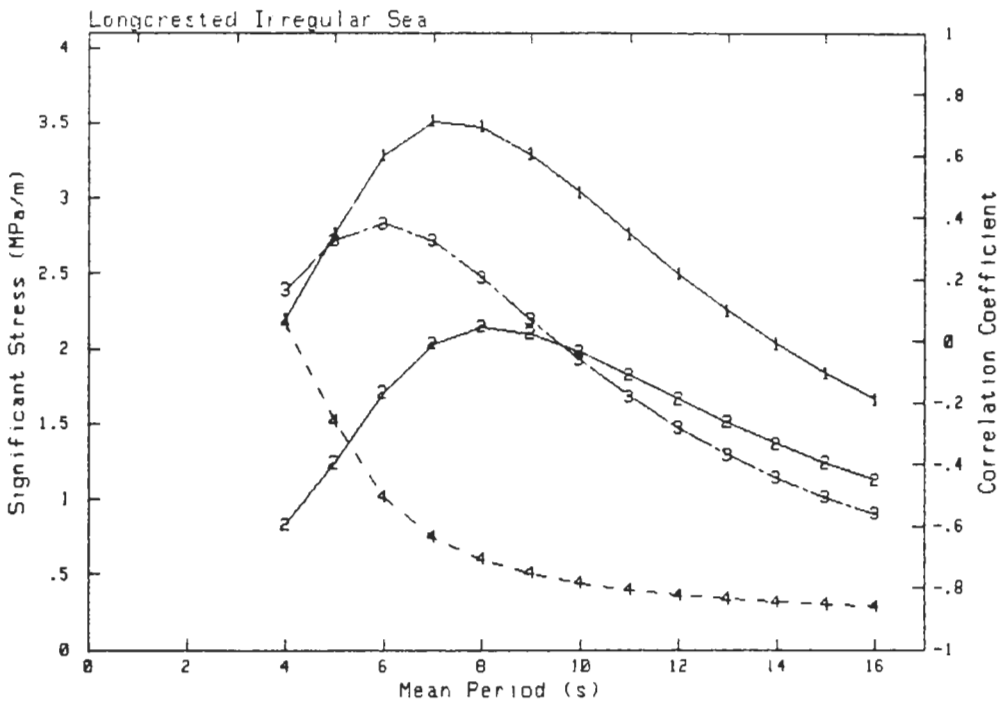

90°

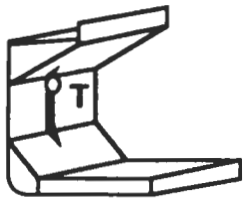

1: Pressure
2: Mass Force
3: Combined linear
4: Correlation Coefficient
Pressure/Mass Force

Side Frame, Position T Hold 2
Normal Stress Components

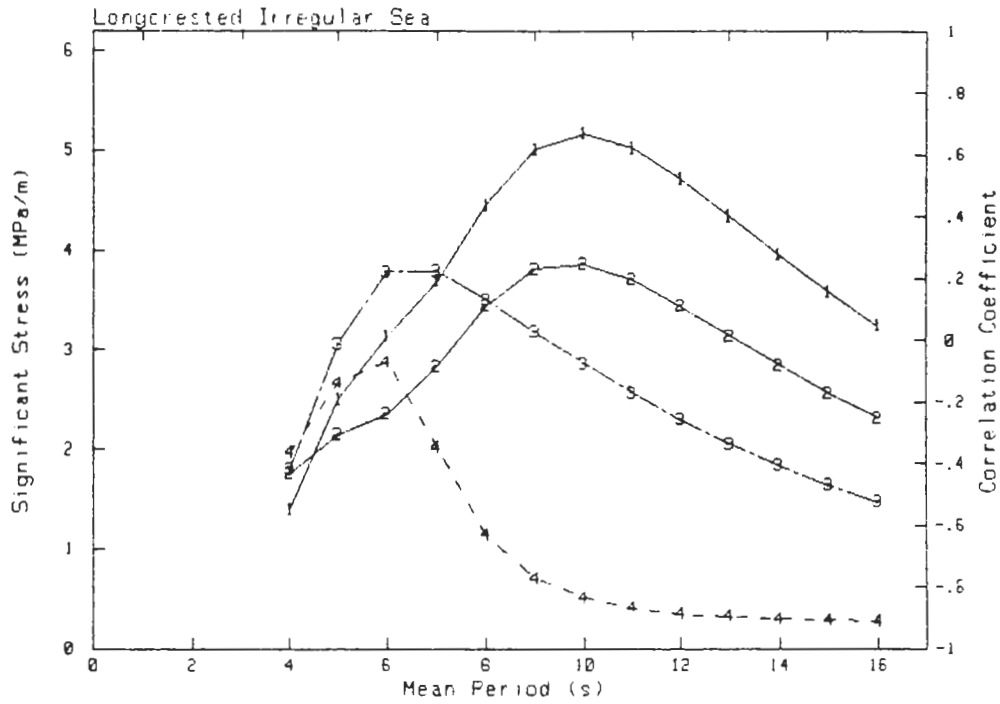

135°

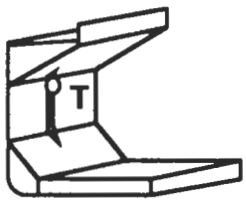

1: Pressure
2: Mass Force
3: Combined linear
4: Correlation Coefficient
Pressure/Mass Force

Side Frame, Position T Hold 2
Normal Stress Components

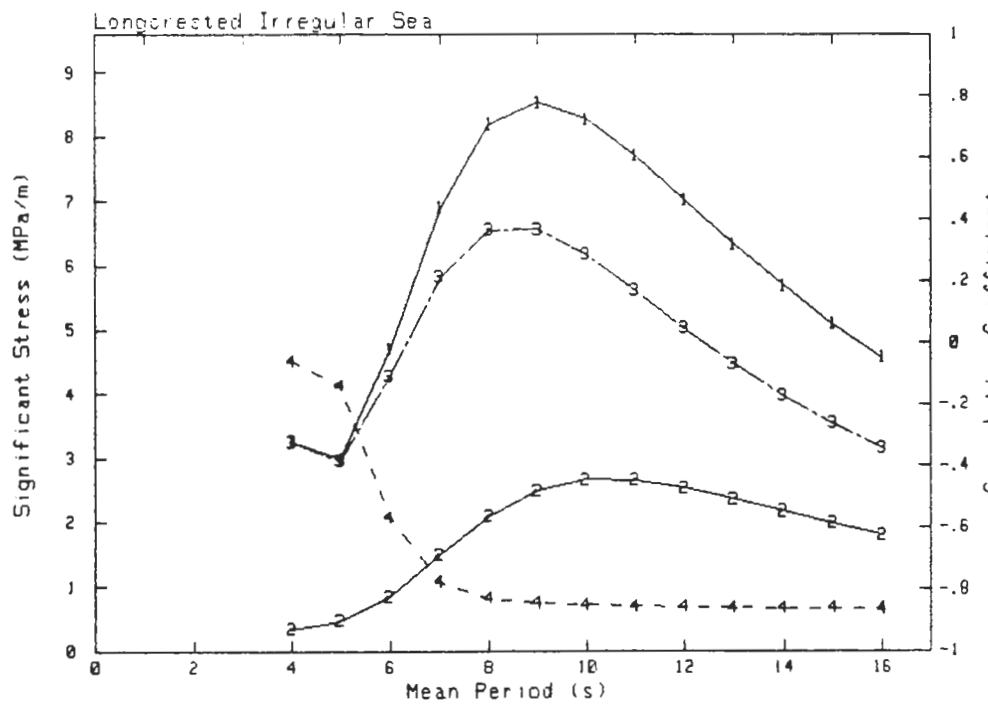

Side Frame, Position T Hold 2
Normal Stress Components

180°

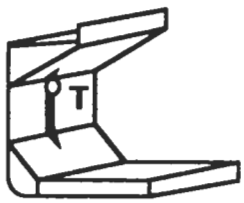

1: Pressure
2: Mass Force
3: Combined linear
4: Correlation Coefficient Pressure/Mass Force

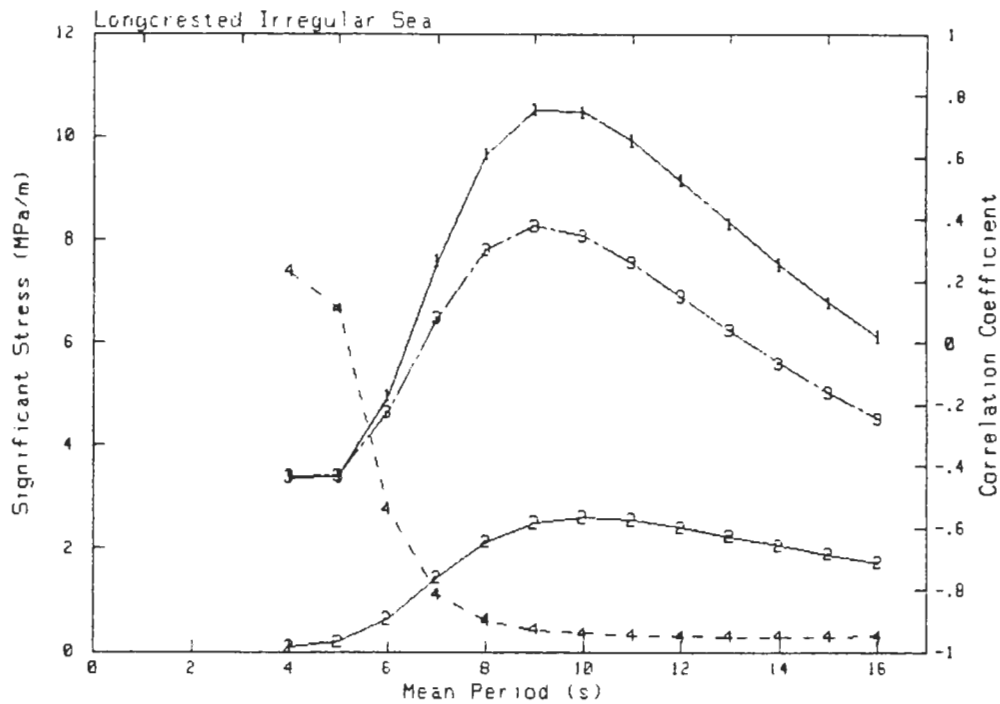

Side Frame, Position T Hold 2
Normal Stress Components

-135°

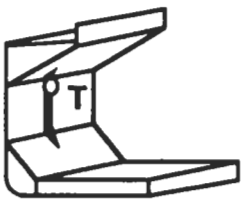

1: Pressure
2: Mass Force
3: Combined linear
4: Correlation Coefficient Pressure/Mass Force

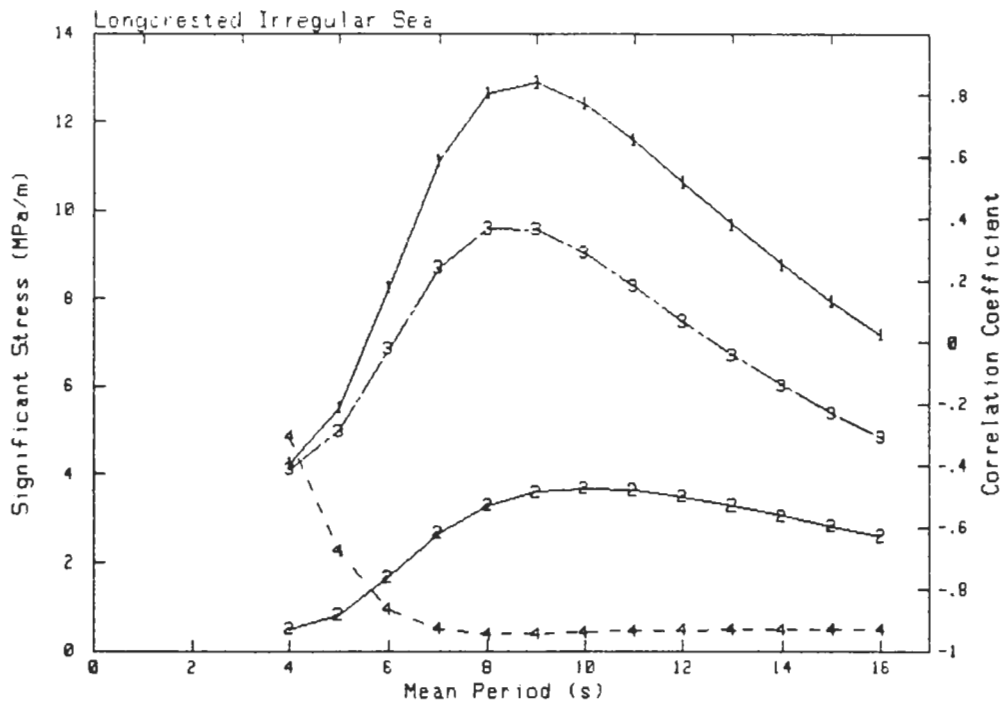

Side Frame, Position T Hold 2
Normal Stress Components

-90°

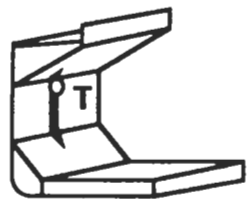

1: Pressure
2: Mass Force
3: Combined linear
4: Correlation Coefficient
Pressure/Mass Force

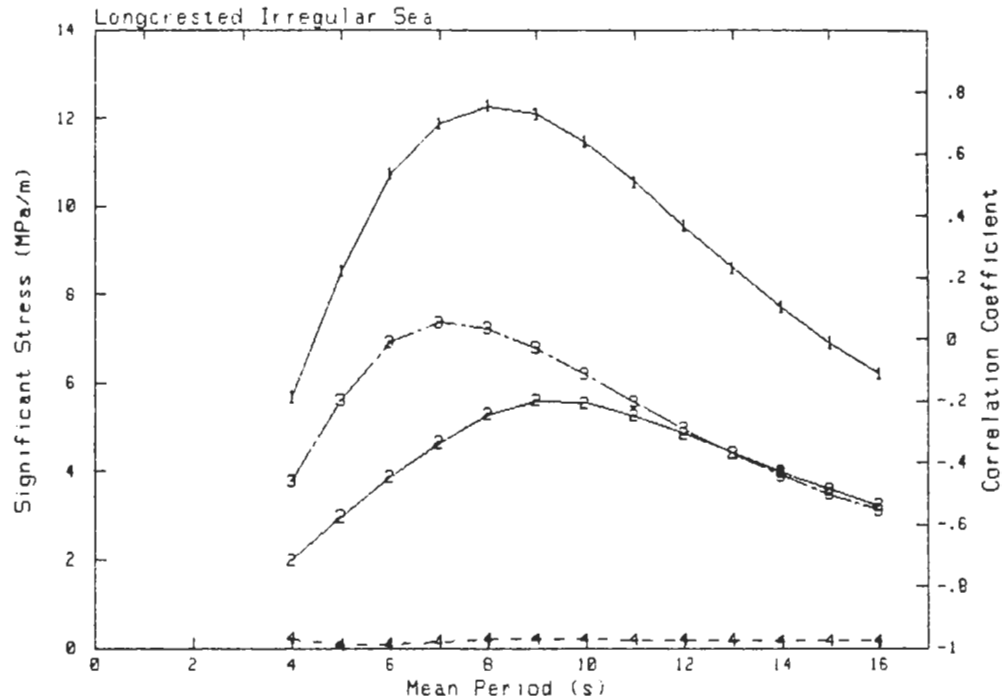

Side Frame, Position T Hold 2
Normal Stress Components

-45°

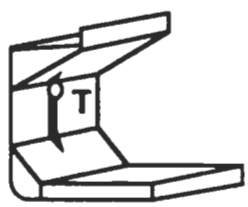

1: Pressure
2: Mass Force
3: Combined linear
4: Correlation Coefficient
Pressure/Mass Force